To the Graduate Council:

I am submitting herewith a dissertation written by Allen Kem Fronabarger entitled "Petrogenesis of the Calhoun Falls, Mt. Carmel, and Greenwood Complexes, South Carolina, and Modeling of Heat Transfer in Gabbro." I have examined the final copy of this dissertation for form and content and recommend that it be accepted in partial fulfillment of the requirements for the degree of Doctor of Philosophy, with a major in Geology.

Harry Y. McSween
Major Professor

We have read this dissertation
and recommend its acceptance:

Accepted for the Council:

The Graduate School

PETROGENESIS OF THE CALHOUN FALLS, MT. CARMEL, AND GREENWOOD COMPLEXES, SOUTH CAROLINA, AND MODELING OF HEAT TRANSFER IN GABBRO

A Dissertation

Presented for the

Doctor of Philosophy

Degree

The University of Tennessee, Knoxville

Allen Kem Fronabarger

December 1984

Copyright © Allen Kem Fronabarger, 1985

All rights reserved

ACKNOWLEDGMENTS

Travel and analytical expenses for this study were funded in part through the Department of Geological Sciences Honorary Fund and the South Carolina Geological Survey. Paul Nystrom of the South Carolina Geological Survey was especially helpful in providing valuable literature about the study area and in guiding me in mapping heavily weathered terrains. EG & G ORTEC in Oak Ridge, Tennessee, put its analytical materials and skills at my disposal so that I could obtain the bulk rock and trace element analyses presented herein. Nancy Jacobus of ORTEC provided invaluable hours of help and expertise in the actual analysis of more than 100 samples. The Oak Ridge National Laboratory Environmental Sciences Division funded me through a fellowship for all of the time spent on the study. Their generous financial support made the work possible. Each of my committee members: Drs. A. J. Baker, O. C. Kopp, K. C. Misra, and S. H. Stow, as well as my major professor, H. Y. McSween, spent hours of their time in reviewing the manuscript and provided me with valuable criticism along the way. Dr. Baker's patient tutoring of this (often naive) student in the esoterics of the finite element method is especially acknowledged. Dr. McSween's encouragement and instruction throughout my dissertation work simply cannot be adequately recognized. Finally, my wife, Chantal, and my daughter, Saskia, endured all of the trials and tribulations of my work without one word of discontent. My debt to them can never be repaid.

ABSTRACT

The Calhoun Falls, Mt. Carmel, and Greenwood mafic complexes have undergone a distinct fractionation history from similar bodies previously studied to the north. The mafic plutons of the southern Appalachians thus appear to comprise several contemporaneous magmatic centers.

The Calhoun Falls Complex is composed of layered metagabbro, cumulate gabbronorites, troctolites, and serpentinized ultramafic rocks. Ferromagnesian minerals exhibit little iron enrichment and plagioclase is normally zoned. Major and trace elements are also restricted in compositional range. This limited range in mineral and bulk rock chemistry is due to crystal accumulation. The calculated intercumulus liquid composition was tholeiitic.

The Mt. Carmel Complex is composed of unlayered metagabbro, olivine-biotite gabbro, and syenite. Textural and chemical evidence indicate that the samples from this suite represent approximate liquid compositions. Ferromagnesian minerals have extended iron-enrichment trends, and the plagioclase has a broad compositional range. Major and trace element trends suggest that the metagabbro and unmetamorphosed rocks are genetically related.

The Greenwood Complex is poorly exposed and appears to have been barely unroofed. It is composed of a chill zone phase (diorite) probably grading into cumulate gabbronorite. The major element and mineral chemistry are similar to that found in the cumulate

gabbronorites of Calhoun Falls; however, it evidently formed from a distinct parental magma.

In all three plutons, the fractionation sequence is olivine + clinopyroxene, joined later by plagioclase. Plutons to the north fractionated olivine + plagioclase, later joined by clinopyroxene. The late appearance of plagioclase in the fractionation sequence allowed the Calhoun Falls Complex to form the extensive ultramafic sequence.

The thermal effects of heat flow in gabbro due to the emplacement of high-level radioactive waste have been modeled by finite element computational analysis. Results indicate that the maximum temperatures reached would be similar to those other studies have found for granites; however, the solidus temperature is significantly higher for gabbro and can accommodate greater heat flux, thus allowing burial of younger (thermally hotter) waste or more waste per unit volume.

TABLE OF CONTENTS

CHAPTER	PAGE
INTRODUCTION	1
Objectives	1
Location of Study Area	3
I. PREVIOUS WORK	5
Introduction	5
Lowndesville (Kings Mountain) Belt	5
Charlotte Belt	8
Carolina Slate Belt	9
Relationship Between the Charlotte and Carolina Slate Belts	11
Mafic Intrusive Bodies Within the Charlotte and Carolina Slate Belts	12
II. FIELD RELATIONS AND LITHOLOGIC DESCRIPTION OF MAFIC PLUTONS	21
Introduction	21
Mapping and Sampling Techniques	21
Nomenclature	23
Calhoun Falls Complex	24
Mt. Carmel Complex	28
Greenwood Complex	30
Other Plutons	35
III. PETROGRAPHY AND MINERALOGY	42
Introduction	42
Metagabbro	45
Calhoun Falls Complex	46
Mt. Carmel Complex	53
Greenwood Complex	59
Summary	62
IV. BULK ROCK COMPOSITION	64
Introduction	64
Analytical Methods	64
Presentation of Data	67
Chemistry of the Complexes	69

CHAPTER PAGE

V. PETROGENESIS 79

Introduction 79
Mt. Carmel Complex 80
Calhoun Falls Complex 92
Greenwood Complex 101
Relationship of the Study Area to Other Mafic Intrusives in the Charlotte Belt 106
The Metagabbro Problem 112

VI. HEAT FLOW IN GABBROIC ROCKS 120

Introduction 120
Theoretical Development 122
Finite Element Method 124
Materials Properties 132
Assumptions and Limitations 140
Error and Sensitivity Analysis 141
Results 154

VII. CONCLUSIONS AND RECOMMENDATIONS 161

Summary 161
Thermal Heat Modeling in Mafic Intrusives 163

BIBLIOGRAPHY 164

APPENDICES 178

Appendix A 179
Appendix B 193
Appendix C 195

VITA 200

LIST OF TABLES

TABLE		PAGE
1.	Previous Studies of Mafic Intrusives in the Kings Mountain, Charlotte, and Carolina Slate Belts of the Southern Appalachians	13
2.	Operating Conditions for the ORTEC 6110 TEFA Energy Dispersive X-Ray Fluorescence Apparatus	65
3.	Estimated Minimum Detectable Concentrations (MDC) of Reported Analyses	66
4.	Percent Change of the Mean Concentrations Reported in This Study and the Best Values of Flanagan (1973) Reported in Decreasing Order of Accuracy	68
5.	Average Compositions of Metagabbro, Gabbro, and Syenite in the Mt. Carmel Complex	86
6.	Results of Mass Balance Computations for the Mt. Carmel Complex Using the Method of Wright and Doherty (1970)	88
7.	Results of the Intercumulus Liquid Calculations of the Gabbros from the Calhoun Falls Complex	100
8.	Summary of the Differences Between the Northern Magmatic Center as Characterized by the Concord Complex (McSween et al., 1984), and the Southern Complex as Characterized by the Mt. Carmel Complex (This Study)	107
9.	Thermal Properties for Several Rock Types Found in the Study Area, Daly et al. (1966)	121
10.	Thermal Decay Curves for Waste Derived from Boiling Water Reactors, Pressurized Water Reactors, and Defense High-Level Waste	135
11.	Packaging and Burial Conditions for Defense High Level Waste and Pressurized Water Reactor Waste	137
12.	Regression Equations Used for the Heat Source	139
13.	True, Reference, and Nondimensional Values Used in the Finite Element Procedure for Defense High-Level Waste and Pressurized Water Reactor Waste	143

TABLE PAGE

14. Sensitivity of Time and Temperature to Changing Rock and Waste Properties 154

A1. Representative Modal Analyses from Calhoun Falls Complex 180

A2. Representative Modal Analyses from Mt. Carmel Complex . . 181

A3. Representative Modal Analyses from Greenwood Complex . . 182

A4. Representative Electron Microprobe Analyses: Plagioclase 183

A5. Representative Electron Microprobe Analyses: Olivine 184

A6. Representative Electron Microprobe Analyses: Pyroxene 185

A7. Representative Electron Microprobe Analysis: Amphibole 186

A8. Major Element Constituents and CIPW Normative Mineralogy for Calhoun Falls Complex 187

A9. Major Element Constituents and CIPW Normative Mineralogy for Mt. Carmel Complex 188

A10. Major Element Constituents and CIPW Normative Mineralogy for Greenwood Complex 189

A11. Trace Element Constituents for Calhoun Falls Complex . . . 190

A12. Trace Element Constituents for Mt. Carmel Complex 191

A13. Trace Element Constituents for Greenwood Complex 192

B1. Units Used in Heat Flow Modeling and Sample Problem Set Up 194

LIST OF FIGURES

FIGURE		PAGE
1.	Generalized Geologic Map of the Southern Appalachian Piedmont Province Showing the Major Belts, the Location of the Study Area, and the Mafic Intrusives in the Kings Mountain, Charlotte, and Carolina Slate Belts	2
2.	Generalized Geologic Map of the Study Area	6
3.	Mesoscopic Layering in Sparolitized Serpentinites Within the Calhoun Falls Complex	27
4.	Aeromagnetic Map of the Greenwood Complex, Showing the Depression in the Magnetic Intensity Between the Northern and Southern Plutons	32
5.	Sketch Map of the Abbeville Pluton in the Abbeville West and Abbeville East 7.5 Minute Quadrangles	37
6.	Sketch Map of the Verdery Pluton Located in the Verdery 7.5 Minute Quadrangle	38
7.	Sketch Map of the McCormick Pluton Located in the Northeastern Corner of the McCormick 7.5 Minute Quadrangle	40
8.	Sketch map of the Winterseat Pluton Located in the Winterseat 7.5 Minute Quadrangle	41
9.	Petrologic Classification of the Rocks (Streckeisen, 1973) in the Calhoun Falls, Mt. Carmel, and Greenwood Complexes	43
10.	Compositions of Silicates in the Calhoun Falls, Mt. Carmel, and Greenwood Complexes	44
11.	Photomicrographs of Samples from the Calhoun Falls Complex	47
12.	Photomicrographs of Samples from the Mt. Carmel Complex in Cross-Polarized Transmitted Light	54
13.	Photomicrographs of Samples from the Greenwood Complex in Cross-Polarized Transmitted Light	60

FIGURE PAGE

14. Expanded Normative Basalt Tetrahedron Showing Calculated CIPW Values for Samples from the Calhoun Falls, Mt. Carmel, and Greenwood Complexes 70

15. Total Alkalis vs. Silica Diagram for Samples from the Calhoun Falls, Mt. Carmel, and Greenwood Complexes 73

16. AFM Diagram of Samples from the Calhoun Falls, Mt. Carmel, and Greenwood Complexes. 74

17. Harker Variation Diagrams for the Three Complexes Studied 76

18. Titanium vs. Magnesium Number for Samples from the Calhoun Falls, Mt. Carmel, and Greenwood Complexes . . . 77

19. Four Representative Two-Element Extract Diagrams Showing the Early Fractionation of Clinopyroxene and Olivine in the Mt. Carmel Complex 81

20. Isomolar Basalt Phase Diagram (Elthon, 1983) Showing Analyses of Metagabbro, Gabbro, and Syenite from the Mt. Carmel Complex 83

21. Minor and Trace Element vs. the Larsen Index for the Mt. Carmel Complex 90

22. Correlation of Volume Percent Cumulus Material to CaO + MgO in the Calhoun Falls Cumulate Gabbros 93

23. Schematic Diagram Showing How the Intercumulus Liquid Composition of Cumulate Gabbros Samples from Calhoun Falls Complex Is Calculated 97

24. Total Alkali vs. Silica Diagram Used to Calculate the Intercumulus Liquid Composition of the Calhoun Falls Complex Cumulate Gabbros 98

25. Total Alkali vs. Silica Diagram of Cumulate Gabbro Samples from the Greenwood Complex Showing That the Calculated Intercumulus Liquid Compositions Do Not Cross the Mt. Carmel Trend 102

26. Polybaric Phase Diagrams (O'Hara, 1976) for the Calhoun Falls, Mt. Carmel, and Greenwood Complexes . . . 104

FIGURE PAGE

27. Map of the Southern Appalachians Showing the Proposed Transform Fault (Kane, 1983) Separating the Northern and Southern Mafic Magmatic Centers in the Charlotte Belt 111

28. Total Alkali vs. Silica Plot of Average Compositions of Lithologies from the Mt. Carmel, Barber (Strange, 1983), and Mecklenburg (Hermes, 1968) Complexes 114

29. Variation of Thermal Conductivity with Temperature for Various Igneous Rock Types 133

30. Thermal Decay Curves for Waste Derived from Pressurized Water Reactors, Boiling Water Reactors, and Defense High-Level Waste 136

31. Schematic Drawing of Burial Conditions for Defense High Level Waste and Pressurized Water Reactor Waste 138

32. Idealized Section Through a Waste Canister Showing the Quarter Section Region Used in the Problem 140

33. Finite Element Grid Used in the Near-Field Error and Sensitivity Analysis 145

34. Time-Temperature-Space Curves Showing the Results of the Reference Run for the X-Direction and the Y-Direction 146

35. Time-Temperature-Space Curves Showing the Effect of Changing the Grid Size for the X-Direction and the Y-Direction 148

36. Time-Temperature-Space Curves Showing the Effect of Using a Quadratic Interpolation Equation in the Y-Direction 151

37. Time-Temperature-Space Curves Showing the Effect of Changing the Time Interval between Temperature Calculations for the Y-Direction 152

38. Isothermal Curves at t = 0.89 Years for Defense High Level Waste in Gabbro 155

39. Isothermal Curves at t = 1.8 Years for Pressurized Water Reactor Waste in Gabbro 156

LIST OF PLATES

PLATE

1. Generalized Geology of the Study Area . . . . . In Pocket
2. Aeromagnetic Intensity . . . . . In Pocket
3. Calhoun Falls Complex . . . . . In Pocket
4. Mt. Carmel Complex . . . . . In Pocket
5. Greenwood Complex . . . . . In Pocket

INTRODUCTION

Objectives

The occurrence of mafic intrusive bodies within the Charlotte and Carolina Slate belts of the southern Appalachians is well documented (e.g., King, 1955; Overstreet and Bell, 1965a, 1965b; Butler and Ragland, 1969; Fullagar, 1971; Hatcher et al., 1980; Glover et al., 1983; and McSween et al., 1984). These intrusives (Fig. 1) form a regional northeast-southwest chain. A cluster of mafic intrusives along the South Carolina-Georgia border and within the Charlotte belt (Fig. 1) has not been studied in detail, however. This cluster is separated from other mafic plutons in the Charlotte belt by regions containing few if any mafic intrusives. Thus, the chain of mafic plutons in the Charlotte belt can be subdivided into what appear to be two magmatic centers. The first objective of this study is to understand the petrogenesis of the three largest mafic plutons in this cluster, and to compare them to other, similar plutons in other magmatic centers. The presence of any significant differences in the petrogenesis of mafic plutons that occur along strike will affect our understanding of the evolution of the southern Appalachians. It is to this end that this study has been undertaken.

The second objective of this work is to model the heat flow through gabbroic rocks in both time and space due to the hypothetical storage of high level radioactive waste. The three plutons investigated in this study represent a wide range of petrographic, lithologic,

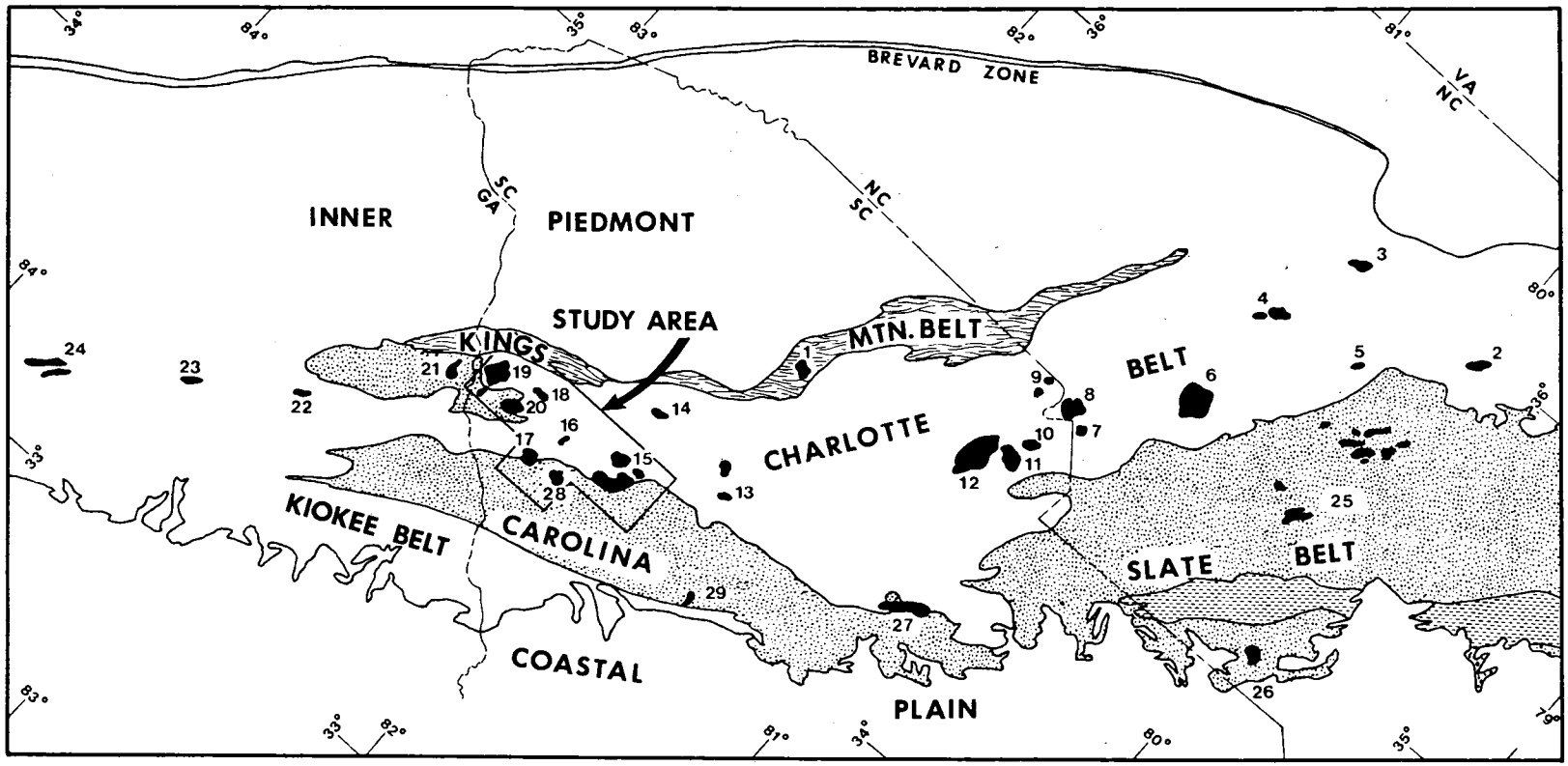

Figure 1. Generalized geologic map of the southern Appalachian Piedmont Province showing the major belts, the location of the study area, and the mafic intrusives in the Kings Mountain, Charlotte, and Carolina Slate belts. (Modified from Butler and Ragland, 1969; and Misra and McSween, 1984.) Numbered plutons are identified in a later table.

and chemical characteristics, and are probably representative of most mafic intrusives found within the United States. Thus, the extremes of variation in the thermal character that are due to the variations in the physical and chemical character can be modeled using data obtained from these rocks. Some of the data collected for the first part of this study are used in conjunction with the finite element method in modeling this heat flow. The U.S. Department of Energy has considered burial of radioactive waste in salt, basalt, shale, and granite (U.S. DOE, 1977, 1979; and ONWI, 1979). Gabbroic rocks have advantageous properties that other rock types do not have, however.

Location of Study Area

The study area is located in parts of Greenwood, Abbeville, and McCormick counties, South Carolina, within the Charlotte belt of the southern Appalachians (Fig. 1) and comprises fourteen 7.5 minute quadrangles. Several mafic intrusive bodies are found in this area, most notably the Calhoun Falls, the Mt. Carmel, and the Greenwood mafic intrusive complexes, but numerous other smaller named and unnamed mafic plutons also occur (Overstreet and Bell, 1965a, 1965b; Griffin, 1978, 1979; Chalcraft et al., 1978; and Pirkle, 1982). Relatively flat, topographically mature terrain and extensive saprolitic soils characterize this part of the Charlotte belt. The primary human activity includes agriculture and foresting and a relatively good system of state and county roads transects the region. The three major

towns in the area are Greenwood to the east, Abbeville in the center part of the region, and Calhoun Falls at the western limit.

The study area is bounded to the northwest by the Lowndesville belt and to the southeast by the Carolina Slate belt. The Lowndesville belt is the southern extension of the Kings Mountain belt (Griffin, 1978) and is considered to represent a major structural boundary between the inner and outer Piedmont subprovinces. The Carolina Slate belt represents stratigraphically higher rocks of lower metamorphic grade relative to those of the Charlotte belt.

CHAPTER I

PREVIOUS WORK

Introduction

Rocks within the study area can be subdivided into several discrete packages, which are, from northwest to southeast (Fig. 2 and Plate 1): (1) the Inner Piedmont belt, (2) the Lowndesville (Kings Mountain) belt, (3) the Charlotte belt, (4) an inlier of the Carolina Slate belt, correlative to the northern Little River belt in Georgia, and (5) the Carolina Slate belt, correlative to the southern Little River belt in Georgia (Griffin, 1978, 1979). The Inner Piedmont belt rocks are separated from the other subprovinces by the Lowndesville belt and no further discussion of them will appear herein. The stratigraphy, structure, and metamorphic history of each belt is summarized with a synthesis of the correlation of the Charlotte and Carolina Slate belts, and is followed by a synthesis of previous studies of the mafic intrusives in the southern Appalachians.

Lowndesville (Kings Mountain) Belt

King (1955) defined the Kings Mountain belt to be distinguished by mica schists, quartzites, marbles, and conglomerate and Overstreet and Bell (1965a, 1965b) extended it to the South Carolina-Georgia border on the basis of amphibolites and sericite schists that they mapped. Price (1969) and Griffin (1970a, 1971, 1972) mapped a major shear zone in Abbeville county, South Carolina and showed it to be

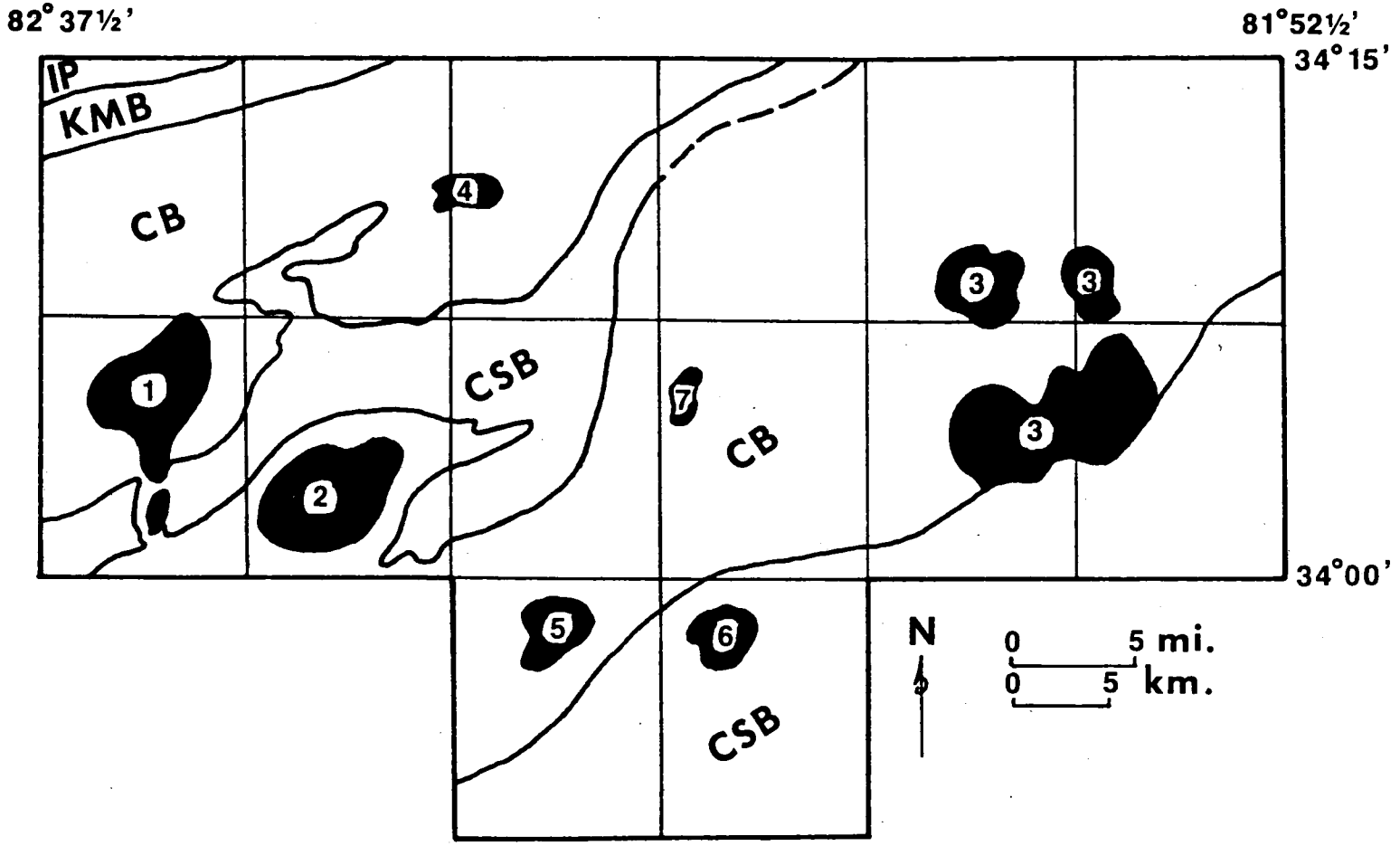

Figure 2. Generalized geologic map of the study area. The belts are: Inner Piedmont (IP), Kings Mountain belt (KMB), Charlotte belt (CB), and the Carolina Slate belt (CSB). The mafic intrusives are: Calhoun Falls (1), Mt. Carmel (2), Greenwood (3), Abbeville (4), McCormick (5), Winterseat (6), and Verdery (7). The grid system outlines 7.5 minute quadrangles indexed on Plate 1. (After Griffin, 1978, 1979, and this study.)

the southern extension of the Kings Mountain belt. Although this extension of the Kings Mountain belt was disputed by Kesler (1972) who suggested the term "Lowndesville belt" for the southern zone, later workers (e.g., Griffin, 1978, 1979, 1981; Rozen, 1981; and Nelson, 1981) confirmed the correlation.

Griffin (1981) described the belt within the study area to be characterized primarily by a muscovite/sericite quartz phyllonite which has been cataclastically foliated and is associated with quartzites which become micaceous along strike. Fine grained, schistose amphibolites, manganiferous (graphitic) biotite schists, and isolated pods of ultramafic rocks can be found in association with the phyllonite in the study area.

Griffin (1981) noted that although the stratigraphic relations have been obscured in the Lowndesville belt by this cataclasis, the phyllonite appears to be mineralogically similar to units in the Inner Piedmont and Carolina Slate belts. On this basis, he suggested that the belts may be stratigraphically correlative.

Nelson (1981) summarized the following sequence of events for the formation of the Lowndesville belt: (1) development of regional metamorphic foliation (S_1) parallel to the mylonitic foliation (S_m) in the shear zone, (2) possible folding of S_m forming rootless isoclinal folds, (3) late stage ductile deformation forming penetrative cleavage (S_2), (4) folding that produced NNE trending folds and slip cleavage (S_3), and (5) one or more periods of fracturing during or after the formation of mylonites. Isotopic evidence (Horton, 1981) suggests a

minimum age of ductile deformation to be 450 my, at or near the end of the peak of Taconic metamorphism. Late fracturing events occurred during the Alleghanian and also possibly during the Triassic and Jurassic Periods.

Charlotte Belt

The Charlotte belt within the study area (Fig. 2 and Plate 1) consists of (1) the Latimer complex, composed primarily of mafic orthogneiss, (2) granitoid gneiss, (3) mica schists and gneisses, (4) quartzites, and (5) cataclasites, as well as late granitic and gabbroic intrusive plutons.

Griffin (1978) named a group of amphibolite grade rocks consisting of amphibolite, metagabbro, greenstone, metabasalt, and metadiorite and located near Calhoun Falls (Plate 1) the Latimer Complex. He stated that both intrusive (metagabbro) and extrusive (metabasalt) rocks occur in the complex. The more felsic rocks in this complex formed through migmatization at depth due to later intrusion of granitic plutons. Weisenfluh and Snoke (1978) reinterpreted the Latimer complex to be a trondhjemitic, volcanic-plutonic complex and redefined the unit within the Latimer complex to consist of hypabyssal dikes, quartz keratophyre, biotite trondhjemite, and a hornblende-rich unit, all of which represent an Eocambrian-Cambrian epizonal igneous center located in an island-arc system on oceanic lithosphere.

Both biotite gneiss and mica schist are found in the Charlotte belt rocks. They do not make up a large proportion of the rocks within

the area. Most of the cataclastic rocks are found in the Cold Springs shear zone (named by Griffin, 1978) to the northwestern edge of the study area. This cataclasis postdated other activity in the area.

Wagener (1977) and Griffin (1978, 1979) mapped several granitic intrusions in the area which range in composition from granite-adamellite to quartz diorite and form small dikes to large batholitic plutons (Griffin, 1978, 1979). It is these rocks that Griffin considers to have formed the migmatities within the older Latimer complex. Three intervals of granitic intrusive activity have been recorded: 595-520, 415-385, and 325-265 my (Fullagar and Butler, 1979), thus spanning the Taconic and Acadian orogenies whose thermal peak occurred at about 460 my (Hatcher et al., 1980).

Carolina Slate Belt

Within the Charlotte belt, Griffin (1978, 1979) mapped a lithologic package that he considers to belong to the Carolina Slate belt. These rocks are totally isolated from the Carolina Slate belt rocks to the southeast by the Charlotte belt and cannot be easily correlated to them due primarily to poor exposure, folding, and metamorphism. Because these two packages of Carolina Slate belt rocks cannot be correlated to one another, they are considered separately (Fig. 2 and Plate 1).

Isolated Carolina Slate Belt Rocks

These units have been mapped and described by Griffin (1978, 1979) and are equivalent to the Little River belt in Georgia. Griffin mapped mafic metavolcanics, felsic and intermediate metavolcanics,

metadacite, phyllite, and metalamprophyre dikes. He considered the rocks to represent metamorphosed supracrustal units whose original textures are often preserved due to the low metamorphic grade.

The mafic metavolcanics consist of tuffs, metabasalt and metadiabase sills, dikes and possibly flows. Felsic to intermediate metavolcanics range in composition from rhyolite, dacite, to andesite. Phyllite is common to the Carolina Slate belt rocks and consists of muscovite and sericite quartz schist. Metalamprophyre dikes occur locally and crosscut all other lithologies. The dikes contain well developed cleavage or foliation suggesting that they were intruded prior to the development of regional metamorphic cleavage (Griffin, 1978).

Main Body of the Carolina Slate Belt

The main body of the Carolina Slate belt occurs to the southeast and provides a more or less distinct boundary of the study area (Pirkle, 1977, 1978, 1982). Pirkle showed an interbedded sequence of argillites and volcanics, all metamorphosed to greenschist facies, as well as a granite and a gabbro pluton. All of the beds trend northeast and are part of a fold system whose axis plunges 6° NE. In the northwestern corner of Winterseat quadrangle, he mapped the contact between the Charlotte and Carolina Slate belts as consisting of a mafic metavolcanic unit grading into, or in contact with a biotite gneiss/ amphibolite.

In Whitney et al. (1978), part of the area mapped is the same as that mapped by Pirkle and their stratigraphic descriptions are in good

agreement. They found this region to consist of the basal, or "lower sequence," Lincolnton metadacite, a felsic pyroclastic sequence consisting of interbedded quartz and diorite tuffs, and an upper sedimentary sequence composed of banded argillite. This sequence was deformed into a single generation of vertical, isoclinal folds dipping northeastward. Carpenter et al. (1982) dated the Lincolnton metadiorite at 554 ± 20 my (Rb-Sr) and 568 my (U-Pb, zircon).

Relationship Between the Charlotte and Carolina Slate Belts

Various workers have suggested that there is structural and stratigraphic continuity between the Charlotte and Carolina Slate belts (Whitney et al., 1978; Bourland and Farrar, 1980; and Secor et al., 1982). Furthermore, the regional magnetic and gravity highs corresponding to both the Charlotte belt and most of the Carolina Slate belt are interpreted by Hatcher and Zietz (1980) as a single belt underlain by mafic crust. Glover et al. (1983) constrained the timing of dynamothermal metamorphism to a single Taconic (480-435 my) event in both belts in the study area. Furthermore, Bourland and Farrar (1980) were able to demonstrate that all metamorphic textures and structural features present in the Winsboro area, straddling the Charlotte-Carolina Slate belt boundary, were due to a single regional orogenic event.

The boundary between the two belts separates greenschist facies rocks of the Carolina Slate belt from the amphibolite facies rocks of the Charlotte belt. The intrinsic differences in petrology and

metamorphic grade between the two belts (predominantly mafic rocks of medium grade in the Charlotte belt and predominantly intermediate to felsic rocks of low grade in the Carolina Slate belt) recognized by McCauley (1961) and Griffin (1978, 1979) suggest that the Slate belt lithologies represent a stratigraphically higher and younger sequence than the Charlotte belt. Furthermore Ellwood (1982), Barton and Brown (1983), and Dooley (1983) noted that little or no relative movement has occurred across the Charlotte-Carolina Slate belt boundary. The large volume and nature of volcanic, volcaniclastic and intrusive rocks found in the two belts probably indicate that they represented an evolving volcanic arc (Butler and Ragland, 1969). Secor et al. (1983) were able to demonstrate that the Carolina Slate belt is an exotic terrain on the basis of fossil evidence. Thus, the Charlotte and Carolina Slate belts appear to represent one single stratigraphic package, subdivided on the basis of metamorphic grade.

Mafic Intrusive Bodies Within the Charlotte and Carolina Slate Belts

Over 35 mafic intrusives within the Kings Mountain, Charlotte and Carolina Slate belts have been mapped (Fig. 1, p. 2), of which a number have been studied in detail. Table 1 summarizes the principal investigations made to date. The following summary of these plutons is drawn from these references.

Table 1. Previous studies of mafic intrusives in the Kings Mountain, Charlotte, and Carolina Slate belts of the southern Appalachians.

Map Symbol*	Name and Location	Studies
	Kings Mountain Belt	
1.	Buffalo	Medlin, 1968, 1969; Butler and Ragland, 1969; Medlin et al., 1972
	Charlotte Belt	
2.	High Point	Hadley, 1973
3.	Farmington	Butler and Ragland, 1969; Fullagar, 1971; McSween et al., 1984
4.	Barber	Butler and Ragland, 1969; Clark, 1980; Strange, 1983; McSween et al., 1984
5.	Linwood	Constantino-Herrera, 1971
6.	Concord	Bell, 1960; Morgan, 1963; Butler and Ragland, 1969; Cabaup, 1969; Price, 1969; Fullagar, 1971; Olsen, 1982; Olsen et al., 1983
7.	Pineville	
8.	Mecklenburg	Hermes, 1968, 1970; Butler and Ragland, 1969; Fullagar, 1971; Wilson, 1981
9.	York	
10.	N. Rock Hill	Butler, 1966; Butler and Ragland, 1969; Wagener, 1974
11.	S. Rock Hill	
12.	Ogden	Butler, 1966; Butler and Ragland, 1969; Chalcraft, 1977; McSween, 1981a; McSween et al., 1984
13.	Newberry County	Butler and Ragland, 1969
14.	Coronaca	McSween, 1970
15.	Greenwood	Butler and Ragland, 1969; Chalcraft et al., 1978, 1981
16.	Verdery	Griffin, 1979
17.	McCormick	Butler and Ragland, 1969
18.	Abbeville	Butler and Ragland, 1969; Griffin, 1979
19.	Calhoun Falls	Butler and Ragland, 1969; Griffin, 1978, 1979; Fronabarger and McSween, 1983
20.	Mt. Carmel	Medlin, 1968, 1969; Butler and Ragland, 1969; Griffin, 1978; Fullagar, 1971
21.	Delhi	Butler and Ragland, 1969
22.	Greene County	
23.	Presley's Mill	Myers, 1968
24.	Gladesville	Carpenter and Hughes, 1970; Mathews, 1967, 1969
	Carolina Slate Belt	
25.	Albemarle Area	Misra and McSween, 1984
26.	Pee Dee	Butler and Ragland, 1969
27.	Dutchman's Creek	McSween, 1972; McSween and Nystrom, 1979
28.	Winterseat	Pirkle, 1982
29.	Cloud's Creek	Secor and Snoke, 1978

*Location in Figure 1, p. 2.

Field Relations

Most of the mafic intrusives of the southern Appalachians consist both of gabbro and metagabbro in close association (e.g., Hermes, 1968, 1970; and McSween et al., 1984). Metagabbro usually occurs at the margins of the bodies; however, Fronabarger and McSween (1983) interpreted occasional areas of metagabbro within the interior of the Calhoun Falls complex to be roof pendants isolated from the main body of the metagabbro. Hermes (1968) proposed a similar relationship for the Mecklenburg complex where he found isolated stocks of unaltered gabbro in metagabbro. Hermes suggested that the gabbro was barely unroofed, placing the metagabbro at the roof and periphery of the complex.

Syenite occurs in at least four of the intrusives: the Concord and Mecklenburg complexes, North Carolina, the Mt. Carmel complex, South Carolina, and the Delhi complex, Georgia. Of these three intrusions, little is known of the Delhi which was only mentioned by Butler and Ragland (1969). The other two have been studied in detail, however, and are unique in terms of field relations. The Concord complex consists of a ring dike of syenite enclosing a gabbro cumulate core (Olsen et al., 1983) whereas the Mt. Carmel complex contains lobate bodies of syenite in close association with gabbro and metagabbro (Medlin, 1968, and this study). Of these three bodies, Concord is the largest encompassing about 36 square kilometers, Mt. Carmel about 8 square kilometers and Delhi about 5 square kilometers (Butler and Ragland, 1969).

The mafic intrusives of the southern Appalachians range in outcrop area from about 70 square kilometers (Ogden pluton) to less

than 1 square kilometer for many small plugs (McSween et al., 1984). Geophysical studies of individual bodies (Hermes, 1968; Chalcraft, 1970; Wilson, 1981; Taylor and Butler, 1982; and Olsen et al., 1983) indicate that they are either cylindrical or lopolithic in nature, extending to depths of 2-6 km. Each of the intrusives forms distinct positive magnetic and gravity anomalies (e.g., Talwani et al., 1975; U.S.G.S., 1978; and Hatcher and Zietz, 1980). McSween et al. (1984) noted that the gravity anomalies over gabbro are more intense than over metagabbro, suggesting that the gabbro extends to greater depths than the associated metagabbro.

All of the mafic intrusives form topographic lows relative to the country rocks. Although this topographic difference aids in locating gabbroic bodies, the intense saprolitic alteration often precludes mapping exact contact relations between individual lithologies.

Contact metamorphic aureoles have been noted for some of the bodies that have been mapped in detail, for example Gladesville (Carpenter and Hughes, 1970), Calhoun Falls (Fronabarger and McSween, 1983), and Mt. Carmel (Medlin, 1968, and this study). These metamorphic aureoles occur both at the contact of country rocks and metagabbro and at the contact of country rocks and unaltered gabbro, suggesting that the effects of contact metamorphism were greater than the effects of the regional metamorphism.

Mineralogy and Petrology

Hermes (1968, 1970) catalogued several types of metagabbro within the Mecklenburg complex. He defined three types of

metagabbro on the basis of the degree of alteration of primary minerals and on foliation within the metagabbro. Metagabbros are characterized by the ateration of mafic minerals to green actinolitic hornblende, and the saussuritization of calcic plagioclase. The most altered samples often exhibit metamorphic foliation. A detailed discussion of Hermes' classification of metagabbro is deferred to a later section of this work as it applies to the rocks in the study area.

Unaltered gabbros almost always exhibit cumulate textures. The term cumulus is used here in a textural descriptive sense (Irvine, 1982), and does not necessarily imply gravity settling. McSween et al. (1984), in a review of the Farmington, Barber, Concord, Mecklenburg, and Ogden complexes, and McSween (1972) and McSween and Nystrom (1979) in studies of the Dutchmans Creek pluton, found that most of these gabbros are gabbronorites composed of cumulus plagioclase and olivine with postcumulus clinopyroxene and orthopyroxene, or cumulus plagioclase and clinopyroxene with postcumulus hornblende and orthopyroxene. Occasional troctolites occur, formed from the accumulation of plagioclase and olivine with postcumulus hornblende. All postcumulus minerals exhibit poikilitic textures. The Barber complex, on the other hand, is unique in that it is composed of cumulus orthopyroxene, clinopyroxene, and plagioclase with postcumulus hornblende (Clark, 1980; and McSween et al., 1984). Furthermore, they found this gabbro to be concentrically zoned with the core of the gabbro body containing up to 16% quartz and the margins containing abundant brown hornblende and biotite. Accessory minerals in all of the

gabbros include variable amounts of magnetite, ilmenite, spinel, hematite, pyrite, and pyrrhotite, usually as postcumulus phases.

The syenite of the Concord complex is composed of a groundmass of perthite, plagioclase, microcline, clinopyroxene, biotite, amphibole, and quartz with large phenocrysts of perthite and antiperthite (Olsen et al., 1983), forming a coarse grained, seriate porphyry. Medlin (1968) described the Mt. Carmel syenite to consist of microcline-microperthite, microantiperthite, microcline, plagioclase, amphibole, biotite, chlorite, opaque minerals, epidote, apatite, zircon, and minor quartz.

Very limited iron-enrichment trends of the mafic minerals have been observed for all of the gabbros studied to date. Plagioclase likewise shows limited sodium enrichment in the gabbros (McSween et al., 1984). The plagioclase found in syenite-bearing intrusions does show a greater sodium enrichment trend (Medlin, 1968; and Olsen et al., 1983). This limited iron enrichment for mafic minerals and sodium enrichment for plagioclase is attributable to three possible controlling factors. O'Hara (1977) suggested that repeated intrusion of primitive magma could buffer major element chemistry. McSween et al. (1984) noted that high fO_2 (evidenced by the large amounts of pyroboles and magnetite in the gabbro) or the emplacement of the magmas as crystal mushes would have the same effect.

Geochemistry

Butler and Ragland (1969) collected 103 analyses for metagabbros, gabbros, and syenites throughout the southern Appalachians. Medlin

(1968) analyzed samples from both the Buffalo and Mt. Carmel complexes; Cabaup (1969) analyzed samples from the Concord complex; Hermes (1968) performed analyses for the Mecklenburg complex; and Strange (1983) collected bulk and trace element data for the Barber complex. Furthermore, Carpenter and Hughes (1970) analyzed samples for selected trace elements for the Gladesville pluton, and Price (1966) performed trace element analyses for several plutons including the Concord complex. Results of these analyses have shown that many of the plutons have undergone unique crystallization histories despite the similarities in their petrologic character.

Butler and Ragland (1969) and later Olsen et al. (1983) found that there is a gap between the compositions of the gabbros and the syenites of the Concord complex. This observation was interpreted by both groups of workers as having resulted from differentiation of the syenite at depth from the original magma that formed the gabbro and was subsequently emplaced as a ring dike at a later time. A second type of differentiation history was provided by Medlin (1968) in his study of the Mt. Carmel complex. He saw a continuous compositional trend from gabbro to syenite and concluded that these rocks formed through perfect fractional crystallization at the site of emplacement. In his analyses, he included metagabbro, gabbro, and syenite. Intrusives that do not contain syenite have been more controversial, however. For the Barber (Strange, 1983), Buffalo (Medlin, 1968), Concord (Cabaup, 1969), and Mecklenburg (Hermes, 1968) gabbros, all show limited iron-enrichment trends. Although Medlin (1968), Butler

and Ragland (1969), and Hermes (1968) ascribed this to limited differentiation of the parent magma, McSween et al. (1984), noted that bulk element compositions of cumulate rocks do not reflect the composition of the liquids from which they were derived. Furthermore, Strange (1983) was able to correlate the amount of cumulus minerals to the bulk rock composition.

Timing of Intrusion and Crystallization

Olsen et al. (1983) recalculated a Rb-Sr whole rock isochron age from Fullagar (1971) for the Concord syenite to be 404 ± 21 my using the new Rb decay constant. Olsen et al. (1983) dated the Concord gabbro using the Sm-Nd (cpx-pg) technique and found a crystallization age of 407 ± 36 my. McSween et al. (1984) reported crystallization ages for the Farmington, Ogden, and Barber gabbros using the same technique to be 399 ± 27 my, 406 ± 32 my, and 479 ± 27 my, respectively. S. S. Goldrich (in Medlin, 1968) dated the Mt. Carmel syenite using Rb-Sr (biotite) to range from 380 to 387 my, which Medlin considers to represent minimum age of crystallization, and Fullagar (1971) dated biotites in the gabbro unit using Rb/Sr and obtained an age of 407 my. The Taconic orogeny is considered to have occurred from circa 480 to 435 Ma (Glover et al., 1983) indicating that all of the intrusives that have been dated, with the exception of the Barber pluton, are late- or post-Taconic in age.

Although only one age date has been obtained for the metagabbros, most workers consider them to be syn- or pre-Taconic in age (e.g., Fullagar, 1971; McSween, 1981b; McSween et al., 1984). Butler

and McSween (1983) noted that early granitic bodies occasionally intrude into metagabbros, indicating that the metagabbros were emplaced before the 520 my age of the granites. McSween et al. (1984) reported a preliminary Sm-Nd age for the Barber metagabbro to be 567 ± 50 my.

Relationship Between Gabbro and Metagabbro

McSween (1981b) and McSween et al. (1984) considered the possibility that the gabbros formed from magmas that migrated up along zones of weakness formed by the earlier (pre-Taconic) metagabbro intrusions. In support of this hypothesis they noted the different ages of gabbro and metagabbro and the consistent field association of the two rock types. Furthermore, Strange (1983) was able to differentiate the compositions of the metagabbros and gabbros in the Barber pluton using discriminant analysis, and McSween et al. (1984) noted that the two units in the Mecklenburg complex also differed in composition.

CHAPTER II

FIELD RELATIONS AND LITHOLOGIC DESCRIPTION OF MAFIC PLUTONS

Introduction

The three major complexes in the study area are the Calhoun Falls complex to the west, the Mt. Carmel complex in the center, and the Greenwood complex to the east, while several other smaller plutons are scattered throughout the study area (Plate 1). These smaller plutons include the Abbeville, McCormick, Winterseat, Verdery, and Kirksey plutons (Fig. 2, p. 6, and Plate 1), all of which were recognized by Overstreet and Bell (1965b) but not named. Further field mapping showing the locations and names of these plutons was conducted by: Griffin (1979) for the Abbeville pluton; Butler and Ragland (1969) for the McCormick pluton; Pirkle (1982) for the Winterseat pluton (mapped but not named); and Chalcraft et al. (1981) for the Verdery pluton.

Mapping and Sampling Techniques

The complexes can be separated into three distinct groups: (1) those composed entirely of metagabbro, (2) those composed entirely of unaltered gabbro, and (3) composite bodies of metagabbro and gabbro. Contact metamorphic aureoles mapped by Medlin (1968), Griffin (1978), Pirkle (1982), and Fronabarger and McSween (1983), as

well as crosscutting relationships demonstrated by Griffin (1978, 1979), indicate that emplacement of these mafic complexes was later than the surrounding Charlotte and Carolina Slate belt rocks.

Intense saprolitic weathering of the gabbros within these mafic complexes forms soils conducive to agriculture and detrimental to geologic sampling. Amphibolites, metagabbros and some gabbros form Mecklenburg soils, whereas most gabbros form Iredell soils. Furthermore, this weathering of gabbroic rocks has produced topographic lows in relation to the country rocks. Ultramafic units, on the other hand, form ridges or broad shallow topographic plateaus. Syenites are more resistant to erosion and form sandy soils which are often difficult to differentiate from soils derived from granitic rocks. Dioritic units are very difficult to sample due to the ease with which they weather. Metagabbros containing abundant amphibole resist saprolitic development and are relatively easy to locate and sample. Thus, an inherent sampling bias is probably present in this and previous studies of gabbroic rocks in the Charlotte belt. With the exception of diorite, fresh outcrop can usually be found in stream beds and in many roadcuts.

A regional aeromagnetic survey of South Carolina was conducted by the U.S.G.S. (1978) and includes the study area (Plate 2). All of the mafic intrusives form aeromagnetic highs relative to the surrounding country rocks, providing a means to approximate their sizes and distribution. Amphibolites also form aeromagnetic highs, but they can usually be differentiated on the basis of their shapes and the

slightly lower intensity of the anomaly. All positive aeromagnetic anomalies were field checked and mapped (Plates 1 and 2). A gravity survey of the eastern half of the study area was conducted by Chalcraft et al. (1981) and their data show a gravity anomaly over the Greenwood complex. These data were useful in mapping the extent of the complex in which very little outcrop is present.

Thus, the distributions of the mafic intrusive lithologies found in the study area have been inferred on the basis of limited outcrop, geophysics, topography, and soil distribution.

Nomenclature

Although each complex contains lithologies unique to itself, other lithologies are common to all three. Furthermore, some of the rocks are metamorphosed and others are not; some exhibit distinct cumulate textures whereas others lack such textures. A further difficulty in describing these rocks stems from the wide variety of igneous and metamorphic classification schemes available.

Metamorphic textures are described using Spry's (1969) system. Noncumulate igneous textures are described using the IUGS (Streckeisen, 1973) system, and cumulate igneous textures follow the convention proposed by Irvine (1982, Table 2). All cumulate rock names are cross referenced with the IUGS system for ease of comparison. Irvine's (1982) classification scheme lists a maximum of three cumulus minerals in order of decreasing abundance, with accessory minerals in parentheses. Thus a norite cumulate would be called a

plagioclase-orthopyroxene cumulate gabbro in which plagioclase is more abundant than orthopyroxene. The following abbreviations are used herein (for ease of description): olivine = O, plagioclase = P, orthopyroxene = oP, clinopyroxene = cP, ilmenite = I, and magnetite = M. Therefore, the norite of the previous example would be called a PoP gabbro.

Calhoun Falls Complex

Field Relations

Two distinct bodies make up the Calhoun Falls complex (Plate 3); a roughly elliptical northern body (∿3 km x ∿6 km) and a southern satellite body (∿3 km x ∿1 km) separated by a narrow zone of amphibolite. Iredell soils (Camp and Herren, 1980) are formed from rocks within the complex which are, in turn, surrounded by a ring of Mecklenburg soils. Mecklenburg soils probably represent both contact metamorphic hornfels formed during intrusion of the complex and amphibolites. The intense positive aeromagnetic anomaly (Plate 2) is continuous from the northern to the southern body suggesting that they are connected at depth. The aeromagnetic signature of the amphibolites to the northwest and south of the main body is intermediate between the felsic country rocks and Calhoun Falls rocks. At the northwest limit of the complex there is a low in this aeromagnetic signature correlative to a pelitic schist mapped by the author in this region. On this basis, the northwestern contact between the Latimer and Calhoun Falls complexes has been slightly modified from Griffin's

(1978, 1979) maps. At the western limit of the southern satellite body (Plates 1 and 3), another contact metamorphic aureole has been mapped by Griffin (1979) and includes several gabbroic dikes radiating into the country rocks. As noted earlier, this aureole and the one mapped to the north clearly demonstrate that the Calhoun Falls intrusive event postdates the regional dynamothermal (Taconic) event that Glover et al. (1983) indicate to have affected the country rocks. Glover et al. (1983) noted that the Calhoun Falls complex cuts fold structures and foliation of the country rocks. A pelitic schist that was mapped during this study on the northwestern boundary of Calhoun Falls is deflected and exhibits progressive contact metamorphism toward the complex.

Calhoun Falls Lithologies

The Calhoun Falls complex has extensive mesoscopic layering seen at the map scale, in outcrop, and in hand sample. The complex is comprised of (1) metagabbro, (2) metasomatised ultramafics, (3) pyroxenite, (4) PO gabbro (troctolite), and (5) PcPO gabbro (gabbronorite). The metagabbro occurs in two regions within this complex (Plate 3), first in the entire western portion, and second as a narrow north-south trending band in the central portion of the northern body. Metagabbro is easily distinguished from other lithologies by its green and white speckled pattern in hand-sample produced by amphibolite and plagioclase. Sampling control in the extreme western limit of the complex is hindered by the town of

Calhoun Falls, after which the complex was named. This town covers much of the western portion of the complex and the existence of metagabbro is inferred at that locality on the basis of other outcrop further east and the character of the soil in the town. Good exposures of metagabbro can be found, however, further east where housing development is less intense. Metamorphosed ultramafics are located in the central part of the northern body and in the entire southern body. For the most part, they are highly weathered, making it difficult to find fresh samples. They form boulder-strewn ridges composed of dark green, often talcose rocks. Mesoscopic layering within the ultramafic units can be seen in saprolitized outcrop (Fig. 3). Only one fortuitous sample (CF-14) of pyroxenite was found in the southern satellite body. The relationship of the pyroxenite and meta-ultramafic rocks is discussed elsewhere in this study. The PO and PcPO gabbros are indistinguishable in the field, forming dark spherical boulders in cultivated fields and fresh outcrop in some stream beds. The PO gabbro is restricted to a narrow zone (Plate 3). The PcPO gabbro is found at the extreme eastern limit of the complex both in the northern and southern bodies. Griffin (1978) mapped an undifferentiated gabbro unit on the western side of the southern satellite, but this author considers the gabbro at this locality to consist of radiating dikes, emanating from the pluton. Although the PcPO gabbro is mapped on the eastern side also, it may be one of these dike systems. It is very fine-grained, suggesting the presence of a chill zone or a dike.



Figure 3. Mesoscopic layering in saprolitized serpentinites within the Calhoun Falls complex. The dark band near the hammer is interpreted as an ultramafic layer and the light band is interpreted as a gabbroic layer. Strike is N-S and dip is 45°W.

Mt. Carmel Complex

Field Relations

The areal extent of the Mt. Carmel complex, as mapped in this study, remains substantially unchanged from Medlin's (1968) work. The body is roughly circular and about 6.5 km in diameter (Plate 4). Glover et al. (1983) discussed the metamorphic aureole around Mt. Carmel as mapped by Medlin (1968) and the country rock structures that are deflected around it as mapped by Griffin (1978). Coupled with the K-Ar (biotite) ages (358 my) reported by Medlin (1968), they speculated that Mt. Carmel is Early Devonian/Silurian or older and that the country rock metamorphic fabric could be as late as Taconic.

A positive aeromagnetic signature (Plate 2) clearly defines the limits of the complex. To the north of the complex, the aeromagnetic intensity is depressed into an east-west trending linear anomaly relative to both the complex to the south and the Carolina Slate belt rocks to the north. Griffin (1978) mapped an interbedded amphibolite/granite gneiss unit corresponding to this negative anomaly. This author verified the mapping by Griffin in this area and noted that it was primarily amphibolite. One would expect the felsic to intermediate metavolcanics and metasediments to the north to have a lower magnetic signature than the amphibolite between them and the complex. One possible explanation for this apparent contradiction is that Carolina Slate belt rocks underly the Charlotte belt rocks in the vicinity of the Mt. Carmel complex. This interpretation contradicts the accepted

relative position of the two units. Structural data by Griffin (1978) indicate that the beds form upright or plunging folds in the vicinity of Mt. Carmel. Another interpretation is that the Carolina slate belt rocks are thinner than suggested by Griffin (1978, plate 5) and are underlain by rocks more mafic than those found in the vicinity of Mt. Carmel.

Mt. Carmel Lithologies

Medlin (1968) mapped three units within the Mt. Carmel complex: (1) gabbro, (2) syenite, and (3) diorite. Although the distribution of the three units (Plate 4) remains essentially unchanged from Medlin's work, the naming of these units has been changed to conform to current nomenclature. Medlin's gabbro has been renamed metagabbro, diorite has been named olivine gabbro, and the syenite remains unchanged. This reassignment of terminology is not arbitrary. Medlin (1968, p. 105) described his "gabbro" in the following manner.

> The Mt. Carmel gabbro is a gray to dark-green, medium- to coarse-grained rock composed of plagioclase, brown pyroxene, olivine, brown and green amphibole, epidote, chlorite, pyrite and opaque minerals. The variation in color and mineralogy is due to the degree of alteration: the less altered rocks are essentially light to dark-gray and are composed of olivine, plagioclase, pyroxene, brown amphibole and the opaque minerals; the more altered rocks are dark-green and are composed of green amphibole, plagioclase, epidote, chlorite and the opaque minerals.

However in his appendix C (Medlin, 1968, pp. 266-328), only two of the 17 samples (126-8 and 126-25) collected in the gabbro unit do not contain modal green amphibole. On this basis, these samples represent what Hermes (1968) called metagabbro in the Mecklenburg

complex. The two other samples appear to represent isolated pockets of olivine gabbro and are so indicated on Plate 4 of this study.

Metagabbro occurs principally in the northern half of the complex but extends to the south also. Gabbros and syenites are restricted to the southern half of the complex with the exception of a small isolated pocket of gabbro near the northern extremity. All units form lobate structures within the body.

Greenwood Complex

Field Relations

Of the three major complexes in the study area, Greenwood exhibits the poorest exposure and the most complex areal geometry, making it the most difficult to study. Overstreet and Bell (1965a, 1965b) mapped the extent of the Greenwood complex on the basis of soils, and Chalcraft et al. (1978) subsequently modified that work in a sketch map in which they included details of the country rocks near the complex. The areal distribution of gabbros in the Greenwood complex (Plate 5) has been extensively revised on the basis of aeromagnetic data (U.S.G.S., 1978), soil data (Herren, 1980; and Camp and Herren, 1980), topography, partial simple Bouger gravity data (Chalcraft et al., 1981), and additional field mapping. The Greenwood complex consists of three separate intrusions that may be connected at depth.

The southern body is by far the largest, about 8 km in the east-west direction and about 3 km in the north-south direction. It

forms well defined magnetic and gravity highs relative to the country rocks. A sharp break in the topographic elevation is present in the southern body and coincident with the occurrence of extensive Iredell soils surrounded by Mecklenburg soils.

The character of the two northern bodies is entirely different, however. The northwestern body, located between Greenwood and Ninety-Six, is about 3 km by 2.5 km in size, and the northeastern body, located just south of Ninety-Six, is roughly 2.5 km in diameter. The aeromagnetic anomalies (Fig. 4) coincident with these two bodies are less intense as compared with the southern body; a local high of 53,980 gammas for the northwestern body and 54,232 gammas for the northeastern body as compared to 55,151 gammas for the southern body. The gradient from country rock (about 53,100 gammas) to the peak along the flanks of the three bodies is the same, however. The simple Bouger anomaly map partially covering the complex by Chalcraft et al. (1981) shows a similar trend. A local gravity high of 24 mgals is present in the southern body. This gravity high is stretched towards the two northern bodies forming a broad ramp in the gravity contours without local highs for the two northern bodies. Iredell soils are practically absent in the northern bodies and abundant in the southern body. Mecklenburg soils on the other hand are extensive in the northern region. Furthermore, there is a conspicuous absence of any clearcut topographic breaks in the north. All of the above data suggest that the Greenwood complex consists, in fact, of three separate plutonic bodies.

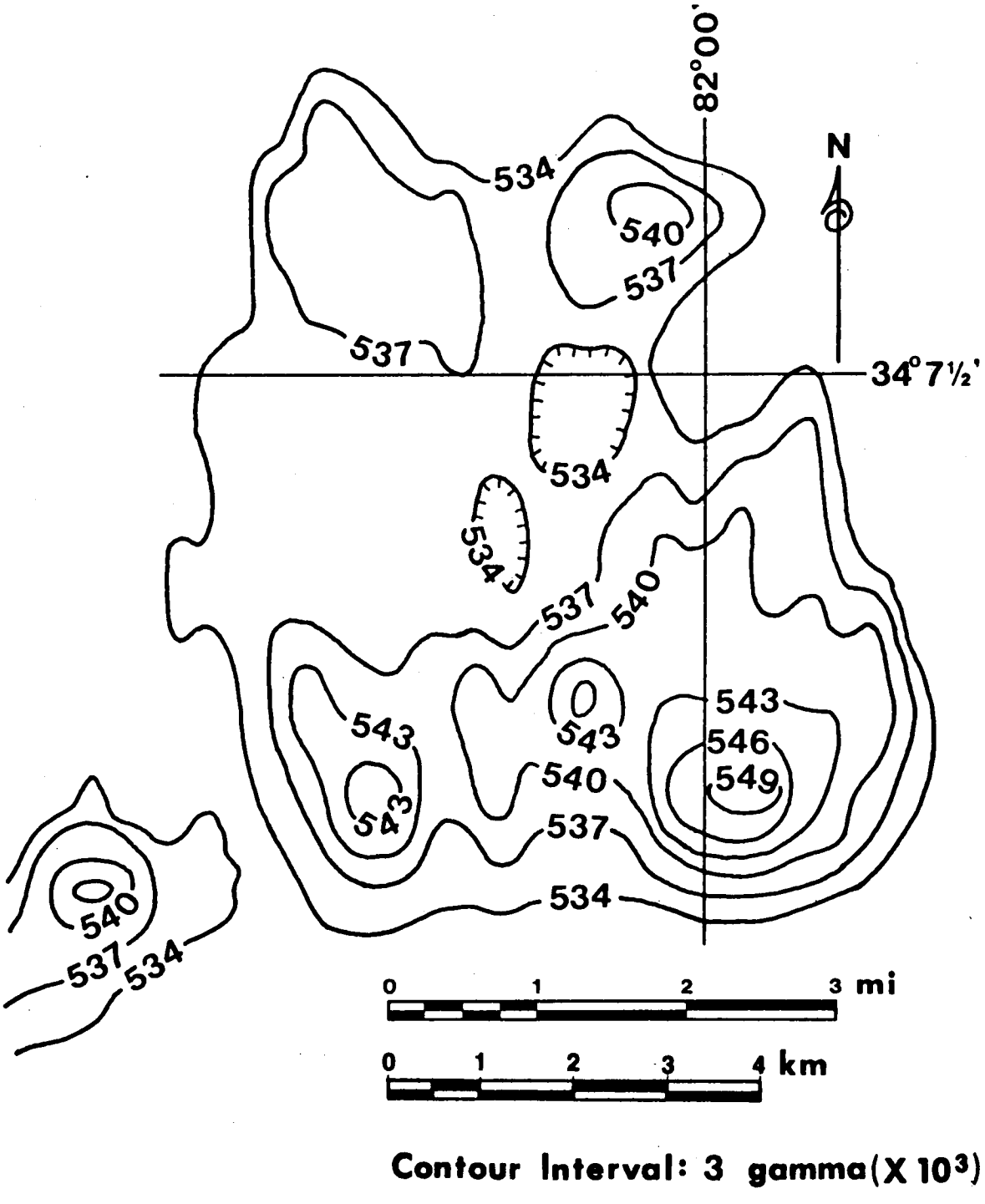

Figure 4. Aeromagnetic map of the Greenwood complex, showing the depression in the magnetic intensity between the northern and southern plutons. The magnetic high to the southwest is an amphibolite. (After U.S.G.S., 1978.)

The more intense magnetic and gravity anomalies in the southern body coupled with the well developed Iredell soils suggest that this pluton is well exposed (in a relative sense) and that the two northern bodies appear to have been barely unroofed by erosion. As will be demonstrated in subsequent chapters, the rocks of Greenwood complex are often fine-grained which is probably conducive to more rapid weathering, thus limiting exposure. In the extreme eastern part of Kirksey Quadrangle and in Good Hope Quadrangle (Plate 5), fairly good exposures of gabbroic rock can be found in some stream beds and along unpaved county roads. In the central part of Kirksey Quadrangle, however, outcrop again becomes scarce due to extensive agricultural activity and the expansion of Ninety-Six into this area.

In an effort to outline the complex and understand the relationship of the complex to the country rocks, the rocks immediately surrounding the body were remapped (Plate 5). Three principal rock types are in contact with Greenwood: (1) Carolina Slate belt metavolcanics and metasediments, (2) granite gneiss, (3) Charlotte belt amphibolites, biotite gneiss, interbedded with granite gneiss. The gabbro cross-cuts the metasediments and metavolcanics and deforms some of the granite gneisses. The southern limit of the complex is bounded by the main body of the Carolina Slate belt; however, two isolated interbedded rhyolite/pelitic units were mapped within the Charlotte belt. These units occur both on the western and northeastern sides of the complex and are metamorphosed to low grade (probably greenschist facies) away from the complex. No contacts

between these or any other country rocks were observed, thus no contact metamorphic aureoles were mapped. Granite gneiss occurs primarily in the central region separating the northern and southern bodies, although several other bodies of granite gneiss were also mapped (Plate 5). The granite gneiss is highly contorted in many areas near the contact with the gabbro. The Charlotte belt rocks in contact with the complex were mapped following the convention of Griffin (1978, 1979), where the most abundant rock type within a discernible lithologic package is listed first followed by the lesser abundant rocks. They occur on all sides of the complex, even to the southeast where a deep embayment into the complex is filled by Charlotte belt rocks. Local schistosity and foliation trends about N45°E in all metavolcanics and metasediments.

Greenwood Complex Lithologies

Due to the poor exposure in the Greenwood complex, the distribution of the various rock types cannot be discerned. Three rock types have been noted, however: (1) fine- to medium-grained diorite, (2) metagabbro, and (3) POcP gabbro (gabbronorite). Although no contacts between these three rock types have been shown on Plate 5, the locations of the samples with separate symbols for each rock type are indicated.

The diorites occur almost exclusively at or near the contact with country rocks, suggesting that they represent chill zones within the complex. Chalcraft et al. (1978) mapped several diorites to the west and north of the northern bodies, but most appear to be fine-grained

amphibolite of the Charlotte belt. The abundant Mecklenburg soils present in the northern bodies may form from some of the diorites mapped by Chalcraft and his associates.

Metagabbro is rare when compared to the other intrusives in the southern Appalachians, but when present it appears to crop out along the margins of the complex as is characteristic of many of the mafic intrusives.

All of the cumulate gabbros were found in the large southern body. This observation, coupled with the geophysical and soils data further support the concept that the southern body has been more deeply eroded than the two northern bodies. Cumulate rocks would not be expected at the extreme margins of a convecting magma chamber where rapid cooling occurs.

Other Plutons

Although the main thrust of this study is directed toward the three major complexes in the study area, several samples were also collected from many of the smaller plutons. As a complete petrochemical study of the three large complexes and five minor plutons is outside of the scope of the present work, preliminary mapping and petrographic results are presented herein for the sake of completeness.

Abbeville Pluton

Located almost entirely within the town of Abbeville, in the Abbeville East and Abbeville West 7.5 minute quadrangles, this pluton

consists of metagabbro with a small appendage of syenite and olivine gabbro to the southwest (Fig. 5). Excellent exposure of metagabbro occurs along State highway 71 that passes through the main part of town. Two small blocks of amphibolite have been mapped within the body (Fig. 5), consisting of hornfels/amphibolite country rocks. This author was unable to sample the syenite/gabbro pendant; however, Griffin (1979) describes it as being similar to the rocks found in Mt. Carmel.

Verdery Pluton

The Verdery pluton, originally mapped by Overstreet and Bell (1965a, 1965b) on the basis of soils, is located within the Verdery 7.5 minute quadrangle just south of the Ceder Springs intersection and east of where McCormick, Abbeville, and Greenwood counties meet at a triple point (Fig. 6). Reedy Branch flows along the southwest margin of the pluton.

Reconnaissance mapping of this pluton has shown it to be smaller than originally mapped by Overstreet and Bell (1965b). A north-south trending amphibolite which is cut by the pluton appears to be responsible for the rather large aeromagnetic anomaly in the area. Soils and topography support this conclusion. Mecklenburg and Iredell soils (Camp and Herren, 1980; and Herren, 1980) occur only in the small isolated topographic low where the pluton is mapped. A traverse over the body of the pluton proved fruitless however, and the nature of the gabbro remains unknown.

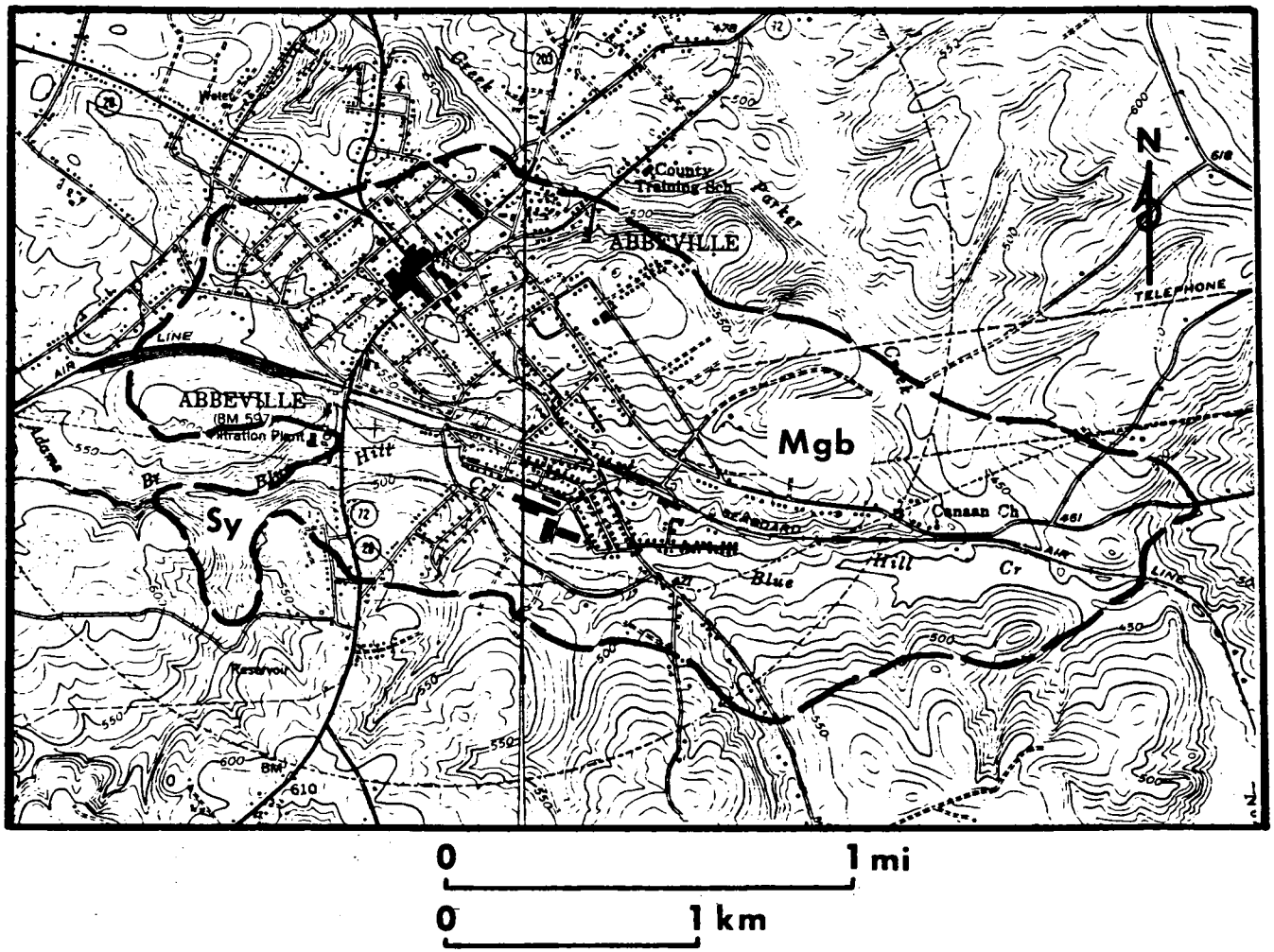

Figure 5. Sketch map of the Abbeville pluton in the Abbeville West and Abbeville East 7.5 minute quadrangles. Contacts taken from Griffin, 1979. Metagabbro (Mgb) and syenite (Sy) make up the body.

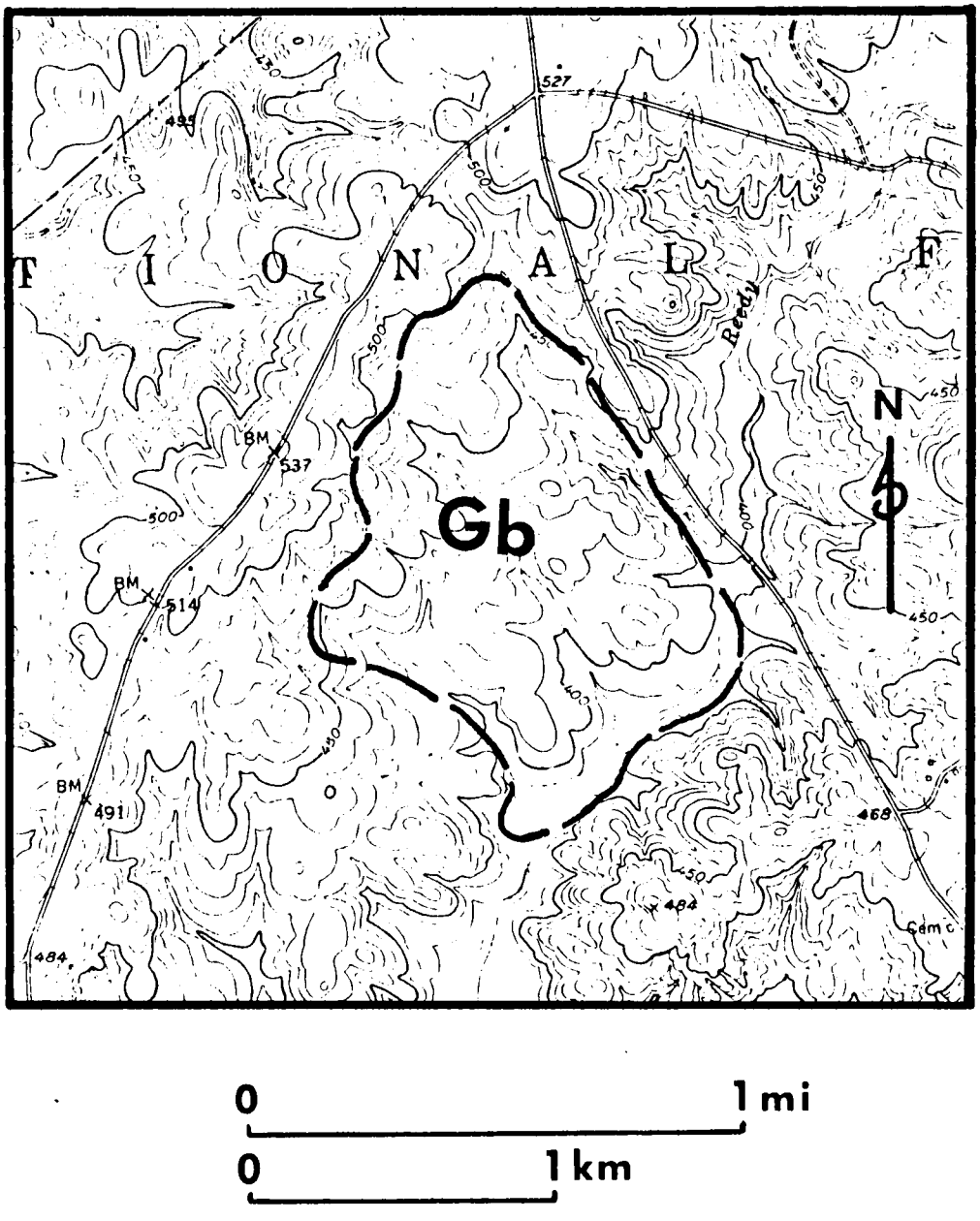

Figure 6. Sketch map of the Verdery pluton located in the Verdery 7.5 minute quadrangle. The pluton consists of undivided cumulate gabbro (Gb).

McCormick Pluton

The McCormick pluton, located north of the town of McCormick and in the town of Troy in Greenwood and McCormick counties (Fig. 7) forms well developed Iredell and Mecklenburg soils. The complex is composed of two separate bodies; a larger lobate body to the east and a small circular plug to the west in Troy. These two bodies are separated by amphibolites and hornfels, trending approximately north-northwest along the county line. Aeromagnetic data (Plate 2) suggest that these two bodies are connected at depth.

Three rock types are found in the McCormick pluton; a PcPO cumulate gabbro with postcumulus hornblende, clinopyroxene, opaques, and biotite (gabbronorite), a PO cumulate gabbro (troctolite) with rare postcumulus opaques and hornblende, and a metagabbro. The troctolites were found at the extreme northern margin of the western plug (Fig. 7) and exhibit anastomosing microfractures propagating through the olivine grains into the plagioclase.

Winterseat Pluton

The Winterseat pluton is located at the intersection of Hard Labor Creek and the Greenwood-McCormick county line (Fig. 8), and forms Iredell and Mecklenburg soils. It consists of PcPO cumulate gabbro (gabbronorite) with postcumulus hornblende, ortho- and clinopyroxene, opaques, and biotite. A well-developed hornfels aureole can be seen in a roadcut just west of the pluton. Pirkle (1982) mapped such a contact metamorphic aureole surrounding the entire pluton.

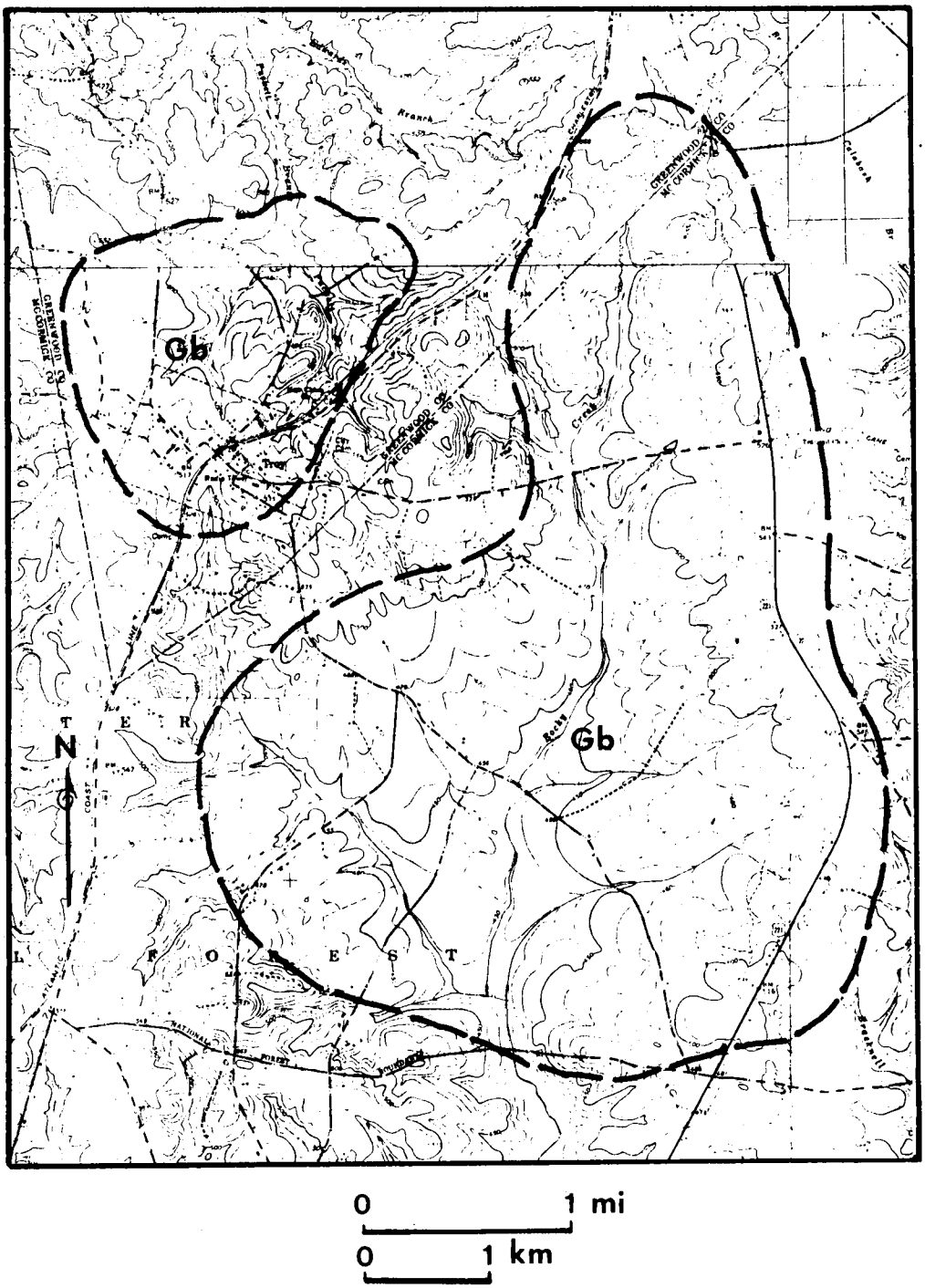

Figure 7. Sketch map of the McCormick pluton located in the northeastern corner of the McCormick 7.5 minute quadrangle. The pluton consists of undivided cumulate gabbro (Gb).

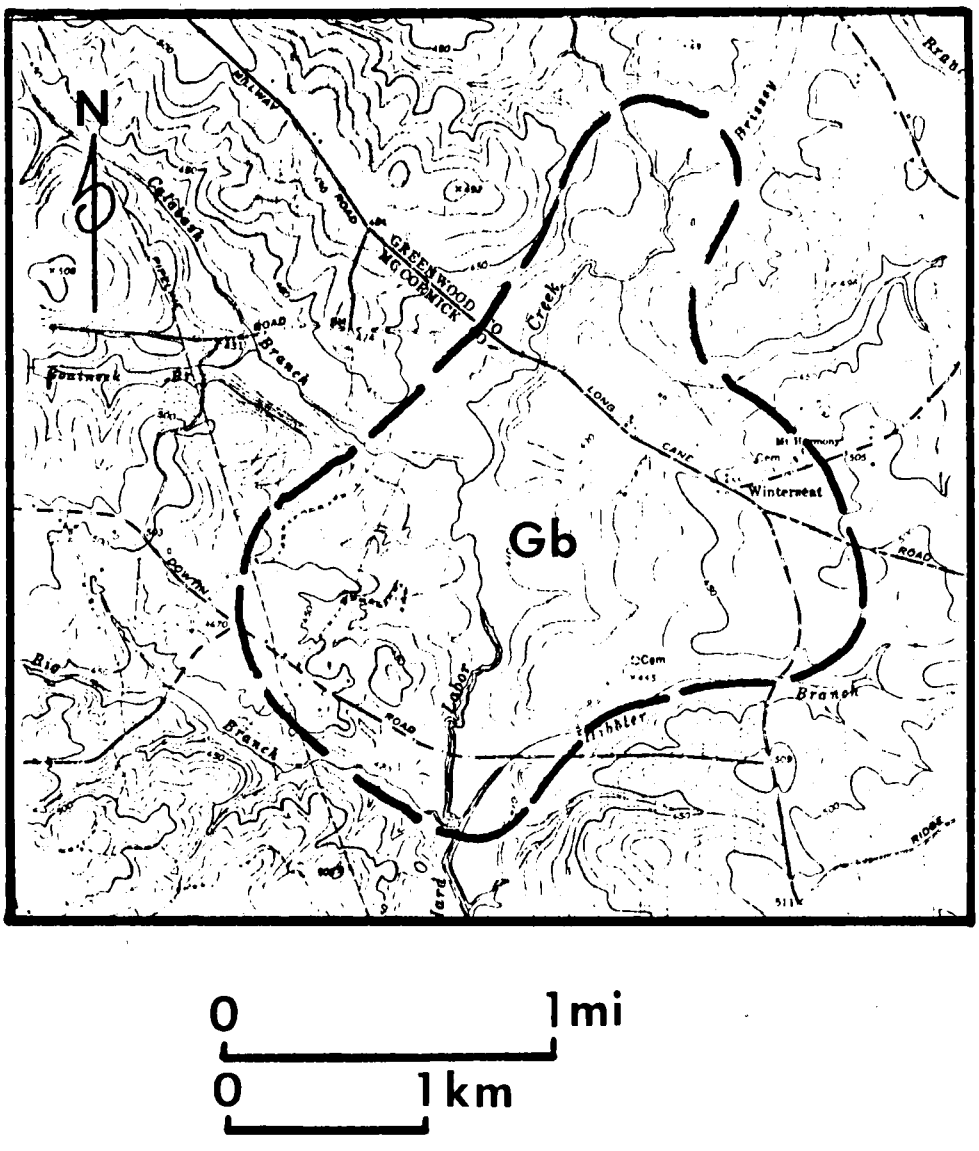

Figure 8. Sketch map of the Winterseat pluton located in the Winterseat 7.5 minute quadrangle. The pluton consists of undivided cumulate gabbro (Gb).

CHAPTER III

PETROGRAPHY AND MINERALOGY

Introduction

As noted in the previous section on field relations of the three complexes, despite their close physical proximity, each intrusive is unique in lithologic character. This uniqueness is also evident in thin-sections. Some similarities are evident however. Metagabbro occurs in each of the complexes and does not exhibit significant textural or mineralogical variation from one intrusive to the next. For this reason, metagabbro is discussed separately, but the reader should recall that it occurs in all of the complexes in the study area.

Modal analyses of representative rocks are presented in Tables A1 through A3 in the appendix. An estimation of error for these data is less than 10% using the method of Van der Plas and Tobi (1965). Figure 9 presents these data using the system recommended by the I.U.G.S. (Streckeisen, 1973).

An automated MAC 400S electron microprobe, with appropriate natural and synthetic standards, was used to obtain mineral compositions (Tables A4 through A7 in the appendix, and Figure 10). Correction procedures of Bence and Albee (1968) and the data of Albee and Ray (1970) were utilized to reduce the data. Operating conditions of the microprobe were 15 kv, 0.03-0.05 μa beam current and a beam diameter of 5-15 μm, depending on the mineral to be analyzed. Those minerals containing significant sodium (e.g., plagioclase and

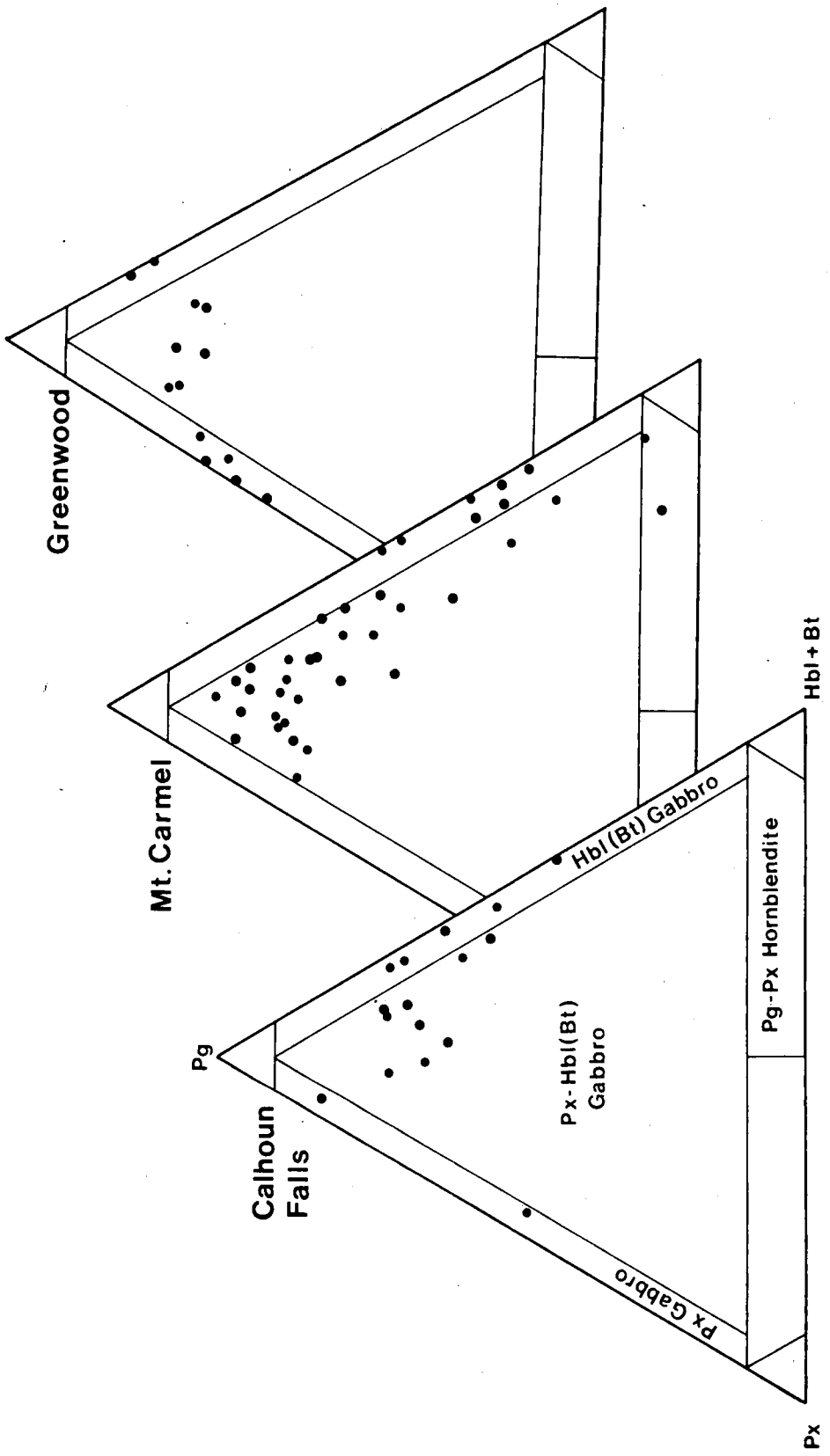

Figure 9. Petrologic classification of the rocks (Streckeisen, 1973) in the Calhoun Falls, Mt. Carmel, and Greenwood complexes.

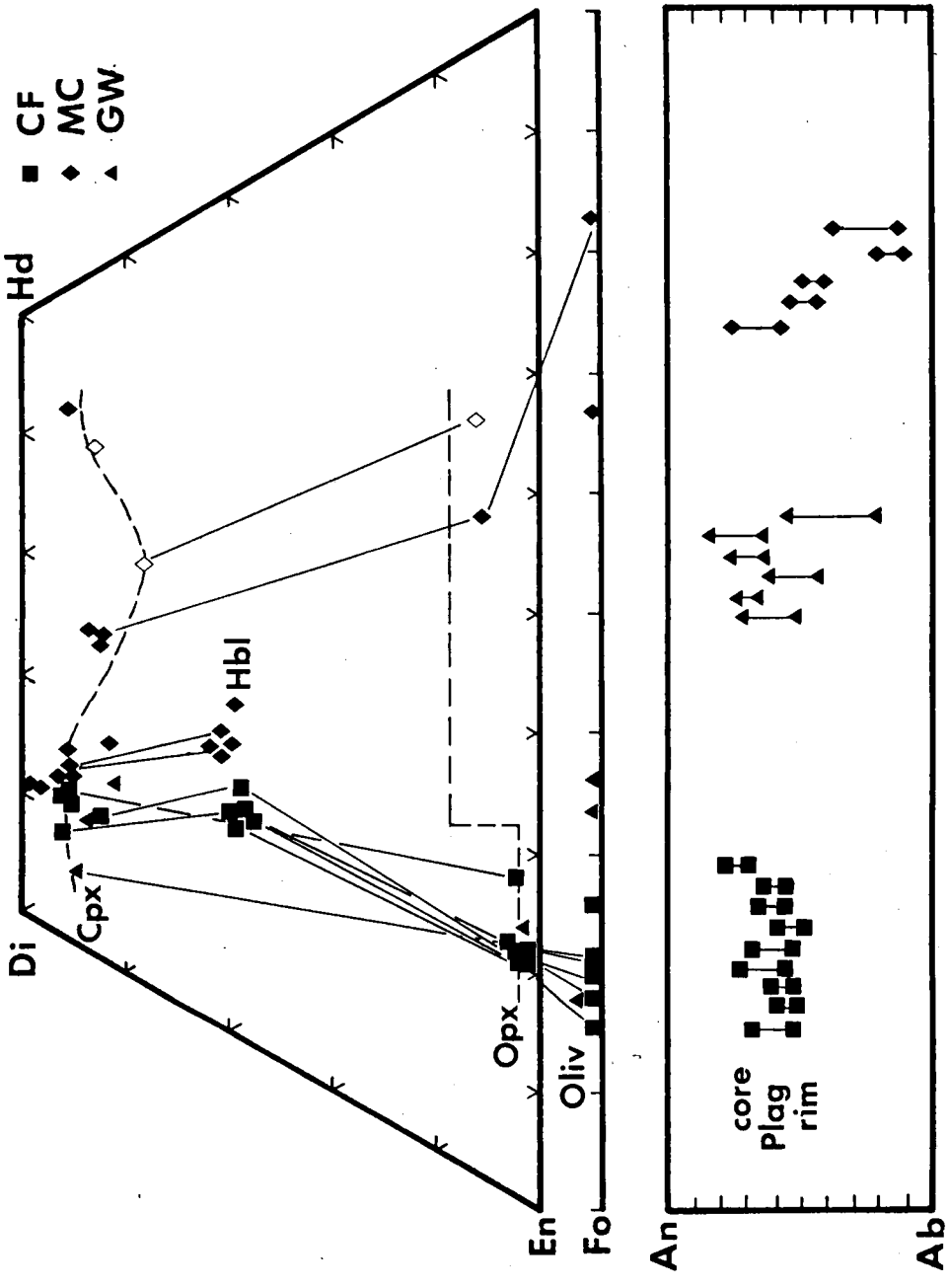

Figure 10. Compositions (mole %) of silicates in the Calhoun Falls (CF), Mt. Carmel (MC), and Greenwood (GW) complexes. Coexisting ferromagnesian minerals are joined by tielines. Coexisting core and rim analyses of plagioclase grains are joined by tie lines. The three open diamonds represent analyses reported in Medlin (1968) for the Mt. Carmel complex. The dashed lines in the quadralateral are trends for Stillwater pyroxenes.

amphiboles) were analyzed at 0.03-0.04 μa with a defocused beam to avoid volatilization of the alkalis. Amphibole analyses were stochiometrically balanced using Leake's (1978) method.

Metagabbro

Hermes (1968, p. 291) distinguished gabbros and metagabbros on the basis of whether olivine was present or absent. This basis of classification is certainly acceptable when unaltered gabbros contain modal olivine, as is the case with the Mecklenburg complex that Hermes studied, but breaks down when studying unaltered plutonic rocks that are olivine-free, as is the case in some units in the present study. For this reason, unaltered gabbros are herein considered to be those that do not contain actinolite, and metagabbros are those that do contain this mineral.

Hermes (1968) subdivided metagabbros into three categories based on the extent of recrystallization present. Type 1 metagabbros retain igneous textures and contain many relict minerals that are only partially recrystallized. Olivine is conspicuously absent, containing pyroxene or amphibole, while plagioclase is typically saussuritized. Type 2 metagabbros have been recrystallized to form unoriented granoblastic textures. Plagioclase is more sodic than the plagioclase in the protolith and is completely recrystallized. Olivine is absent and orthopyroxene is uncommon; clinopyroxene and green amphibole make up the bulk of the mafic minerals. Type 3 metagabbros exhibit distinct banding due to the linear orientation of plagioclase and

amphibole. As Hermes points out, all gradations may be found between these three types.

All three types of metagabbro can be found in the study area, but their distribution is apparently random, and the contacts with other units are never seen but appear to be fairly sharp over the distance of a few meters. Essential minerals include plagioclase and green amphibole with accessory recrystallized ilmenite, hematite, magnetite, and relict orthopyroxene, clinopyroxene, brown hornblende, and biotite. Apatite and epidote are also present. All relict ferromagnesian minerals are without exception surrounded by intergrowths of metamorphic green amphibole and opaque minerals. The oxides commonly form coloform intergrowths.

Calhoun Falls Complex

The Calhoun Falls complex is composed of metagabbro, metasomatized ultramafics, pyroxenite, PO cumulate gabbro (troctolite), and PcPO cumulate gabbro (gabbronorite) (Plate 3). These units trend north-south throughout the complex and show mesoscopic layering in handsample. The Calhoun Falls complex is dominated by cumulus textures and very limited iron-enrichment within the constituent minerals.

Ultramafic Rocks

The ultramafic rocks can be divided into three groups on the basis of mineralogy and texture: bastites, bastitic serpentinites, and orthopyroxenites (Fig. 11). Bastites are defined for the purpose of

Figure 11. Photomicrographs of samples from the Calhoun Falls complex.

a. CF-14. Cumulus orthopyroxenite containing cumulus orthopyroxene, olivine, and clinopyroxene with postcumulus plagioclase and pargasitic hornblende. Photo taken under cross-polarized transmitted light.
b. CF-4. Bastite from the ultramafic zone. Talc pseudomorphic after cumulus pyroxene. Photo taken under cross-polarized transmitted light.
c. CF-27. Serpentinite from the ultramafic zone. Serpentine pseudomorphic after cumulus olivine with opaque minerals in the intercumulus region. Photo taken under cross-polarized transmitted light.
d. CF-50. Cumulus plagioclase, olivine, clinopyroxene, and opaques with postcumulus pargasitic hornblende and opaques in the PcPO cumulate gabbro (gabbronorite). Photo taken under transmitted light with uncrossed nicols.
e. CF-32. Cumulus plagioclase, olivine, and opaques with postcumulus hornblende and opaques in the PO cumulate gabbro (troctolite). Orthopyroxene rim surrounds the olivine. Photo taken under cross-polarized transmitted light.

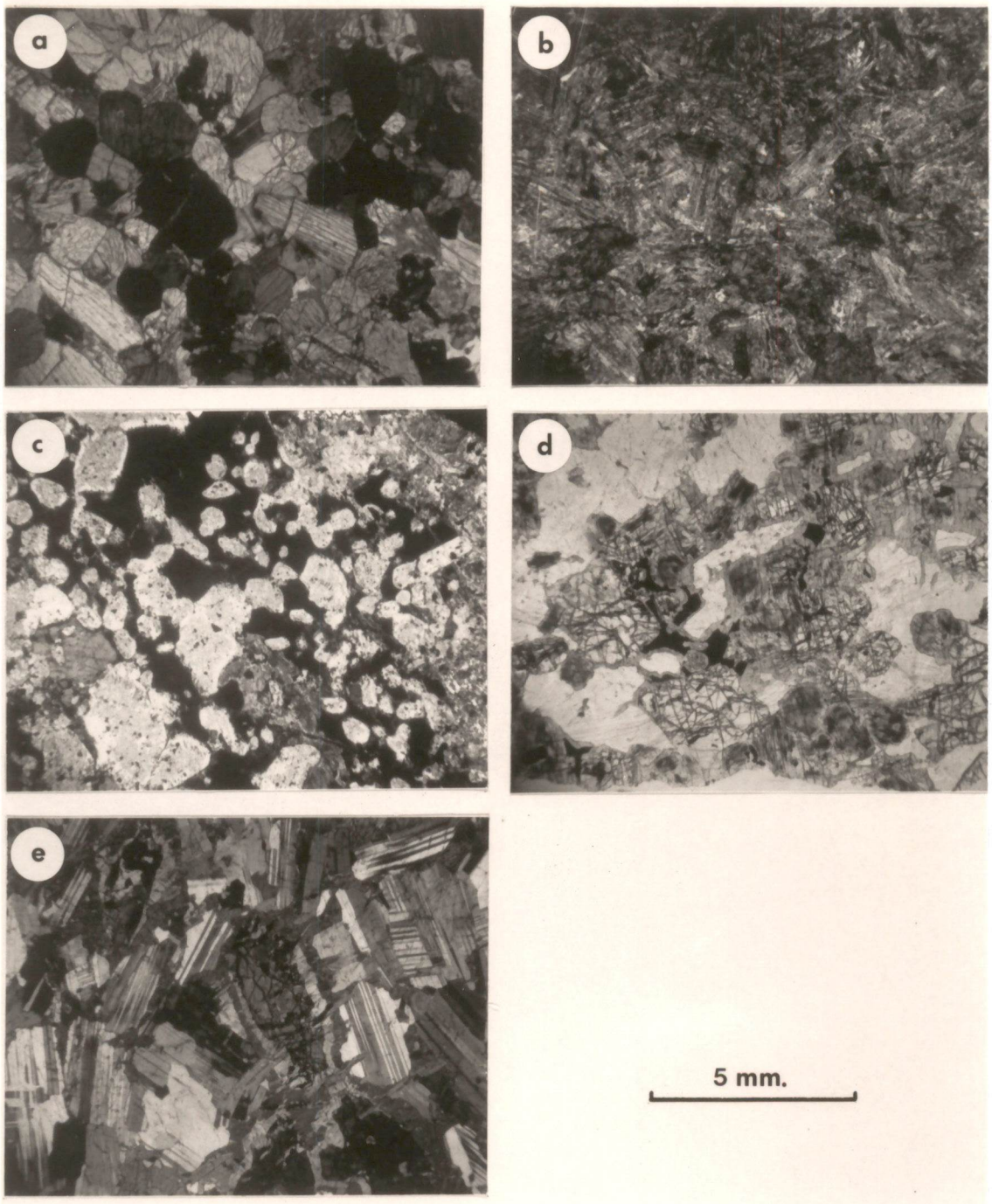

Figure 11.

this study as being rocks formed from the alteration of orthopyroxenites producing a characteristic olive-green, blackish-green, or brownish serpentinite, occurring as foliated masses often characterized by schiller luster (A.G.I., 1974, and Wicks and Whittaker, 1977). Serpentinites are defined as rocks formed from the alteration of dunites and peridotites, producing serpentine family minerals such as lizardite, chrysotile, or antigorite. Neither the bastites nor the serpentinites exhibit any signs of metamorphic fabric as is evident in many of the structurally more competent metagabbros. For this reason they presumably were altered after the last deformation episode that affected the study area, which is considered to be Taconic by Glover et al. (1983). Alteration of these rocks occurred either through autometasomatism or through hydrothermal alteration by fluids originating from the country rocks.

The bastites are represented by samples CF-4, CF-8, CF-11, and CF-18 (Appendix A, Table A1). They consist primarily of serpentine, which is pseudomorphic after orthopyroxene, with minor magnetite, brucite(?), talc, and hematite (Fig. 11b). The hematite appears to be an oxidation product after magnetite due to saprolitization of some of the samples. Very rare relict grains of brown hornblende can be found in a few samples altering to magnetite plus brucite(?). The bastites retain the same textural features as the pyroxenite (compare Figs. 11a and 11b). All of the pseudomorphs formed from pyroxene exhibit subparallel lamination, and are euhedral, prismatic crystals with magnetite at the serpentine grain boundaries.

Serpentinites are represented by samples CF-2, CF-27, CF-36, CF-45, and CF-46. Their mineralogy is more complex than the bastites, being composed of serpentine, magnetite, brucite(?), with minor chlorite, talc, and relict clinopyroxene, brown hornblende, and rare orthopyroxene. Their textures are reminiscent of the mafic clots seen in many of the gabbronorites (compare Figs. 11c and 11d). The serpentine is pseudomorphic after cumulus olivine and pyroxene with burcite(?) and magnetite forming from postcumulus brown hornblende and opaques. Thus, these rocks are interpreted as having formed through the alteration of peridotite layers in the ultramafic zone.

Wicks and Whittaker (1977) and Wicks et al. (1977) related serpentine textures to eight distinguishable regimes in which they could have formed. These regimes are functions of temperature gradients, shearing stress, and nucleation of antigorite. On the basis of the presence of lizardite plus brucite (Fig. 11c), these rocks were probably altered at low temperatures, thus forming what Wicks and Whittaker (1977) call type 3 serpentinites where there is an absence of shearing.

Only one sample of unaltered orthopyroxenite (CF-14) was collected. It was found in a bastite zone in the southern satellite body (Plate 3) and is undoubtedly part of the same. The orthopyroxenite consists of cumulus orthopyroxene and postcumulus plagioclase. Accessory clinopyroxene, brown hornblende and opaque minerals also occur (Appendix Table A1). All cumulus minerals are euhedral and fine-grained ($\sim$1 mm), and the postcumulus plagioclase is

anhedral and interstitial (Fig. 11a). Poorly developed subparallel lamination of the pyroxene is present in parts of this sample, but other places exhibit no lamination.

The pyroxene composition of the orthopyroxenite is shown in Appendix Table A6 and the plagioclase compositions in Appendix Table A4. The orthopyroxene composition is not significantly more magnesian than those found in the gabbros, indicating that very little iron-enrichment has occurred in this phase. Plagioclase is not zoned and has a composition of An60.

Gabbros

The troctolitic zone is characterized by cumulus plagioclase and olivine with postcumulus brown hornblende, biotite, orthopyroxene, and accessory ilmenite, apatite, magnetite, and spinel. Normally zoned plagioclase is subhedral while olivine is typically euhedral and forms a loose framework that is surrounded by postcumulus material. Minor biotite and optically continuous hornblende make up the bulk of the postcumulus volume and commonly subpoikilitically enclose the cumulus crystals (Fig. 11e).

The modal amounts of minerals in the gabbronorites vary from one outcrop to another, but consist of cumulus olivine, plagioclase, and clinopyroxene, or cumulus ortho- and clinopyroxene, and plagioclase. Postcumulus minerals include hornblende, orthopyroxene and accessory ilmenite, magnetite, spinel, and biotite (Fig. 11d). Olivine and pyroxene are not zoned, but plagioclase shows normal zonation and is anhedral to subhedral. Clinopyroxene exhibits ilmenite exsolution

along {001} planes. The mafic minerals often form clots which are enclosed by postcumulus brown hornblende. The oxides are often associated with olivine and form clots surrounded by cumulus plagioclase. At the extreme eastern margin of the southern body a very fine grained gabbronorite zone was mapped and may be a chill margin of the parental magma that formed the PCO cumulate gabbro (Plate 3).

Plagioclase dominates the gabbros (Appendix Table A1), and shows subparallel lineation. The composition of plagioclase ranges from An75 in the cores to AN54 in the rims but the composition of individual grains is more limited (Appendix Table A4). Plagioclase is medium to coarse grained, and is subhedral. This layering is not necessarily considered to have formed through the process of gravity settling, but could have been developed through convective flow processes.

Olivine (Fo84-77) commonly exhibits subsolidus reaction texture with plagioclase. Olivine is often resorbed, forming a halo of enstatite (En80-72) around the olivine. The enstatite is, in turn, often surrounded by hornblende plus biotite (Fig. 11e). A second reaction commonly observed is symplectic orthopyroxene plus spinel forming from olivine and plagioclase.

Poikilitic clinopyroxene compositions are shown in Figure 10, p. 44, and in Appendix Table A6. It often forms oikocrysts surrounding the plagioclase and sometimes, olivine. This augitic pyroxene shows very little iron enrichment contrary to similar pyroxenes in other layered intrusions (e.g., Irvine, 1980).

Large brown hornblende is commonly found in association with biotite, occurs as reaction rims around the pyroxene and olivine. The hornblende compositions are bastitic according to the classification of Leake (1978). These two minerals form intimate intergrowths and probably formed from late magmatic liquid high in water. The rimming effect seems to indicate that these minerals are formed from intercumulus liquid, but they could also have formed from some type of subsolidus reaction as suggested by Otten (1983) who described similar textures in Swedish gabbros.

Opaque minerals include magnetite, ilmenite, and very minor pyrite and pyrrhotite. They are most commonly found in the postcumulus material suggesting that they formed late in the crystallization history of the gabbros. Other oxides, however, are found as exsolution material from olivine and hornblende.

Mt. Carmel Complex

Metagabbro, olivine-biotite gabbronorite, and syenite make up the lithologies of the Mt. Carmel complex (Plate 4). As Calhoun Falls was characterized by layering and cumulate textures, Mt. Carmel is characterized by a conspicuous absence of cumulus textures (Fig. 12) common in plutons in the southern Appalachians and by lobate outcrop patterns. Some cumulate textures are present in the rocks of Mt. Carmel, but they are restricted to the most primitive metagabbros containing no plagioclase. These cumulates appear to have formed from olivine + pyroxene that were subsequently metamorphosed. As

Figure 12. Photomicrographs of samples from the Mt. Carmel complex in cross-polarized transmitted light.

a. MC-35. Hypidiomorphic granular texture in syenite, with plagioclase, potassium feldspar, perthite, clinopyroxene, and oxides. Seriate intergranular textures along the feldspar grain boundaries are visible.
b. MC-24. Hypidiomorphic granular texture in the olivine-biotite gabbronorite with plagioclase, olivine, clinopyroxene, biotite, pargasitic hornblende, and opaques.

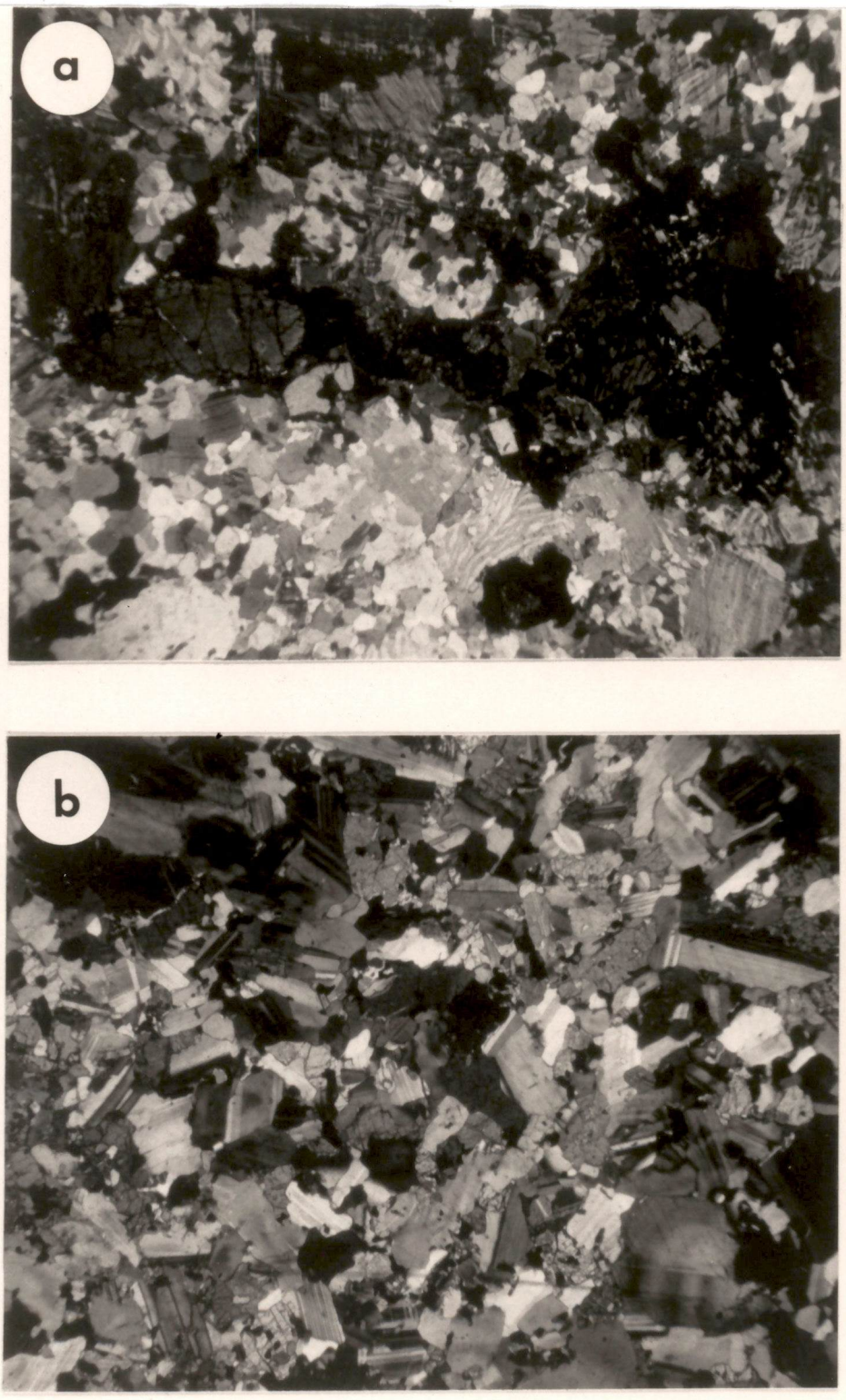

Figure 12.

would be expected from an intrusive that evolved in situ from a tholeiitic gabbro to a syenite, iron-enrichment of mafic minerals and sodium-enrichment of plagioclase are more pronounced in this intrusive than in the others.

Olivine-Biotite Gabbronorite

Essential minerals include plagioclase, clinopyroxene, olivine, biotite, and brown hornblende. Accessory minerals are magnetite, ilmenite, and minor orthopyroxene and zircon (Fig. 12b). In thin-section, the rock is hypidiomorphic granular with euhedral olivine and biotite, the other species exhibiting subhedral to anhedral morphologies. This lithology is generally equigranular, but very rare sub-poikilitic phenocrysts of clinopyroxene can be found enclosing olivine. The ferromagnesian minerals sometimes form glomerophyres. Occasional reaction rims of orthopyroxene and hornblende form at the expense of olivine. Plagioclases rarely show subparallel lineation, rather, random orientations are common. Biotite makes up to 10 modal percent of the rocks suggesting higher water fugacities during crystallization than the plutons with less modal biotite. When present, olivine occurs as small euhedral crystals dispersed throughout the rock. The clino-pyroxene is commonly twinned in the gabbro.

Syenite

The Mt. Carmel syenites (Fig. 12a) are usually porphyritic with phenocrysts of pyroxene ranging in size up to 5 mm in cross section, and a matrix grain size of about 0.5 mm in cross section. Locally,

equigranular varieties exist with grain sizes tending to the smaller extreme. In the porphyritic varieties, the phenocrysts consist of zoned plagioclase, twinned microcline, and perthite. The grains are subhedral with seriate and lobate boundaries; the matrix material consists of plagioclase, microcline, clinopyroxene, perthite, quartz, ilmenite, and accessory zircon, apatite, eipdote or zoisite, and biotite. Myrmekite and graphic intergrowths of quartz and plagioclase are common. In all samples, clots of ilmenite, orthopyroxene, zircon, and apatite occur. Sample MC-35 exhibits complex intergrowths of ilmenite with sericitic muscovite, and ilmenite with apatite. Rosettes of biotite growing into the feldspar nucleate on anhedral grains of opaques. The orthopyroxene is always armored by either green or brown hornblende. Euhedral zircon crystals up to 1 mm in cross section occur as isolated grains. When present, clinopyroxene crystals are twinned and zoned.

Mineralogy of the Gabbro and Syenite

Plagioclase dominates the gabbro (Appendix Table A4), and is normally zoned but is less common in the syenites. Its composition is An78-38 in the gabbro and An42-5 in the syenite. A continuous range in the composition of plagioclase is seen between the two lithologies (Fig. 12 and Appendix Table A4). As seen in Fig. 12, the range in composition for individual plagioclase grains is less than for the total suite.

Perthite and antiperthite, as well as alkali feldspar, can be found in the syenites. These potassium rich feldspars are absent in the

gabbro, however. From staining of the samples, alkali feldspars appear to dominate the syenites, but due to the very fine grain size, point counting proved to be inaccurate, an observation also made by Medlin (1968).

Clinopyroxene dominates the ferromagnesian minerals in the gabbros and syenites. Its composition ranges from Wo48-En39-Fs13 to Wo42-En30-Fs28 in the gabbros and Wo40-En27-Fs33 to Wo45-En11-Fs44 in the syenites (Fig. 12 and Appendix Table A6). Like the plagioclase, the pyroxene compositions are continuous between the syenites and gabbros. They have the greatest iron enrichment of all three plutons studies and are similar to those described by Olsen et al. (1983) for the Concord complex. Clinopyroxene commonly shows twinning and is pale blue under uncrossed polars. Rare exsolution lamellae of magnetite and ilmenite can be found along the {100} direction.

Olivine (Fo33-18) is euhedral in form and found only in the gabbros. It sometimes forms glomerophyric clots, separated from the plagioclase in the more primitive gabbros. Some grains exhibit serpentinization along fractures in the olivine. This may be due to deuteric alteration shortly after crystallization or it may be due to hydrothermal action attendant to the saprolitic alteration of the region. Bastitic hornblende and orthopyroxene (En41) commonly form reaction rims around the olivine, similar to the textures described in the Calhoun Falls complex gabbros. The enstatite is pale pink and very slightly pleochroic.

Greenwood Complex

The three lithologies encountered in Greenwood are POcP cumulate gabbro (gabbronorite), diorite, and metagabbro (Plate 5 and Fig. 13). Unlike the Mt. Carmel and Calhoun Falls complexes, the Greenwood complex appears to be barely unroofed, containing abundant fine grained diorite that crystallized rapidly along the magma chamber margins. There appears to be a systematic variation in the outcrop pattern between the diorite and the cumulate gabbro. The diorites grade into the cumulate gabbro in the southern portion of the complex, but limited outcrop in this pluton makes this observation tentative at present.

Cumulate Gabbro

Texturally, the cumulate gabbro in the Greenwood complex is very similar to that seen in Calhoun Falls. Plagioclase appears to be cumulus along with olivine and clinopyroxene. Orthopyroxene occurs as a late magmatic or subsolidus phase, forming at the expense of olivine. Hornblende occurs as a postcumulus phase as it encloses the cumulus minerals. As in the Calhoun Falls complex, the opaques form both as postcumulus phases and as exsolution phases in olivine and hornblende.

Diorite

The diorites occur only in the Greenwood complex and consist of acicular plagioclase, euhedral olivine, ortho- and clinopyroxene,

Figure 13. Photomicrographs of samples from the Greenwood complex in cross-polarized transmitted light.

a. GW-13. Fine-grained diorite sample showing acicular plagioclase and intergranular clinopyroxene and olivine.
b. GW-14. Medium-grained diorite sample showing acicular plagioclase with intergranular clinopyroxene and olivine.
c. GW-11. Coarse-grained gabbro sample grading into cumulate gabbro showing subhedral plagioclase and clinopyroxene and euhedral olivine.
d. GW-22. Cumulate gabbro showing cumulus plagioclase, clinopyroxene, and olivine with postcumulus opaques.

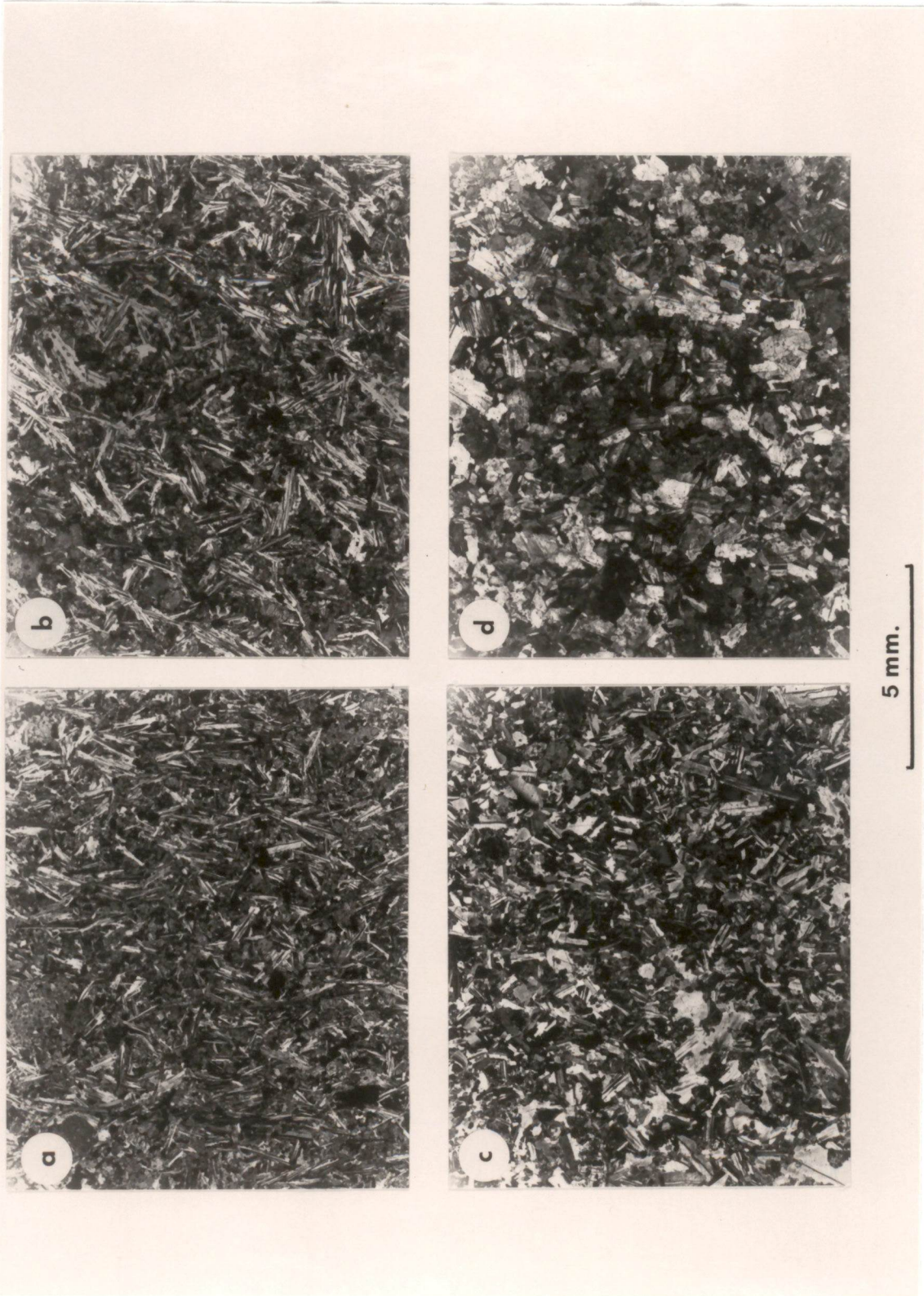

Figure 13.

biotite, and opaques. The crystal habit of the plagioclase indicates rapid growth due to rapid cooling relative to the cumulate gabbros.

Mineralogy

Plagioclases in the cumulate gabbro (An87-62) show normal zonation and have more variation in composition than the plagioclases in the diorites (An64-22). This is probably due to the fact that the diorites represent chill zones with short crystallization times.

The olivine in the cumulates are similar to those found in the Calhoun Falls complex. Their compositions are shown in Figure 10, p. 44, and in Appendix Table A5, making them slightly more magnesian than those found in the Calhoun Falls cumulates. Clinopyroxene compositions (Fig. 10 and Appendix Table A6) are essentially the same as the Calhoun Falls rocks. There is very little iron enrichment in the Greenwood cumulate ferromagnesian minerals. Orthopyroxene compositions, like those in the Calhoun Falls complex, have limited compositions (Fig. 10 and Appendix Table A6).

Summary

Each of the three complexes studied herein exhibits different textures. The Calhoun Falls complex is dominated by mesoscopic layering and abundant cumulus textures. This cumulus character of Calhoun Falls is reflected in the limited iron enrichment found in the ferromagnesian minerals and the normal zonation of the plagioclase.

The wide range in rock type and mineral chemistry found in the Mt. Carmel complex indicates that this pluton underwent greater

fractionation than the other two plutons studied. The extensive iron enrichment in the olivine and pyroxene (relative to Calhoun Falls and Greenwood) also suggests a large degree of fractionation. The textures in Mt. Carmel indicate that the individual samples probably have compositions close to the liquids from which they crystallized.

The Greenwood complex appears to have been barely unroofed due to the transition observed from diorite to cumulate gabbro away from the margins of the complex. Limited iron enrichment in the ferromagnesian minerals from the cumulates suggests that Greenwood underwent a similar evolution to Calhoun Falls. The fact that no mesoscopic layering was observed may be a function of the depth to which the pluton has been exposed.

CHAPTER IV

BULK ROCK COMPOSITION

Introduction

As an aid to modeling the evolution of the magmas from which these complexes were formed, bulk rock analyses were obtained using x-ray fluorescence. The analytical method is first described, including sample preparation, run conditions, and error associated with the data. The results of these analyses are subsequently presented, but interpretation of the data is deferred to the next chapter as all data obtained in this study must be used to understand the petrogenesis of the complexes.

Analytical Methods

Samples were selected to represent all lithologies in each complex and weathered samples were rejected. Approximately 1 kilogram of fresh material from each sample was reduced to pebble size using a steel jaw-crusher. Although no iron filings were observed, the samples were subsequently hand-picked to avoid the possibility of such contamination. The sample was then ground for 1 minute in a tungsten carbide container of a Spex shatter box. For each sample, 0.2000 ± .0005 g of sodium stearate was added to 8.0000 ± .0005 g of sample as a grinding aid and then reground for 6 minutes in the shatter box. After grinding, each sample was pelletized with CP-grade boric acid as an encapsulating agent at a pressure of

2.066×10^8 pascals (15 tons/in^2) for 30 seconds. These prepared pellets were stored in a dessicator for future analysis.

An ORTEC 6110 TEFA energy dispersive x-ray fluorescence (EDXRF) apparatus was used for the analysis under the operating conditions shown in Table 2. Reference standards used for the analysis were DTS-1, PCC-1, BHVO-1, BCR-1, STM-1, AGV-1, GSP-1, G-2, and RGM-1. Both striping and exponential correction equations (Wheeler, 1982) were used in the correction matrix. As a check of accuracy, BCR-1 or DTS-1 was analyzed after each 16 samples and no significant deviations from the published values were found. Seven U.S. Geological Survey samples were analyzed during the same period of time under the same operating conditions (Fronabarger, 1984). Since several of the U.S.G.S. samples were mafic and ultramafic rocks, accuracy and precision for them should be the same as for the rocks of this study.

Table 2. Operating conditions for the ORTEC 6110 TEFA energy dispersive x-ray fluorescence apparatus.

Operating Conditions						
Voltage (KV)	Amperage (μA)	Livetime (sec)	Energy Range (KeV)	Filter	Anode	Elements
10	100	200	0-10	--	Rh	Na, Mg, Al Si, P, K Ca, Ti, V Cr, Mn, Fe
50	200	400	0-10	Sr	W	Ni, Cu, Zn Pb, Rb, Sr Y, Zr, Nb

In almost all cases, a relatively high degree of precision for each sample was obtained for the major oxides. This degree of precision was not maintained, however, for all trace elements. Chromium, nickel, and strontium show poor analytical precision. Furthermore, as with almost all analytical studies, the precision of the determinations of most trace elements decreases with decreasing concentration, suggesting that the minimum detectable concentrations are approached (Table 3).

Table 3. Estimated minimum detectable concentrations (MDC) of reported analyses.

Oxide (in weight percent)	MDC	Element (in parts per million)	MDC
SiO_2	0.03	Cr	9
Al_2O_3	.07	Nb	1
Fe_2O_3	.01	Ni	12
MgO	.16	Pb	5
CaO	.01	Rb	2
Na_2O	.15	Sr	2
K_2O	.01	Th	3
TiO_2	.01	Y	1
P_2O_5	.01	Zr	1
MnO	.01		

Best values for three U.S. Geological Survey samples, BIR-1, W-2, and DNC-1, were obtained from F. J. Flanagan (personal communication). These best values represent the population means

calculated from data submitted by various laboratories that analyzed the samples. The percent change between the data obtained in this study and the best values has been used to estimate accuracy (Table 4). This method is, at best, elementary because no quantifiable test for accuracy can be made. Assuming that the best values are the true concentrations of the constituents within these samples, then the method used in this study, under the operating conditions of Table 2, yields "highly" accurate data (less than 10% change) for SiO_2, CaO, Y, Al_2O_3, Fe_2O_3, and MnO, and "accurate" data (less than 20% change) for TiO_2, Na_2O, MgO, and Th. These limits can only be considered arbitrary and other analysts may impose more strict or more flexible definitions of accuracy of this data.

Presentation of Data

Major oxide (in weight percent) constituents and CIPW norms for each complex are presented in Appendix Tables A8 through A10. Iron was analyzed as Fe_2O_3 (total) and subsequently separated into FeO and Fe_2O_3 using $Fe^{2+}/(Fe^{2+} + Fe^{3+})$ values for similar rock types from Le Maitre (1976). Values are given in Appendix Tables A8 through A10. Trace element (in ppm) constituents for each sample are presented in Appendix Tables A11 to A13. Twenty samples were analyzed from the Calhoun Falls complex, 21 from Mt. Carmel, and 25 from Greenwood. The 18 additional samples from Mt. Carmel analyzed by Medlin (1968) are also considered for comparison. All samples collected in this study are labeled by a two letter prefix and a numerical suffix

Table 4. Percent change of the mean concentrations reported in this study and the best values of Flanagan (1973) reported in decreasing order of accuracy.

Oxide/ Element	Percent Change			Absolute Mean % Change
	BIR-1	W-2	DNC-1	
SiO_2	0.10	2.07	0.40	0.86
CaO	-5.26	-.73	-1.12	2.37
Y	-1.25	.00	-7.50	2.92
Al_2O_3	-9.55	-2.22	-3.47	5.08
Fe_2O_3	11.19	3.45	4.09	6.24
MnO	16.67	4.38	5.71	8.92
TiO_2	15.66	9.48	15.24	13.46
Na_2O	-18.02	-12.70	-11.04	13.92
MgO	-9.77	-10.03	-24.63	14.81
Th	ND	-19.67	ND	19.67
Sr	29.16	24.68	21.01	24.95
Cr	-12.35	-60.21	-12.59	28.38
K_2O	-16.67	-9.28	-13.33	29.76
Zr	-47.43	20.48	-23.00	30.30
Pb	ND	-36.17	ND	36.17
Rb	-68.57	4.50	-41.25	38.17
Nb	-62.33	-32.50	-25.71	40.18
Ni	80.87	ND	18.75	49.81
P_2O_5	-87.65	-41.25	-63.16	64.02

*A positive percent change indicates that the value reported in this study is greater than the best value and a negative percent change indicates that the value is less than the best value.

(e.g., MC-11) and Medlin's analyses are labeled by numbers only (e.g., 126-7).

Chemistry of the Complexes

The normative mineralogy of each of the complexes was calculated using the CIPW system, and the results are presented in Fig. 14. Each of the complexes occupy different regions of normative olivine, diopside, hypersthene, quartz space.

All of the troctolites from Calhoun Falls are nepheline normative while the gabbronorites and metagabbros are diopside-olivine-hypersthene normative. The ultramafic rocks all fall near the diopside-hypersthene join, some being quartz normative. This high silica nature of the ultramafics must be due to silica enrichment relative to other major oxides during metamorphism. Thus, the original compositional character of the ultramafic rocks is not represented by the results of analyses presented in Appendix A. The troctolites and gabbronorites form a continuous trend along the olivine-diopside join, which are the major ferromagnesian cumulus phases in these rocks.

Samples from the Mt. Carmel suite span the compositional range, but a systematic variation with rock type is apparent. Metagabbros tend to cluster along the olivine-diopside join, some being nepheline normative and some being hypersthene normative. Gabbros tend to be diopside-olivine-hypersthene normative; however, several exceptions can be found. With the exception of three of Medlin's (1968) samples,

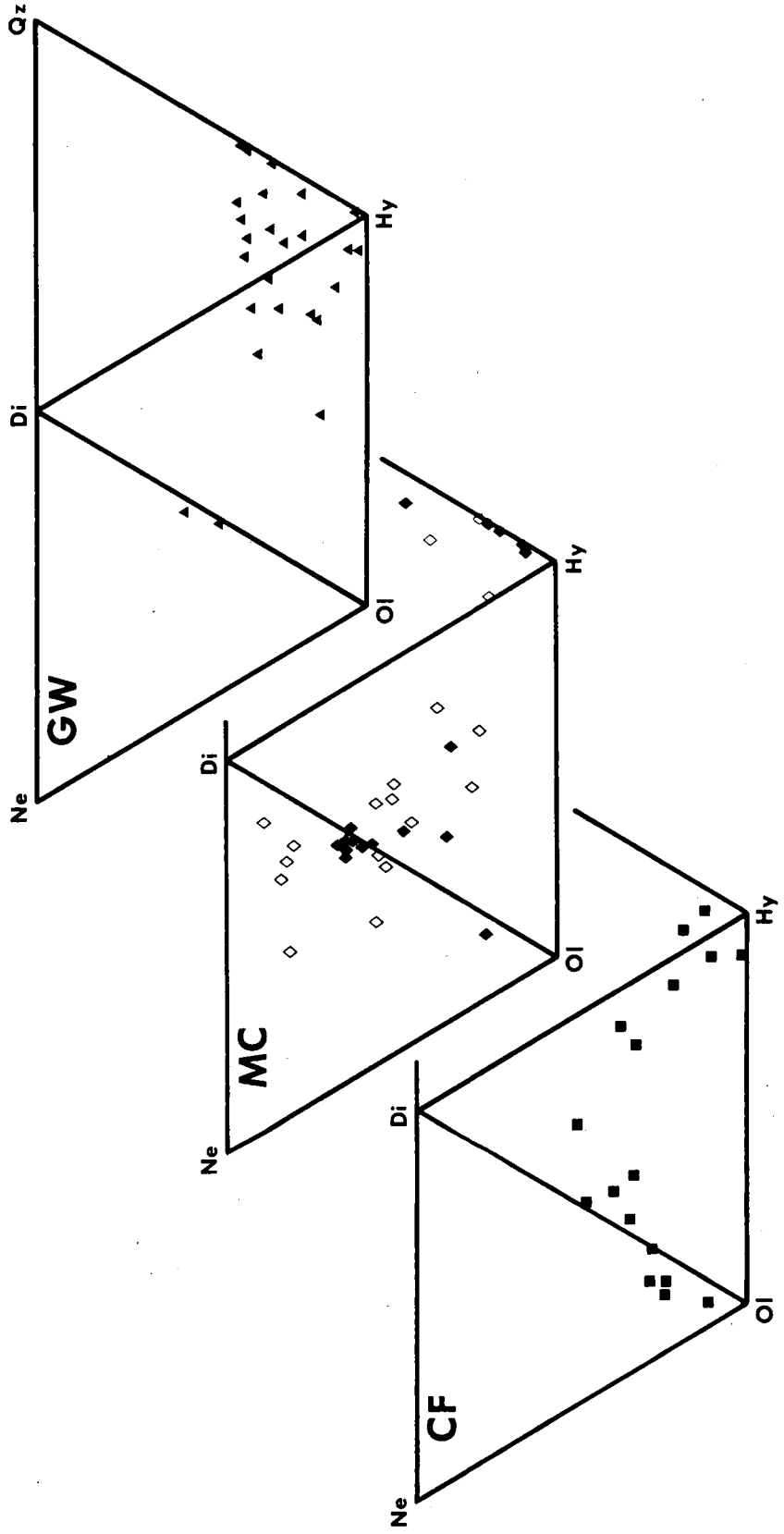

Figure 14. Expanded normative basalt tetrahedron showing calculated CIPW values for samples from the Calhoun Falls (CF), Mt. Carmel (MC), and Greenwood (GW) complexes. Open symbols represent data from Medlin (1968) and closed symbols are from this study.

all syenites are quartz normative. Thus, as would be expected, the correlation seen between bulk chemistry and rock type also holds true for normative mineralogy; metagabbros are most mafic, gabbros are intermediate, and syenites are most felsic in the suite.

The samples from the Greenwood complex fall along the hypersthene-diopside join, many being quartz normative. The normative quartz enrichment in the samples from Greenwood is unlike that seen in Mt. Carmel. In the Greenwood suite, there appears to be no well defined differentiation series, making it very similar to the Calhoun Falls suite, yet it is, on the average, higher in silica than Mt. Carmel rocks.

Irvine and Barager (1971) devised a system whereby volcanic rocks are classified on the basis of bulk rock chemistry. They subdivided volcanic rocks on the basis of three fundamental differentiation series that are commonly found: subalkaline, alkaline, and peralkaline rocks. Of these, the subalkaline and alkaline series are pertinent to the present study. Subalkaline rocks may be further subdivided into a tholeiitic and a calc-alkali basalt series, whereas the alkaline rocks series can be subdivided into alkali olivine basalt and feldspathoidal series. The subalkaline series forms a differentiation series of tholeiite to rhyolite and the alkaline series forms a differentiation series starting with an alkalic basalt and evolving ultimately to a phonolite. Difficulties arise however, in determining precise boundaries between these series (Kuno, 1959, 1966, 1968; Macdonald and Katsura, 1964; Macdonald, 1968; Upton, 1974).

These difficulties become evident when considering the rocks of these complexes. Irvine and Baragar (1971) used the variation diagram of alkalis versus silica to separate subalkaline and alkaline series (Fig. 15). Clearly the Mt. Carmel suite belongs to the alkaline series using Irvine and Baragar's (1971) line, but are subalkaline using Upton's line. The Calhoun Falls and Greenwood samples form clusters in the subalkaline region; but their nature is indeterminate because the individual samples from these two plutons do not represent liquid compositions. When considering the same rocks on the alkali-total iron-magnesium (AFM) ternary plot (Fig. 16), they clearly plot as a tholeiite suite, a subgroup of the subalkaline series. Upton's (1974) line separating alkaline and subalkaline series (Fig. 15) resolves this problem, but some justification must be made to use one dividing line over the other. This justification comes from considering the textures of the rocks. Many authors (e.g., Kuno, 1968; Macdonald and Katsura, 1964; and Irvine and Baragar, 1971) note that in subalkaline suites, olivine commonly is resorbed, reacting to form either hypersthene or pigeonite. Such textures are common in this suite collected from the study area. On this basis, the dividing line of Upton (1974) is accepted for the purpose of this study. The AFM ternary plot (Fig. 15) shows that the series is tholeiitic and not calc-alkaline.

Another difficulty arises when attempting to classify the chemical nature of the rocks in the study area. The major element chemistry of samples containing cumulus textures does not necessarily represent the

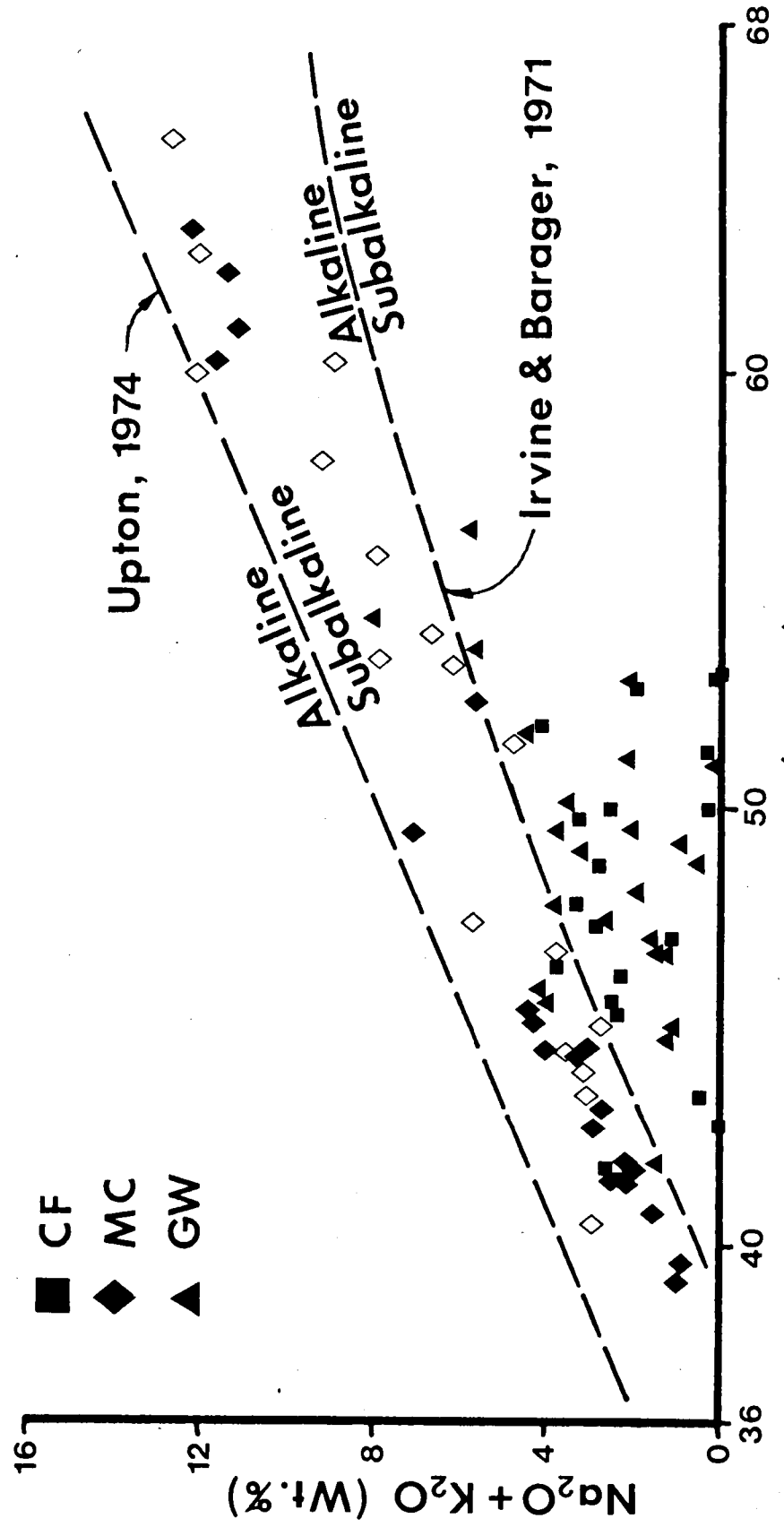

Figure 15. Total alkalis vs. silica diagram for samples from the Calhoun Falls (CF), Mt. Carmel (MC), and Greenwood (GW) complexes. Filled symbols represent analyses from this study and open symbols represent analyses taken from Medlin (1968).

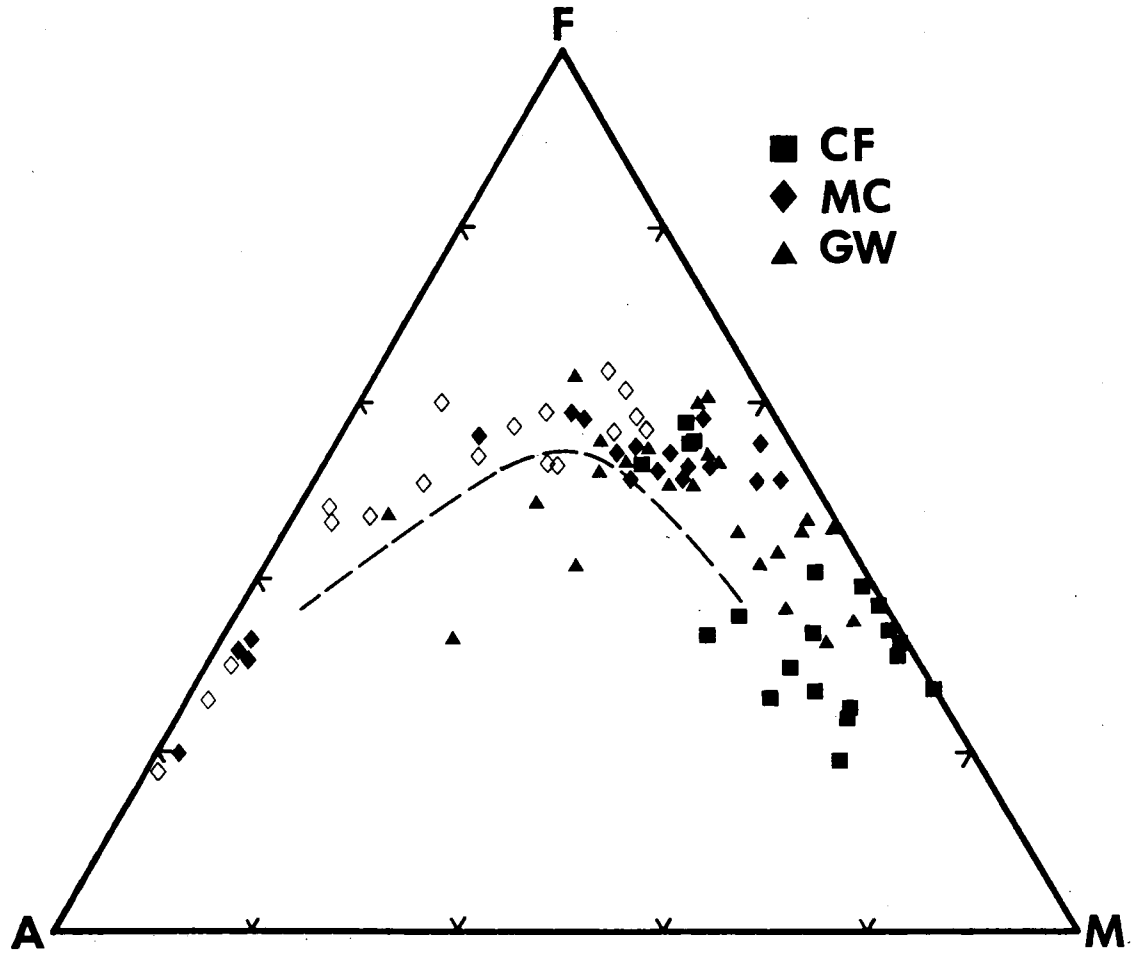

Figure 16. AFM diagram of samples from the Calhoun Falls (CF), Mt. Carmel (MC), and Greenwood (GW) complexes. Filled symbols represent analyses from this study and open symbols from Medlin (1968). The dashed line represents the separation between alkali olivine (below) and tholeiitic (above) basalts.

composition of the liquids from which they crystallized, rather they represent a weighted average of the cumulus phase compositions and the intercumulus liquid. Thus, the samples from the Calhoun Falls and Greenwood complexes do not define a clear differentiation trend (Fig. 15); they cluster in two groups well below the trend formed by the Mt. Carmel suite. Since the Mt. Carmel suite does form a well defined trend and does not contain cumulus textures, individual samples from this suite probably represent liquid compositions, and the trend represents a liquid line of descent. This does not appear to be the case for the Calhoun Falls or the Greenwood suites. This problem is addressed in more detail elsewhere in this chapter.

The variation diagrams (Fig. 17) further show the inherent differences between the Mt. Carmel suite and the Calhoun Falls and Greenwood suites. Most of the major elements vary systematically within the Mt. Carmel suite (Fig. 17), but the Calhoun Falls and Greenwood suites show poor correlation among the major elements. Again, this lack of systematic variation in the latter two complexes is primarily due to the cumulate nature of many of the rocks within them. This inherent difference is perhaps best exemplified in Fig. 18, a plot of titanium versus magnesium number. Titanium is in many cases an incompatible element, being partitioned into the residual melt during fractional crystallization until ilmenite becomes a crystallizing phase, and thereafter decreasing in concentration in the evolving magma (Hughes, 1982). The Mt. Carmel rocks do not contain cumulus phases, so there is a direct correlation of Ti to Mg* and fractionation

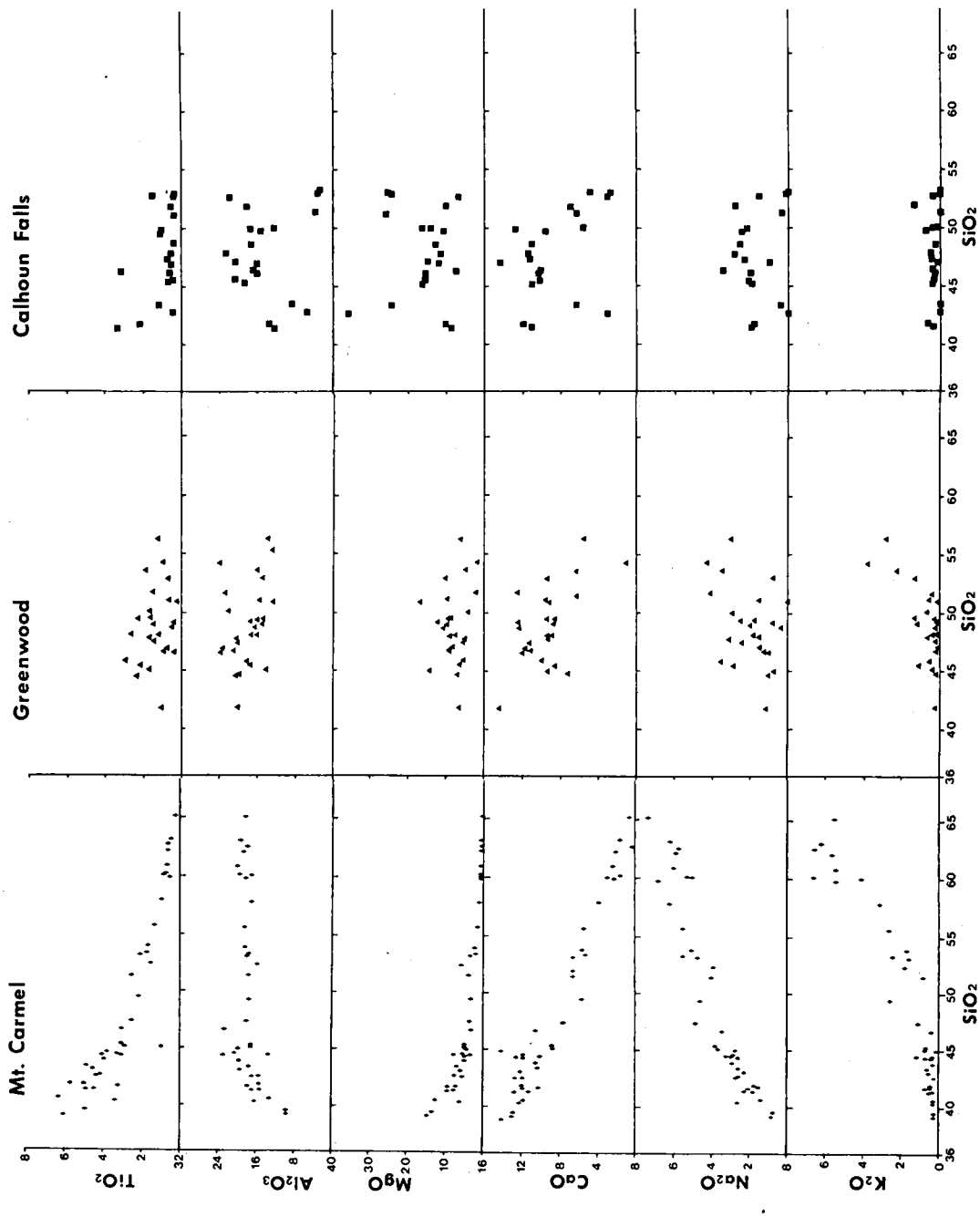

Figure 17. Harker variation diagrams for the three complexes studied. All oxides in weight percent.

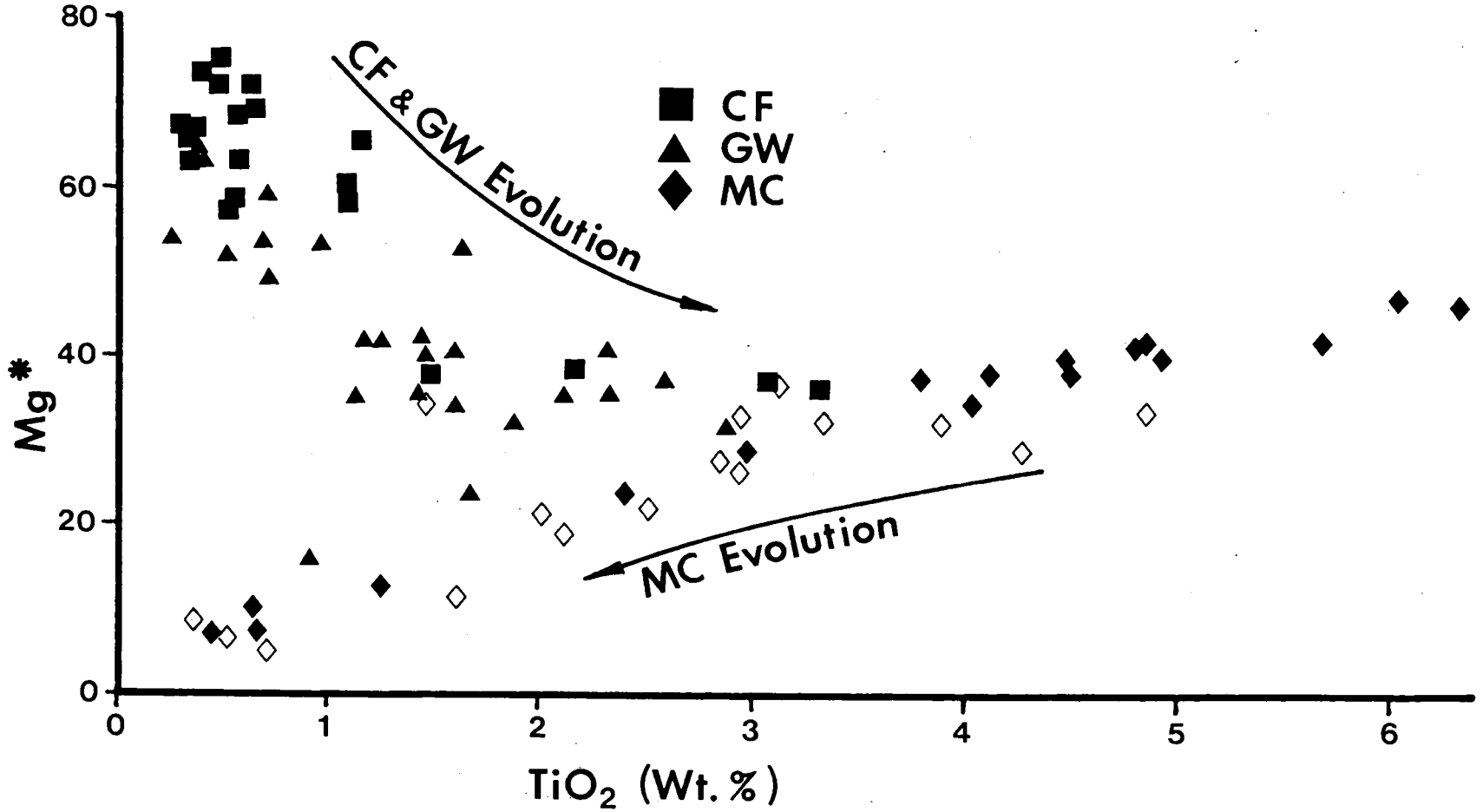

Figure 18. Titanium vs. magnesium number for samples from the Calhoun Falls (CF), Mt. Carmel (MC), and Greenwood (GW) complexes. Filled symbols represent analyses from this study and open symbols represent analyses from Medlin (1968).

continues from right to left in Fig. 18. The Calhoun Falls and Greenwood complexes, on the other hand, contain abundant cumulus ferromagnesian minerals, and ilmenite is restricted to the postcumulus material. Thus, "primitive" rocks containing abundant cumulus olivine and pyroxene are poor in ilmenite relative to more "evolved" rocks containing less cumulus olivine and pyroxene, and the trend of fractionation is reversed, from left to right in Fig. 18.

CHAPTER V

PETROGENESIS

Introduction

Each of the three complexes investigated within the study area shows different textural characteristics. This is surprising because of the close geographic proximity and presumed similar age of emplacement. If these complexes were similar magmas intruded into the same physical environment at the same approximate time, one would expect to observe similar crystallization paths. The fact that each of these intrusives is apparently different suggests that parental magmas were different, or that the parameters that controlled crystallization were different despite their close temporal and spatial proximity. This section will show that the Mt. Carmel and Calhoun Falls complexes can be related by their fractionation trends. The Mt. Carmel complex samples represent approximate liquid compositions and are therefore discussed first. The intercumulus liquid composition of the Calhoun Falls complex is then related to the composition of the early differentiates in the Mt. Carmel complex. Despite the proximity of the Greenwood complex, this section will show that it may not have formed from the same parental liquid as the other two.

The study area is separated from other intrusives within the Charlotte belt by gaps both to the north and the south where no mafic intrusives are found (Fig. 1, p. 2). For this reason, the petrogenetic character of the rocks of this study is summarized and subsequently

compared to others within the Charlotte belt. Finally, the relationship between gabbro and metagabbro as interpreted by Hermes (1968) and McSween et al. (1984) is reevaluated in light of the data presented in this study.

Mt. Carmel Complex

The Mt. Carmel complex provides the most information concerning the evolution of the magmas that formed the mafic intrusives in the Charlotte belt because it is the only complex that does not exhibit abundant cumulus textures. As noted in earlier sections, the rocks in the Mt. Carmel suite appear to represent the liquid compositions from which they formed. Thus, it is possible to determine the nature and degree of fractionation that formed the suite.

Major Element Fractionation

All of the variation diagrams of the Mt. Carmel suite show a continuous fractionation trend from metagabbro to gabbro to syenite. Extract polygons of Cox et al. (1979) were plotted on two element variation diagrams to determine the fractionation control lines for this suite (Fig. 19). Average mineral compositions of olivine, clinopyroxene, and plagioclase for the three rock types are plotted. Plagioclase becomes more sodic, and olivine and clinopyroxene become more iron-enriched during the evolution of the suite. Thus the extract polygon determined by these three minerals changes position and shape during the evolution of the suite. Olivine is not present in

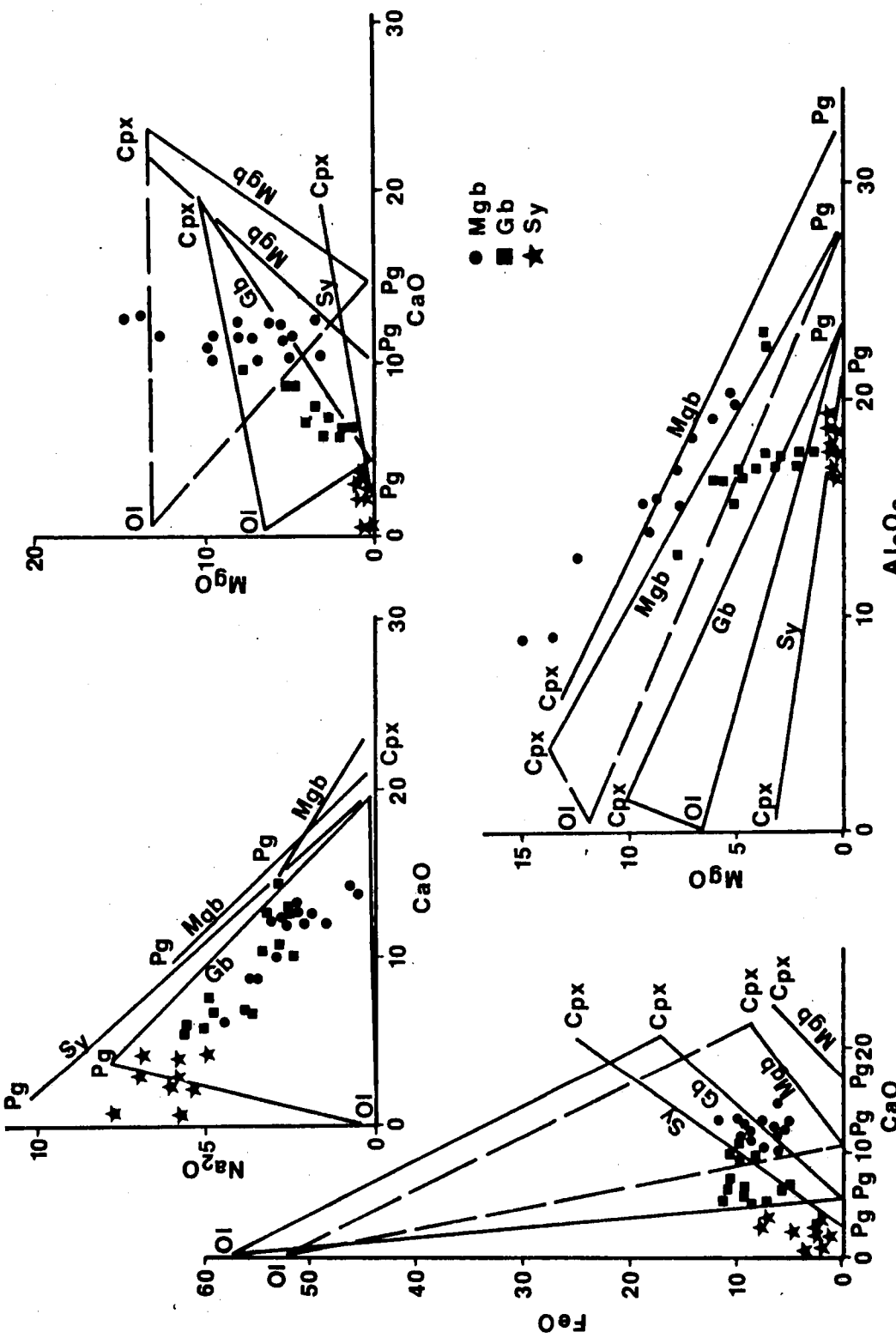

Figure 19. Four representative two-element extract diagrams showing the early fractionation of clinopyroxene and olivine in the Mt. Carmel complex. Dots represent metagabbro (Mgb), squares represent gabbro (Gb), and stars represent syenite (Sy).

the syenites and the extract "polygon" becomes a line joining plagioclase and clinopyroxene for extreme differentiates.

These extract polygons indicate that initial crystallization of clinopyroxene + olivine or clinopyroxene + olivine + plagioclase formed the metagabbros. This is evidenced by the fact that the gabbro samples fall outside the extract polygons along a line connecting the gabbro and metagabbro. The line connecting these two suites point to the olivine-pyroxene join. After all olivine crystallized, fractionation of clinopyroxene plus plagioclase controlled crystallization of the syenites. In the CaO-MgO variation diagram, a distinct bend between the gabbro extraction and the syenite extraction trends is seen. This bend is interpreted as being due to the exhaustion of olivine at the onset of the syenite production.

The bulk rock analyses of samples collected from the Mt. Carmel complex have also been projected from plagioclase onto the diopside-olivine-quartz phase diagram (Fig. 20) and from diopside onto the anorthite-quartz-olivine phase diagram (Fig. 20) using the method developed by Elthon (1983). In this figure

$$Cpx = moles((CaO+Na_2O+K_2O)-(Al_2O_3+Fe_2O_3)),$$

$$Ol = moles((MgO+FeO+MnO-TiO_2)-(CaO+Na_2O+K_2O)+(Al_2O_3+Fe_2O_3))/2,$$

$$Silica = moles((SiO_2)-(MgO+FeO+MnO-TiO_2)+(Al_2O_3+Fe_2O_3)+3(CaO+Na_2O+K_2O))/2, \text{ and}$$

$$Pg = moles\ (Al_2O_3+Fe_2O_3).$$

Included on these diagrams are the pseudo-liquidus phase relations as deduced by Walker et al. (1979) at 1 atm for mid-ocean ridge basalt

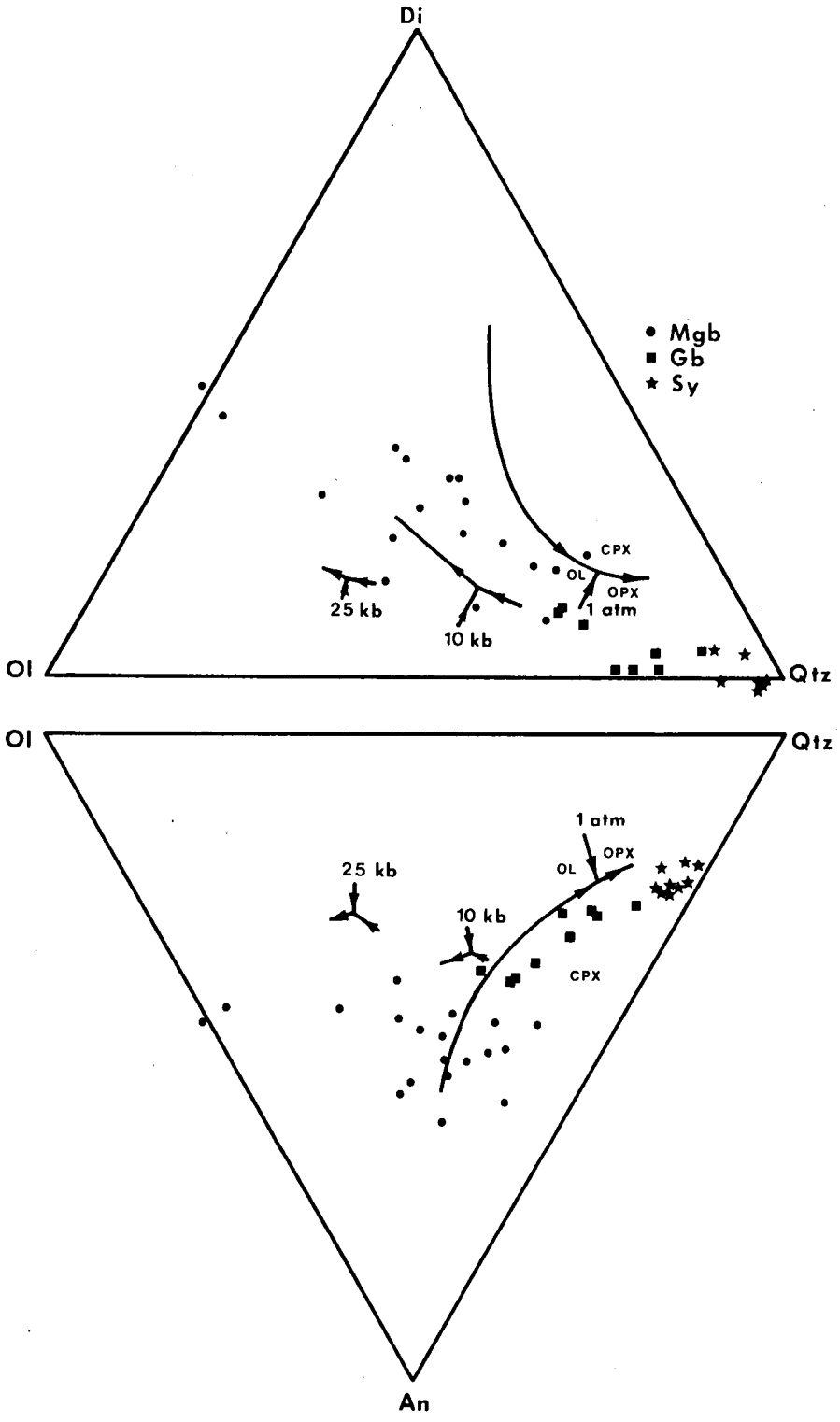

Figure 20. Isomolar basalt phase diagram (Elthon, 1983) showing analyses of metagabbro (Mgb), gabbro (Gb), and syenite (Sy) from the Mt. Carmel complex.

(MORB), and by Elthon and Scarfe (1984) for high-magnesian basalt at 10 and 25 kb. Elthon (1983) points out that these isomolar phase diagrams separate the plagioclase projection point into a line along the anorthite-quartz join. In so doing, the evolution of plagioclase during the crystallization history of the complex must be known to trace the plagioclase-controlled crystallization path on these diagrams. Fortunately, plagioclase is normally zoned in the Mt. Carmel suite, containing calcic cores and sodic rims. The early plagioclase is more calcic on the average than the late crystallization products (Appendix Table A4). This change in plagioclase composition causes the projection point to move continuously from near the anorthite apex for the metagabbros to near quartz (at the albite point) for the syenites in the diopside-olivine-quartz diagram. The final effect is relatively minor since the plot of the data falls along a trend forming a vertical plane coincident with plagioclase solid solution in the quaternary space. The plagioclase effect on the liquid line of descent in the anorthite-quartz-olivine ternary is to pull evolved samples towards the albite projection point.

The Mt. Carmel samples fall between the 1 atm and 10 kb pseudo-liquidus phase relations in the diopside-olivine-quartz diagram (Fig. 20). This is broadly consistent with conclusions of McSween et al. (1984) who determined pressures of crystallization for other gabbros in the southern Appalachians to be about 5 kb using coexisting pyroxene compositions. The samples plot along the 1 atm pseudo-liquidus in the anorthite-quartz-olivine phase diagram (Fig. 20). In

this ternary, however, the distances between the 1 atm and 10 kb liquidus cotectic surfaces are small and it is difficult to discriminate the pressures of crystallization for gabbros.

In both ternary diagrams, there is a distinct bend in the liquid line of descent, but it is most pronounced in the anorthite-quartz-olivine diagram (Fig. 20). The most primitive metagabbros appear to be controlled by olivine and clinopyroxene crystallization until the olivine-plagioclase cotectic is reached. Thus, the evolution of the magma is controlled by fractionation of clinopyroxene + olivine for the metagabbros, clinopyroxene + olivine + plagioclase for the gabbros, and clinopyroxene + plagioclase for the syenites, in agreement with the extract diagrams previously presented.

Least-squares mass-balance computations using a program by Wright and Doherty (1970) for the average major element compositions (Table 5) were used to calculate the amount of residual liquid remaining after fractionating gabbro from metagabbro and syenite from gabbro. In both steps, clinopyroxene, ilmenite, magnetite, plagioclase, and olivine were allowed to fractionate from the parent to produce the daughter magma. In these computations, the compositions of both plagioclase and olivine were allowed to vary over the maximum range observed in the parent lithology. Plagioclase compositions range from An74 to An62 in metagabbro and An62 to An23 in the gabbro. Since no olivine survived metamorphism in the metagabbros, their compositions were assumed to range from Fo84 to Fo77. The olivine compositions in the gabbro were varied between Fo77 to Fo47.

Table 5. Average compositions of metagabbro, gabbro, and syenite in the Mt. Carmel complex.

Major Oxides (wt%)	Metagabbro			Gabbro			Syenite		
	$\bar{X}$	$\sigma_{\bar{x}}$	n	$\bar{X}$	$\sigma_{\bar{x}}$	n	$\bar{X}$	$\sigma_{\bar{x}}$	n
SiO_2	42.64	1.97	19	50.03	4.15	10	61.45	2.17	9
TiO_2	4.17	1.27	19	2.36	.80	10	.54	.22	9
Al_2O_3	16.97	3.69	19	17.13	1.43	10	18.19	1.09	9
Fe_2O_3	3.55	1.07	19	2.53	.97	10	1.69	.84	9
FeO	8.20	1.91	19	9.21	1.18	10	3.80	2.10	9
MnO	.14	.05	19	.25	.07	10	.17	10	9
MgO	7.50	3.27	19	3.62	1.86	10	.43	.17	9
CaO	11.90	1.03	19	6.98	1.70	10	1.86	1.09	9
Na_2O	2.23	.75	19	4.41	.82	10	5.97	.72	9
K_2O	.36	.17	19	1.48	.76	10	5.31	1.12	9
P_2O_5	.49	.61	12	.99	.35	4	.16	.04	4
Total	98.15			98.99			99.57		
Fe_2O_3 (T)	12.43	2.81	19	12.23	12.71	10	5.70	2.25	9
FeO (T)	11.18	-	-	11.00	-	-	5.13	-	-
Trace elements (ppm)*									
Ba	255	30	12	427	199	4	1023	170	5
Cr	22	5	12	19	2	4	<9	-	-
Nb	<1	-	-	110	43	4	86	55	4
Pb	6†	2	5	6	-	3	0	-	3
Rb	10	2	12	18	9	4	43	4	4
Sr	639	249	12	470	96	4	383	294	5
V	845	211	12	513	174	4	26†	-	2
Y	9	5	12	42	14	4	32	19	4
Zr	101	23	12	295	257	4	534	429	4

*Significant variation between Medlin's (1968) data and Fronabarger's (this study) data exists. Mean calculated using data from this study.

†Several values were below the minimum detectable limits and were not included in the mean. True mean is less than the value reported.

$\bar{x}$ = Arithmetic mean.

$\sigma_{\bar{x}}$ = One standard deviation from the mean (n - 1 d.f.).

n = The number of analyses included.

Results of these mass-balance computations (Table 6) indicate that fractionating about 22% clinopyroxene, 8% ilmenite, 2% magnetite, 40% plagioclase (An74), and 11% olivine (Fo84) will produce gabbro, leaving about 7% residual liquid. Although the error values as computed by the Wright and Doherty (1970) program are low, the sum of the squares of residuals is high (.4383). Solutions can be considered acceptable if the residuals are less than unity (Barnes, 1983). This error may be due to the fact that the range of compositions assumed for olivine and plagioclase in metagabbro are poorly constrained. Average syenite can be produced from average gabbro by fractionating about 12% clinopyroxene, 4% ilmenite, 5% magnetite, 45% plagioclase (An52), and 5% olivine (Fo77) leaving 28% residual liquid. This 28% residual liquid is assuming 100% parental gabbro parent magma and converts to about 2% residual liquid when compared to the original 100% parental metagabbro liquid. Both the error and sum of the squares of the residuals (.0049) are low indicating excellent precision.

These results are broadly consistent with the observed field relations. They do not agree totally with the extract diagrams, however, which are not entirely definitive. The earliest participants in fractionation in the Mt. Carmel suite can be either plagioclase + olivine + pyroxene or olivine + pyroxene. In light of the results of these mass-balance computations and the phase diagrams, as well as the textural evidence seen in the most primitive metagabbros, it appears that plagioclase participated in fractionation after significant quantities of olivine and pyroxene crystallized. Metagabbro makes up

Table 6. Results of mass balance computations for the Mt. Carmel complex using the method of Wright and Doherty (1970).

Solution	Avg	Cpx	Ilm	Mag	Plag	Ol	Rock	Weight	Calc.	Diff.
	Fractionation Index Calculation for Mt. Carmel Metagabbro-Gabbro									
SiO_2	51.32	51.33	0.00	0.00	49.89	39.30	43.89	1.00	44.19	-0.29
Al_2O_3	17.57	1.08	0.10	0.69	32.49	0.00	17.47	1.00	17.62	-0.14
FeO	11.79	16.78	43.25	97.81	0.14	15.56	11.73	1.00	11.88	-0.14
MgO	3.72	10.27	3.01	0.40	0.00	45.16	7.72	1.00	7.78	-0.05
CaO	7.16	20.00	0.00	0.00	14.59	0.00	12.25	1.00	12.19	0.07
Na_2O	4.53	0.30	0.00	0.00	2.87	0.00	2.30	1.00	1.82	0.48
K_2O	1.52	0.00	0.00	0.00	0.05	0.00	0.38	1.00	0.14	0.24
TiO_2	2.43	0.28	53.65	1.12	0.00	0.00	4.30	1.00	4.44	-0.14
Solution	7.39	22.25	7.78	2.18	49.41	11.01				$\Sigma R^2 = 0.4383$
Sensitiv	0.66	0.69	0.77	1.26	0.72	0.71				
An Ratio =	100.00									
Fa Ratio =	0.00									
	Fractionation Index Calculation for Mt. Carmel Gabbro-Syenite									
SiO_2	62.03	51.33	0.00	0.00	56.81	38.57	51.32	1.00	51.29	0.04
Al_2O_3	18.37	1.08	0.10	0.69	27.30	0.00	17.57	1.00	17.56	0.02
FeO	5.37	16.78	43.25	97.81	0.16	21.26	11.79	1.00	11.77	0.02
MgO	0.44	10.27	3.01	0.40	0.00	40.19	3.72	1.00	3.71	0.01
CaO	1.88	20.00	0.00	0.00	9.30	0.00	7.16	1.00	7.17	-0.00
Na_2O	6.03	0.30	0.00	0.00	6.35	0.00	4.53	1.00	4.58	-0.04
K_2O	5.36	0.00	0.00	0.00	0.10	0.00	1.52	1.00	1.55	-0.02
TiO_2	0.55	0.28	53.65	1.12	0.00	0.00	2.43	1.00	2.41	0.02
Solution	28.06	12.37	4.03	5.35	44.81	5.42				$\Sigma R^2 = 0.0049$
Sensitiv	0.40	0.31	0.45	0.93	0.38	0.33				
An Ratio =	84.15									
Fa Ratio =	0.00									

the bulk of the Mt. Carmel complex, about 60%, while gabbro and syenite make up proportionately less, about 20% respectively (Plate 4). If the present day erosional surface represents the volumetric proportions of the three constituent lithologies, then the large amount of magma required to produce average gabbro from average metagabbro is to be expected.

Trace Element Trends

Six minor and trace elements from Mt. Carmel are plotted against the Larsen differentiation index which is defined in Fig. 21. The Larsen index has been used in these figures because it shows better correlation than other possible indices. Other trace elements for which analyses were performed do not show systematic variation, possibly due to poor analytical precision, and are not illustrated. Gill (1981) classifies these trace elements on the basis of their behavior in the following manner. Rubidium and barium form large cations and substitute for potassium during crystallization. Strontium on the other hand, substitutes for calcium during crystallization. Lead is an incompatible element and usually increases during the evolution of a magma. Vanadium is a compatible element, commonly substituting for ferrous iron and titanium, increasing during early crystallization.

In the Mt. Carmel suite most of the trends (Fig. 21) follow expected trends for an evolving magma. Due to the incompatible nature of lead and barium, their concentrations increase during crystallization. Rubidium and strontium both exhibit two trends, one for metagabbros, and one for gabbros plus syenites. These two

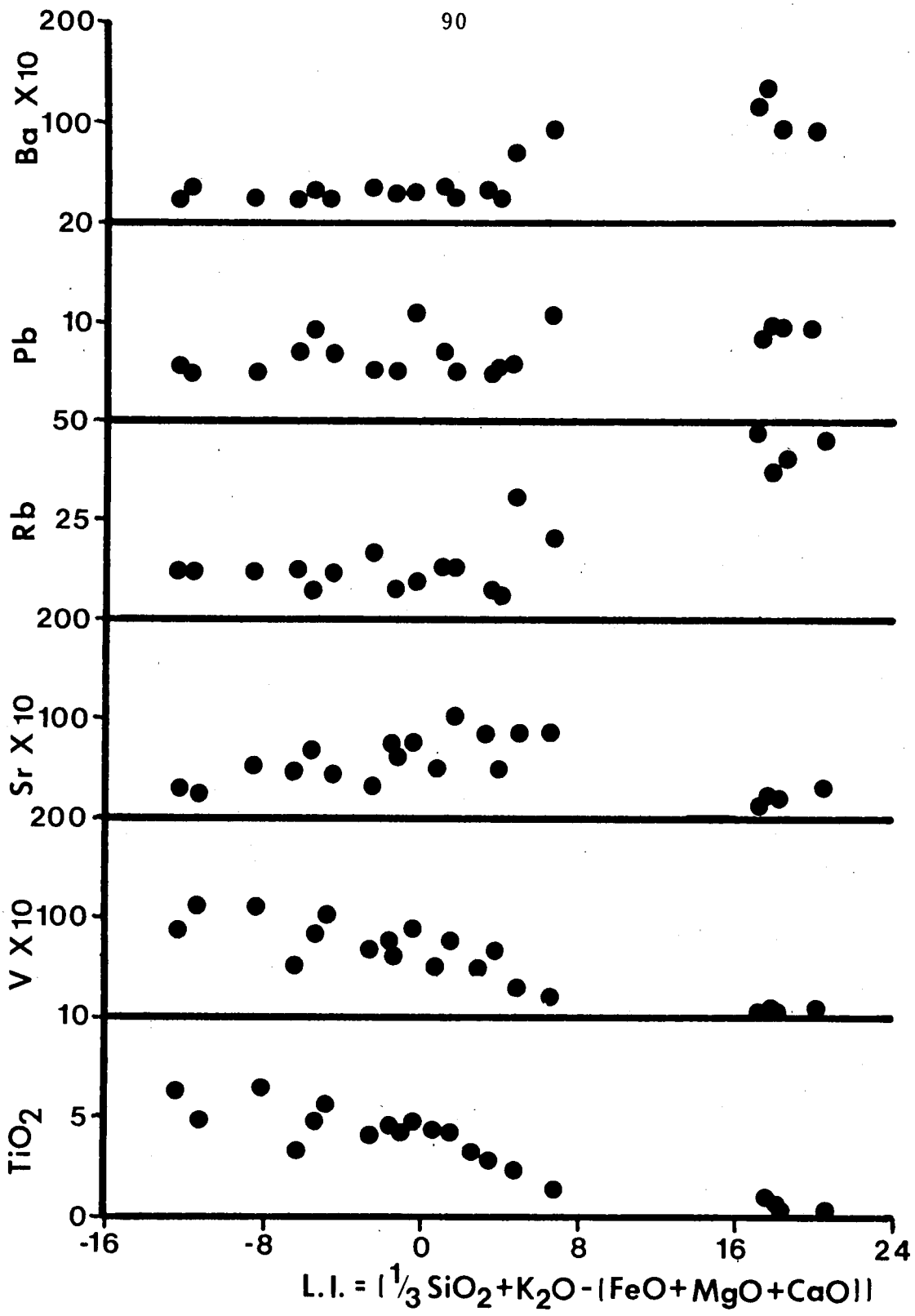

Figure 21. Minor and trace element vs. the Larsen Index (L.I.) for the Mt. Carmel complex. TiO_2 is in weight percent and all others in parts per million.

elements have possibly been redistributed during alteration. Rubidium decreases from about 15 ppm to a few ppm and strontium increases from about 200 ppm to about 1600 ppm in the metagabbros. The gabbro-syenite trends bisect the metagabbro trend due to the compositional overlap of the major elements in the evolved metagabbros and primitive gabbros. The rubidium and strontium slopes are reversed for the metagabbros, indicating that rubidium was depleated and strontium was enriched in the evolved metagabbros relative to the primitive metagabbros. No correlation of the Rb and Sr trends with metagabbro type (Hermes, 1968) was observed however, as type 2 metagabbros predominate in the Mt. Carmel suite. Both vanadium and titanium systematically decrease during crystallization of the Mt. Carmel magma. Vanadium substitutes readily in the magnetite structure which coprecipitates with ilmenite. Thus, the constant decreases in V and TiO_2 indicate that ilmenite and magnetite crystallized early in the magmatic history of Mt. Carmel.

The systematic variation of Ba, Pb, V, and Ti from metagabbro to gabbro in the Mt. Carmel suite suggests that these two rock types crystallized from a single magma, contrary to the conclusions of Hermes (1968) and McSween et al. (1984) for other intrusives in the Charlotte belt. The variation of Rb and Sr is similar to that of potassium, indicating that the rubidium is being partitioned into biotite and K-rich feldspars late in the crystallization history. Strontium, on the other hand, substitutes for calcium and is partitioned into Ca-rich plagioclase early in the crystallization history of the suite.

Calhoun Falls Complex

The Calhoun Falls complex has been shown to be compositionally more mafic than the other two complexes in the study area as it contains abundant ultramafics. Metagabbro, troctolite and gabbronorite are also present, all of which contain cumulus textures, affecting the major element trends. For this reason it is impossible to determine the degree of fractionation that occurred in this intrusive. The intercumulus liquid composition can, however, be estimated.

Intercumulus Liquid Compositions of the Calhoun Falls Cumulates

The major element chemistry of samples containing cumulus textures do not necessarily represent the compositions of the liquids from which they crystallized, rather they represent a weighted average of the total cumulus phase compositions and the intercumulus liquid compositions. This relationship between volume percent cumulus phases and bulk chemistry for two rock types in Calhoun Falls is apparent in Fig. 22. Two parallel lines can be drawn through these samples, one through the troctolites, containing high CaO + MgO and low volume percent cumulus phases, and a second through the gabbronorites. This relationship is primarily due to the amount of cumulus olivine and pyroxene in the respective rock types. In this figure, all plagioclase was assumed to be cumulus. It would be a simple matter to perform a mass balance calculation to obtain the intercumulus liquid composition of each major element analysis if all mineral phases can be

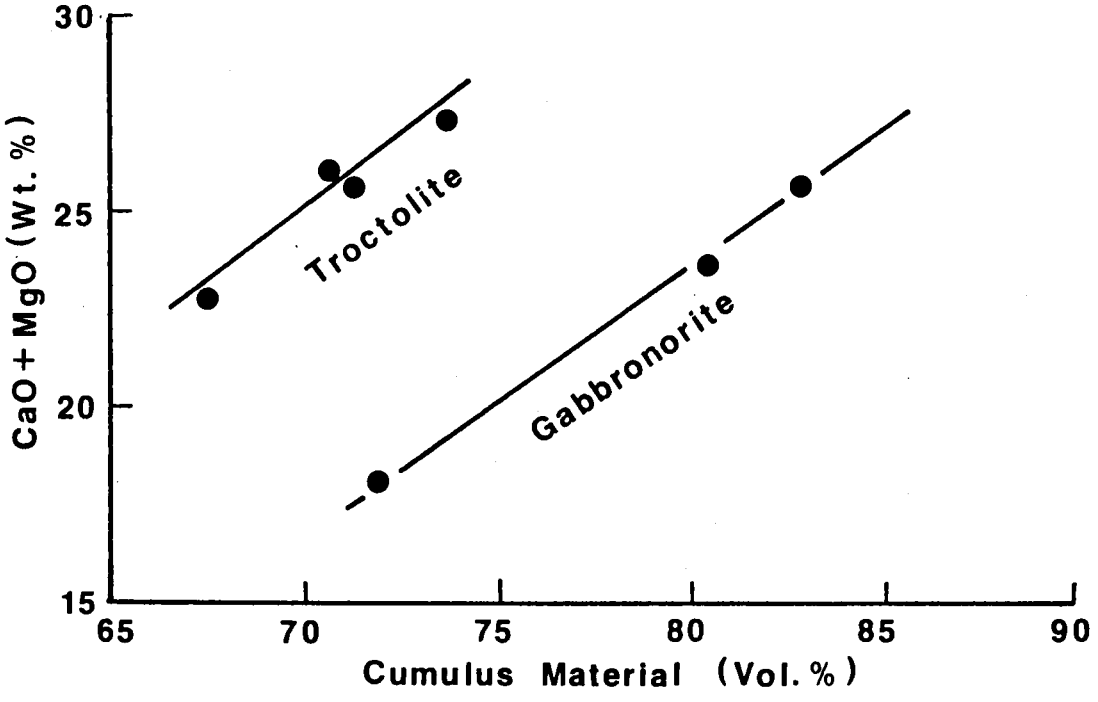

Figure 22. Correlation of volume percent cumulus material to CaO + MgO (wt. %) in the Calhoun Falls cumulate gabbros.

assumed to be either cumulus or postcumulus in nature. Unfortunately, this assumption is not valid, as pointed out by Irvine (1980). Continued growth of cumulus crystals from intercumulus material makes it difficult to determine how much of a given mineral phase is cumulus and how much is postcumulus. As noted in this and previous studies (e.g., Clark, 1980; McSween and Nystrom, 1979; and Olsen, 1982), ferromagnesian minerals in gabbroic samples are unzoned. Some of these mafic minerals could have been derived through adcumulus growth. Furthermore, overgrowths on cumulus plagioclase by the intercumulus liquid would form normally zoned crystals which may or may not exhibit a sharp compositional break at the intersection of cumulus and postcumulus derived material. If some of the plagioclase grew from the intercumulus liquid, then a further difficulty arises in assigning a composition to the postcumulus plagioclase in any mass balance calculation. A further difficulty arises from recent work by Salpas et al. (1983) in which they present chemical evidence that poikilitic grains may form from the cumulus liquid. Thus, on the basis of textures, modes, and bulk chemistry alone, it is impossible to determine the intercumulus liquid composition of the Calhoun Falls samples. By making two simplifying assumptions however, both the intercumulus liquid composition and the percent cumulus plagioclase can be estimated.

First, we will assume that all olivine and pyroxene are 100% cumulus with no adcumulus growth or overgrowth to have occurred. The validity of this assumption will be tested in the subsequent

discussion, but first consider its impact. Modal plagioclase makes up to between 58% and 73% of the troctolites and gabbronorites (Fig. 9, p. 43, and Appendix Table A1) while olivine and pyroxene make up between 5 and 22 modal percent of these rocks. Thus, these ferromagnesian minerals do not comprise a large volume of the total rock and any adcumulus growth must be less than that.

Second, we will assume that the initial liquids from which the Mt. Carmel and Calhoun Falls complexes crystallized were similar. There is no adequate way to test this assumption, and the different nature of the products of crystallization in the two bodies argues against this assumption. Either some compositional or intensive parameters must have been different to give rise to the different crystallization products. The near proximity of the two complexes suggests that the parental liquids were formed in the same regime, however. If the crystallizing liquids were similar in both complexes, then the intercumulus liquid compositions at Calhoun Falls should be the same as the bulk rock compositions at Mt. Carmel. The fact that the crystallization sequences in the two suites are similar supports this assumption.

On the basis of these two assumptions, the following methodology has been employed to determine the intercumulus liquid composition and the percent cumulus plagioclase of the mafic cumulates. If the two complexes are genetically related, then two compositional vectors can be drawn, one the liquid line of descent (LLD) of the Mt. Carmel samples and the other, an intercumulus liquid (ICL) composition vector

connecting the two extreme assumptions of all (100%) cumulus plagioclase and no (0%) cumulus plagioclase in the Calhoun Falls suite (Fig. 23). In this schematic figure, the line labeled LLD represents the Mt. Carmel trend and a line labeled ICL represents a vector connecting the calculated compositions of the intercumulus liquids assuming no cumulus plagioclase (labeled 0%) and all cumulus plagioclase (labeled 100%). The vector ICL1 is calculated in the basis of the most calcic plagioclase found in the rock and ICL2 is calculated on the basis of the most sodic plagioclase found in the rock. The region of intersection (bold line) represents the range of possible intercumulus compositions due to the variation of the plagioclase. If the two liquids are in fact related, then the ICL and LLD vectors must intersect at a point where the intercumulus liquid of Calhoun Falls equals the composition of the Mt. Carmel liquid line of descent. Thus, the total alkalis are plotted against silica for both the Calhoun Falls and Mt. Carmel sample and the point of intersection determines the percent silica and alkalis in the intercumulus liquid. By knowing the weight percent silica in the intercumulus liquid, the weight percent modes, and the compositions of the phases, one can mass balance the cumulus and intercumulus fractions, adjusting the amount of plagioclase as needed to cause silica to balance.

In using this method the data were manipulated in the following manner. First an alkali versus silica variation diagram (Fig. 24) was chosen over other compositional plots because of the excellent linear variation of the LLD of the Mt. Carmel suite. A goodness of fit test

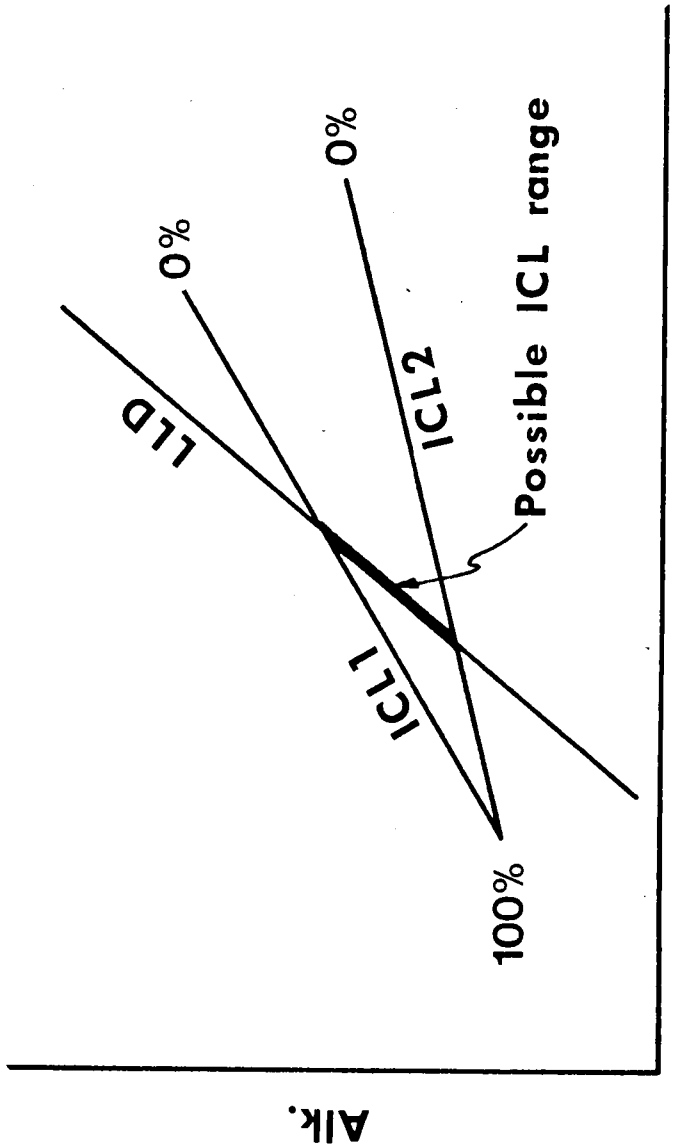

Figure 23. Schematic diagram showing how the intercumulus liquid composition of cumulate gabbros samples from Calhoun Falls complex is calculated.

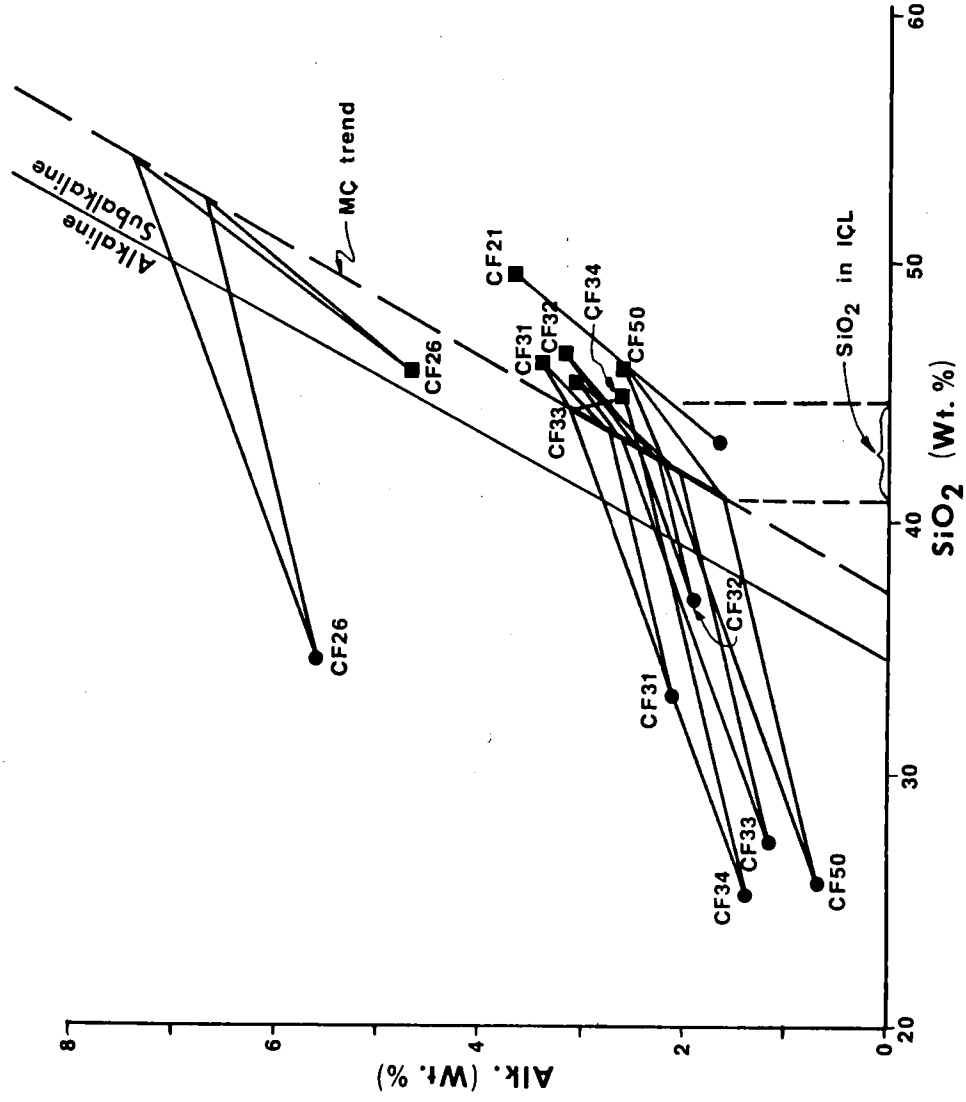

Figure 24. Total alkali vs. silica diagram used to calculate the intercumulus liquid composition (ICL) of the Calhoun Falls complex cumulate gabbros. Dots represent the ICL of samples assuming 100% plagioclase is cumulus and squares represent the ICL of samples assuming no plagioclase is cumulus.

through the Mt. Carmel samples yields an R^2 of 0.95 for a linear regression analysis, thus assuring a low error associated with this projection. Furthermore, this plot was used because the weight percent silica of the intercumulus liquid can be determined. Because silica is the most abundant oxide in these rocks, error is again minimized. Second, all bulk rock and mineral analyses were normalized to 100% anhydrous totals. Because all the cumulus phases that were subtracted are anhydrous, this normalization should not seriously affect the results. Third, the problem of zonation in plagioclase was handled in the following manner. The most calcic and sodic plagioclase analyses were determined for the troctolites and gabbronorites. The slope (alkali/silica) was plotted as vectors on Fig. 24. The region between these two vectors, in which they intersect the LLD, represents the maximum variation one can expect in the diagram due to plagioclase variation for each sample.

Results of this analysis (Table 7) indicate that between 15 and 30 weight percent plagioclase is cumulus. The intercumulus liquid composition for each sample and the mean are also shown. If these are truly intercumulus liquid compositions for the Calhoun Falls suite, then constituents other than silica and alkalis should also be comparable to the Mt. Carmel trend over the range of intersection. To verify this, the mean Mt. Carmel composition was computed over the rang of intersection and a Students t-test was performed, comparing this mean to the mean intercumulus liquid composition. At the 95% confidence level, $t_{0.05}$ (two tailed test) with 14 degrees of freedom, the critical value of

Table 7. Results of the intercumulus liquid calculations of the gabbros from the Calhoun Falls complex.

	Mineral Compositions Used for Intercumulus Liquid Calculations										Calculated Intercumulus Liquid Compositions and Weight % Cumulus Plagioclase					Mean and Std. Dev. for Calhoun Falls ICL (B.)		Mean and Std. Dev. for Intersected Region of Mt. Carmel LLD		
	Pg	CPx	Ol	Opx	Hbl	Ilm	Mag	Epid	Aputite	Bt	CF50	CF31	CF32	CF33	CF34	$\bar{x}_n$=5	$\sigma_{\bar{x}}$	$\bar{x}_n$=11	$\sigma_{\bar{x}}$	t-Test*
SiO_2	51.97	51.18	38.52	54.43	40.45			39.67	52	37.48	42.85	44.57	43.70	43.53	42.36	43.58	.64	43.41	2.37	0.08
TiO_2		.76		.37	3.46	51.9	1.06			2.36	.92	.98	.84	.56	.91	.84	.17	4.06	1.01	8.10
Al_2O_3	30.58	3.73		1.95	11.93	.09	.65	33.66		16.36	14.59	23.69	19.90	24.00	21.06	20.65	3.81	16.85	2.41	.85
FeO	.25	7.11	21.23	13.10	10.59	41.84	92.63			7.67	11.24	2.63	6.29	2.63	3.34	5.23	3.69	10.93	1.96	1.59
MnO				.41	.22	3.13	.14			.04	.30	.10	.11	.08	.11	.14	.09	.15	.07	3.19
MgO		15.84	40.14	28.51	14.44	2.91	.37			19.94	20.47	10.04	14.49	13.73	14.63	14.67	3.74	7.10	2.01	2.02
CaO	13.12	20.84	.02	1.18	11.63			24.68			6.92	14.08	10.86	12.27	13.30	11.49	2.82	11.03	1.97	.17
Na_2O	3.97	.54		.08	2.54					.59	1.73	2.66	2.43	2.28	2.01	2.22	.36	2.45	.83	.81
K_2O	.19				1.14					9.11	.42	.69	.64	.50	.58	.57	.11	.70	.65	.79
P_2O_5									41		.54	.56	.74	.43	.79	.61	.15	.61	.61	.00
(Fe_2O_3)						(4.82)	(58.7)													
Total	100.0	100.0	100.0	100.0	96.37	100.39	101.06			93.55	100.00	100.00	100.00	100.00	100.00					
Wt. % Cum. Pg											27%	15%	30%	15%	15%					

*Two-tailed t-test of the average reported from mean and standard deviation for Calhoun Falls ICL (B.).

**At the 95% confidence level, $t_{0.025}$ with d.f. = 14, the critical value of t = 2.145, the evidence supports the conclusion that all oxide populations except TiO_2 and MnO are the same.

t = 2.145 was not exceeded by any of the major or minor elements except MnO and TiO_2, Table 7, supporting the conclusion that the two liquids are not significantly different. Because MgO and FeO are near the critical value of t = 2.145, 2.02 and 1.59, respectively, it is possible that some small portion of the olivine and clinopyroxene is also postcumulus. This observation is supported by noting the FeO is too low and MgO is too high in the intercumulus liquid, e.g., is that iron-rich ferromagnesian phases must be added to the intercumulus liquid to mass balance the ILC to equal the LLD.

Greenwood Complex

Of the three intrusives studied, the Greenwood complex yields the least amount of information due to its very poor field exposure. This lack of outcrop, on the other hand, is in itself significant when considered with other data. Aeromagnetic intensity maps of the complex (Fig. 4, p. 32) in conjunction with soils surveys by Camp and Herren (1980) indicate that the Greenwood complex is in fact probably two or three separate intrusives in near proximity that may or may not be connected at depth. On the basis of the few samples that were collected from this complex, cumulus rocks appear to be prominent away from the margins and roof pendants, whereas the rocks exhibiting diabasic textures are near the roof pendants and margins. Because these two textural extremes are gradational, it appears that the diabasic samples represent rapidly cooled rocks while the cumulus rocks represent samples from the same magma that cooled slowly.

If the samples from Greenwood that contain diabasic textures are rapidly cooled basaltic magmas, then they should represent liquid compositions. However, they do not fall on the Mt. Carmel alkali versus silica trend, being higher in silica and lower in alkalis in relation to Mt. Carmel (Fig. 15, p. 73), but they are closer to the Mt. Carmel trend than the other rocks from Greenwood. Furthermore, calculations to derive the intercumulus liquid compositions fail to yield acceptable results because the ICL vectors for the Greenwood cumulus suite do not cross the Mt. Carmel liquid line of descent (Fig. 25). These two observations suggest that the magmas that generated the Greenwood suite are different than those that produced the Mt. Carmel and Calhoun Falls complexes. This interpretation is clearly seen when chemical data are plotted on phase diagrams.

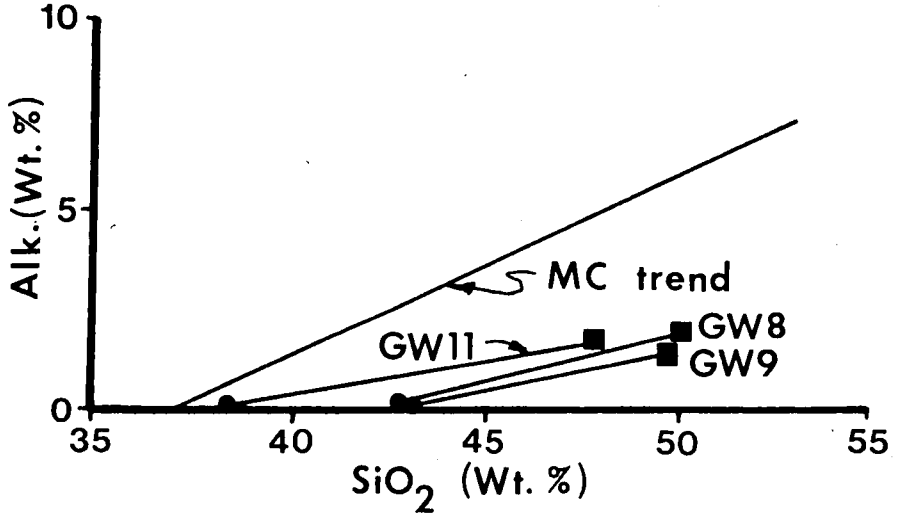

Figure 25. Total alkali vs. silica diagram of cumulate gabbro samples from the Greenwood complex showing that the calculated intercumulus liquid compositions do not cross the Mt. Carmel trend.

The data from the three complexes have been plotted on O'Hara's (1968, 1976) polybaric phase diagrams (Fig. 26). These projections are into the CMAS pseudo quaternary where the plotting parameters are calculated as percentages of

C = (mol. prop. $CaO-3.3P_2O_5+2Na_2O+2K_2O$) x 56.08

M = (mol. prop. $FeO+MnO+NiO+MgO-TiO_2$) x 40.31

A = (mol. prop. $Al_2O_3+Fe_2O_3+Cr_2O_3+TiO_2+Na_2O+K_2O$) x 101.96

S = (mol. prop. $SiO_2-2Na_2O-2K_2O$) x 60.09

Projection is from olivine into the CS-MS-A plane, and from diopside into the C_3A-M-S plane. For the projection to be valid, the mineral through which the projection is made must be present in the rock. Thus, projections through olivine are not valid for syenites (containing no olivine), but they are presented in Fig. 26 for comparison. Cox et al. (1979) caution that distortion due to the oblique projections may occur, and any interpretation of these diagrams should be made with care.

The projection through diopside into the C_3A-M-S ternary shows the approximate normative character of the three complexes (Fig. 26). The Mt. Carmel samples and the unaltered gabbros of Calhoun Falls plot along the olivine gabbro thermal divide indicating that these samples are controlled by olivine-diopside-plagioclase fractionation. The Greenwood samples plot in the plagioclase-enstatite-diopside olivine subquaternary suggesting that they are silica saturated. All three complexes plot along the olivine-garnet periodotite-enstatite-liquid control plane in the CS-MS-A ternary (Fig. 26), suggesting little

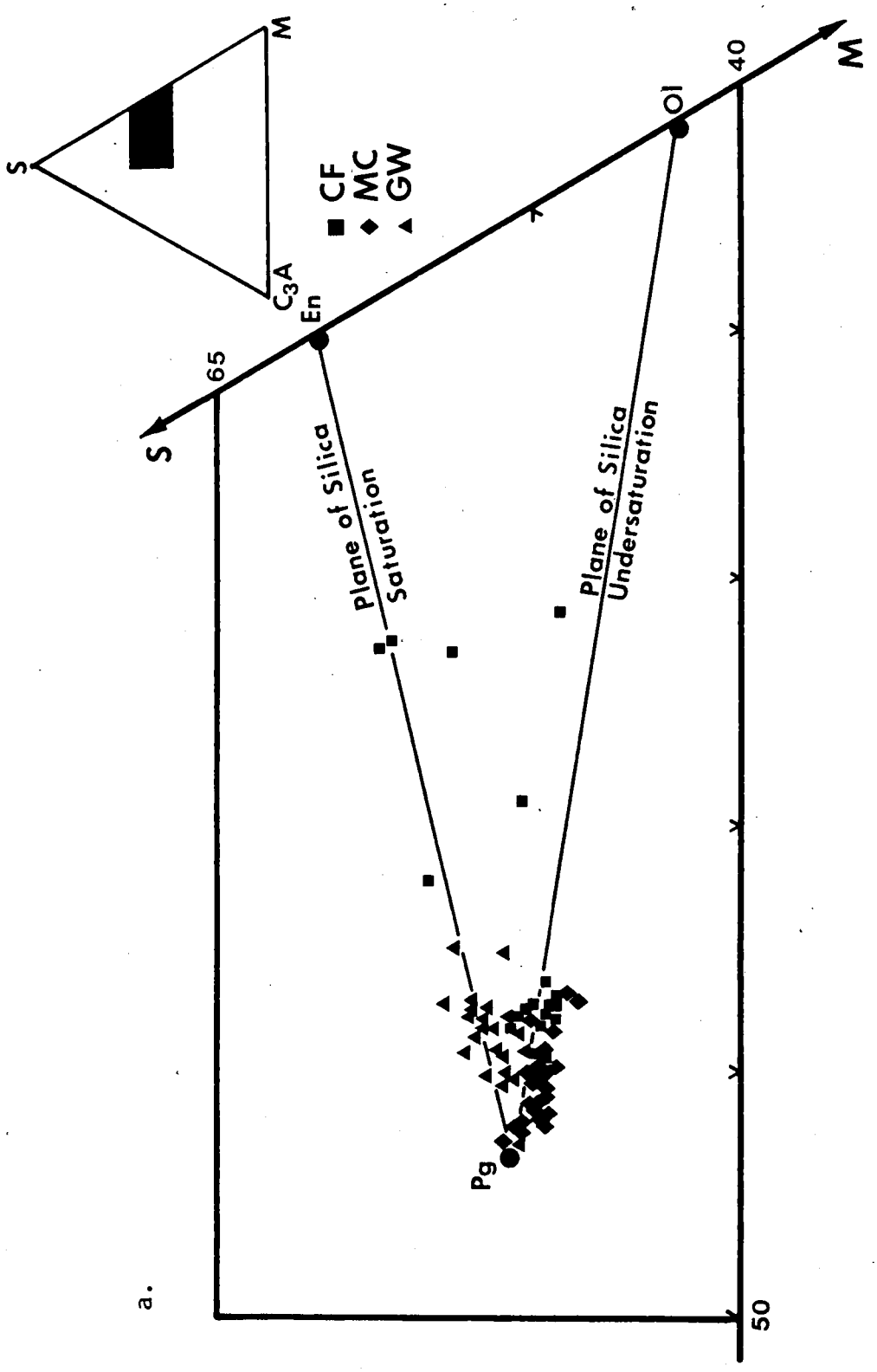

Figure 26. Polybaric phase diagrams (O'Hara, 1976) for the Calhoun Falls (CF), Mt. Carmel (MC), and Greenwood (GW) complexes.

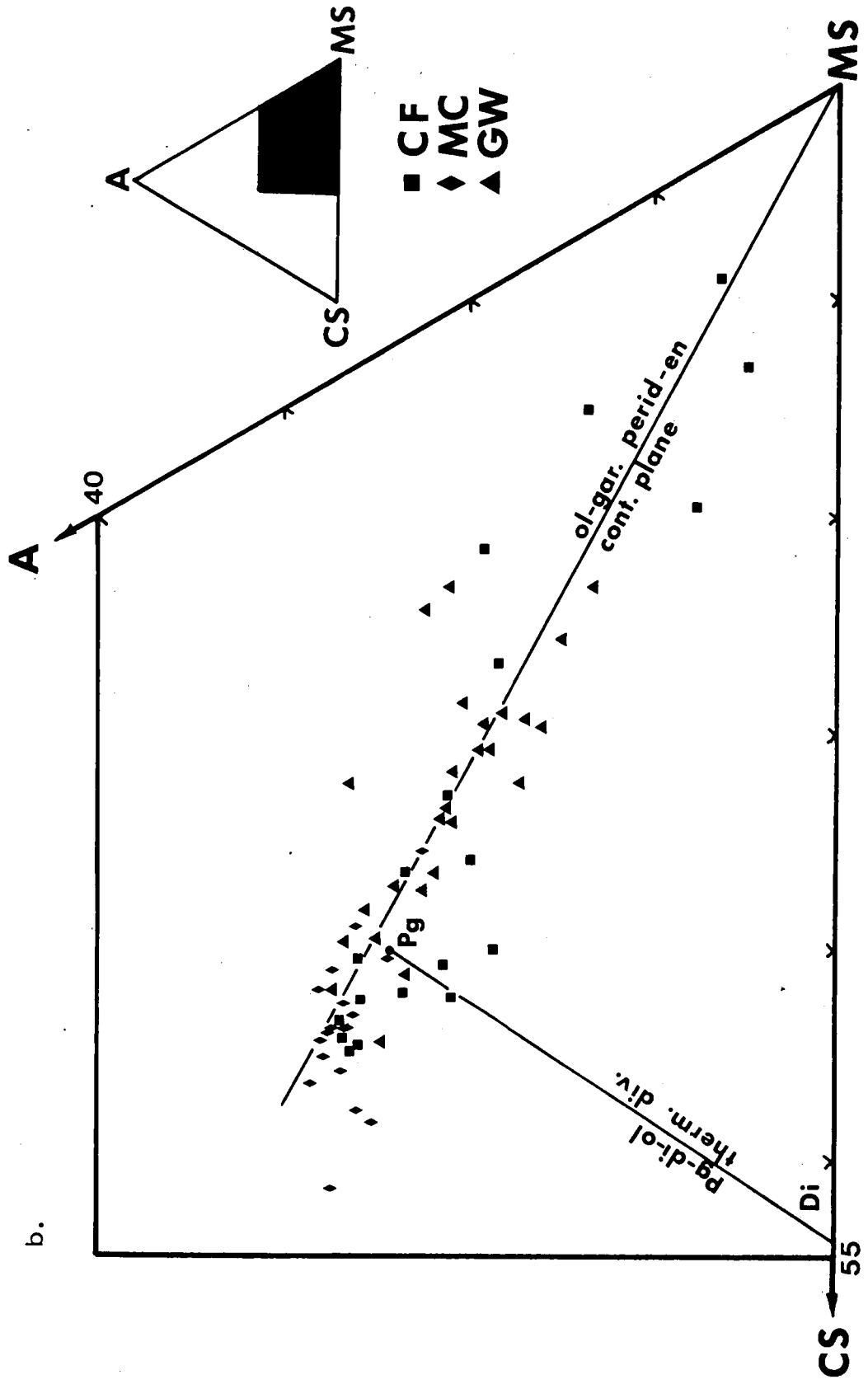

Figure 26 (continued)

crustal contamination during emplacement. The pressure of partial melting can theoretically be determined from these projections for basaltic glasses (O'Hara, 1968); however, such does not appear to be the case with the samples from the study area.

The Greenwood complex appears to have been derived from the same approximate mantle material as the Mt. Carmel and Calhoun Falls complexes, as suggested by their close proximity and the fact that they all lie on the garnet-peridotite line. The silica enrichment of the Greenwood complex does not appear to be due to crustal contamination, but may be due to advanced fractionation from more primitive magma that crystallized at depth relative to the present day erosional surface.

Relationship of the Study Area to Other Mafic Intrusives in the Charlotte Belt

As pointed out in the previous section, significant differences exist between the three complexes in the study area. When compared to the other mafic intrusives in the Charlotte belt, however, there are important similarities among these plutons, making them unique among all the intrusives.

Although they span a wide compositional range which is approximately the same as that for the other mafic intrusives, differences exist between the intrusives in the study area and those to the north (Table 8). All of the intrusives in the study area fractionated olivine + clinopyroxene before plagioclase. Such is not the case with the intrusives outside the study area, where plagioclase participated early

Table 8. Summary of the differences between the northern magmatic center as characterized by the Concord complex (McSween et al., 1984), and the southern complex as characterized by the Mt. Carmel complex (this study).

Summary	North (e.g., Concord)	South (e.g., Mt. Carmel)
Chemistry	Tholeiites	Tholeiites
Textures	Cumulates	Cumulates & Noncumulates
Rock Types	Metagabbro Troctolite Gabbronorite Syenite	Metagabbro Troctolite Gabbronorite Syenite Ultramafics
Fractionation	Early Pg + Ol Later Pg + Cpx + Ol	Early Cpx + Ol Later Pg + Cpx + Ol
Ultimate Fractionation Product	Syenite	Syenite

in the fractionation history (e.g., Hermes, 1968; Butler and Ragland, 1969; Olsen et al., 1983; and McSween et al., 1984). For this reason, ultramafic rocks formed in the study area on a scale not seen elsewhere in the Charlotte belt. It is not clear whether the formation of ultramafic rocks is due to a compositional difference inherent in the parental magmas, due to different conditions of crystallization, or due to both. The presence of biotite and brown hornblende in all of the intrusives, both within the outside the study area, suggests that water fugacities were similar. Similar pressures of crystallization

(about 5 kb) were determined for gabbros outside the study area (McSween et al., 1984) and less than 10 kb in the study area (this work). Although pressure of crystallization and water fugacity are far from being the only conditions that control the phases that crystallize from a magma, their similar character suggests that different magma compositions are, in part, responsible for the different minerals seen in the different regions.

The regional outcrop pattern of the intrusives within the Charlotte belt is further evidence of the unique character of the study area. An approximate north-south trending line of intrusives in North and South Carolina contains ten major plutons from the Farmington pluton in North Carolina to the Chester pluton in South Carolina (Fig. 1, p. 2). The study area forms a kink in the southern extention of this linear trend from the Newberry pluton to the east in South Carolina to the Delhi pluton in Georgia. The trend is separated by a region containing few mafic intrusives. The linearity of these two trends is certainly open to interpretation, and may indeed be considered two distinct groups with no linear relationship. The fact that the two groups are separated by a region where no mafic plutons are formed and that they do contain different intrusive character does suggest that there are two mafic intrusive provinces in the Charlotte belt of North and South Carolina. To the south of the study area the Gladesville intrusive contains some olivine gabbro but is predominated by norite consisting of orthopyroxene and plagioclase (Carpenter and Hughes, 1970). Thus the general trend is early plagioclase

fractionation both to the north and to the south, and no early plagioclase fractionation in the study area. Whether or not these three regions represent distinct and separate intrusive centers or whether they represent variations in one trend is open to interpretation.

It is difficult to speculate on the genetic implications of this trend when the nature of the plate margin that formed the mafic intrusives is so poorly understood (e.g., McSween et al., 1984). None the less, Gill (1981) points out several possible contributing factors affecting along-strike compositional variations in compressional plate boundaries. Variations in crustal thickness encountered by an ascending magma, heterogeneity of source materials, edge effects at places where convergent plate boundaries terminate in tear faults, and differing convergence rates are four possible factors. He notes that with few exceptions, continental crust thickness is not sufficient to produce andesites. The crustal thickness may affect more mafic magma compositions, however, such as those encountered in the study area. A smaller amount of crustal contamination would be needed to change the composition of a gabbroic magma than an andesitic magma. Olsen et al. (1983) demonstrated the Concord gabbro-syenite complex was not contaminated, however, and it seems unlikely that others in the Charlotte belt would be (McSween et al., 1984). Hughes (1982) noted that due to the high liquidus temperature of mafic rocks, they have a tendency to form chill zones during intrusion, thus armoring them from significant country rock contamination. It is impossible to evaluate the effects of source material heterogeneities in the Charlotte belt due to

the controversy surrounding the interpretation of the COCORP data in the region (e.g., Long, 1979; Hatcher and Zietz, 1980; Cook et al., 1981; Cook et al., 1983; and Iverson and Smithson, 1982).

Abrupt changes in the composition of volcanics in modern island arcs occur directly above tear faults in the subducted plates (Gill, 1981). Differing subduction rates can occur along either side of these tear faults, however. Miyashiro (1974) classified volcanic arcs by convergence rate, crustal thickness and percent calc-alkalinity of the extrusive. He noted that in regions with high convergence rates with thin crusts, most eruptives are tholeiitic. In areas with low convergence rates and thicker crusts, few are tholeiitic.

It appears possible, therefore, that the difference in mafic rock types from north to south in the Charlotte belt may be due to a convergent plate system in which there are different subduction rates along strike and where the subducted plates are separated by tear faults. This would account for the different linear trends noted in the mafic intrusives in the Charlotte belt as well as the regions where few such intrusives are encountered. The "kink" in the trend of the mafic intrusives as noted in this study (Fig. 1, p. 2), and the offset noted by Kane (1983) fall along the transform fault that Kane (1983) hypothesized. This transform fault runs from Charleston, S.C., to a region approximately between the two magmatic trends (Fig. 27). On this basis, two petrographic provinces are proposed for the mafic intrusives of the Charlotte belt; the troctolite/gabbronorite province extending from the Farmington to the Chester plutons to the north,

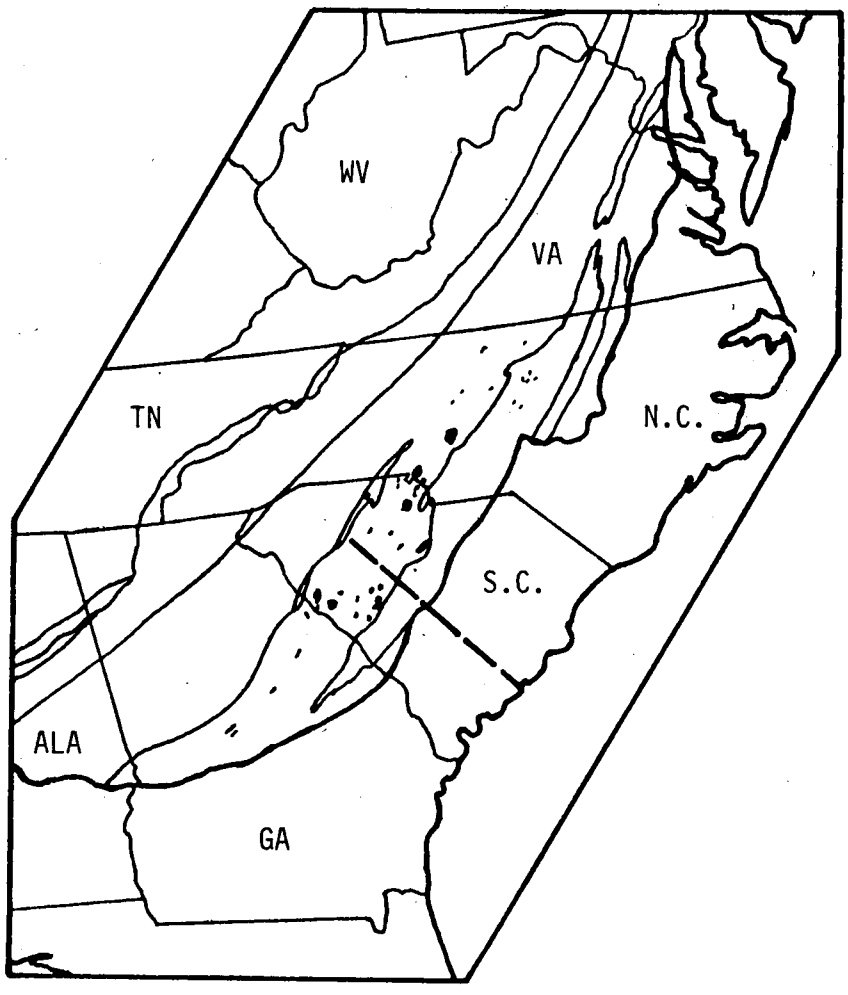

Figure 27. Map of the southern Appalachians showing the proposed transform fault (Kane, 1983) separating the northern and southern mafic magmatic centers in the Charlotte belt.

and the ultramafic/gabbronorite province extending from the Newberry to the Delhi plutons in the south.

The Metagabbro Problem

The Mt. Carmel complex raises some interesting questions concerning the genetic relationship between gabbro and metagabbro. This work has shown the Mt. Carmel complex has undergone what appears to be continuous fractionation from metagabbro, gabbro, to syenite. Evidence for this continuous fractionation include bulk and trace element trends (e.g., Figs. 15 and 17, pp. 73 and 76, respectively), and least-squares regression analysis, relating all lithologies to a single intrusive event. This conclusion is contradicted, however, by the models proposed by Hermes (1968), and McSween et al. (1984). The objectives of this section are two-fold: (1) to test the data obtained from Mt. Carmel against the Hermes (1968) and McSween et al. (1984) model, and (2) to propose an additional model that may also be valid in light of existing evidence. Due to the paucity of the existing data, this section explicitly does not favor one model over the other. By proposing an additional hypothesis, I hope to stimulate other workers to investigate the gabbro-metagabbro association.

The Data

Several lines of evidence used to shed light on this problem include: (1) isotopic age dates, (2) bulk rock chemistry, and (3) textural information. Unfortunately, no contacts between gabbro

and metagabbro have been observed either in this or previous published studies.

McSween et al. (1984) obtained a preliminary plagioclase whole rock isochron age of 567 ± 50 my for a sample of practically unaltered Barber metagabbro, but they also found an age using the same method for the Barber gabbro of 479 ± 24 my, clearly anomalous if the Taconic orogeny was about 460 my as suggested by Glover et al. (1983). As McSween et al. (1984) point out, this age for gabbro is inconsistent with their model if the peak of the Taconic thermal event was 460 my. Furthermore, the Barber complex is unique chemically from all other complexes in the Charlotte belt, being higher in silica and potassium and lower in magnesium (Clark, 1980; and McSween et al., 1984). The Barber age dates and chemistry do not seem to reflect normal conditions of petrogenesis in the Piedmont and cannot be considered in a "general" petrogenetic emplacement model for gabbro-metagabbro associations.

An alkali versus silica plot (Fig. 28) of average gabbro, metagabbro, and syenite for Mecklenburg (Hermes, 1966), Barber (Strange, 1983), and Mt. Carmel (Medlin, 1968, and this study combined) show interesting trends. With increasing alteration from gabbro to type 4 metagabbro, both alkalis and silica increase in both the Mecklenburg and Barber plutons but with very limited variation as compared to other bodies. The opposite is true for the Mt. Carmel trend, however, where metagabbro contains less silica than the gabbro. Although Hermes considered metamorphism to be isochemical,

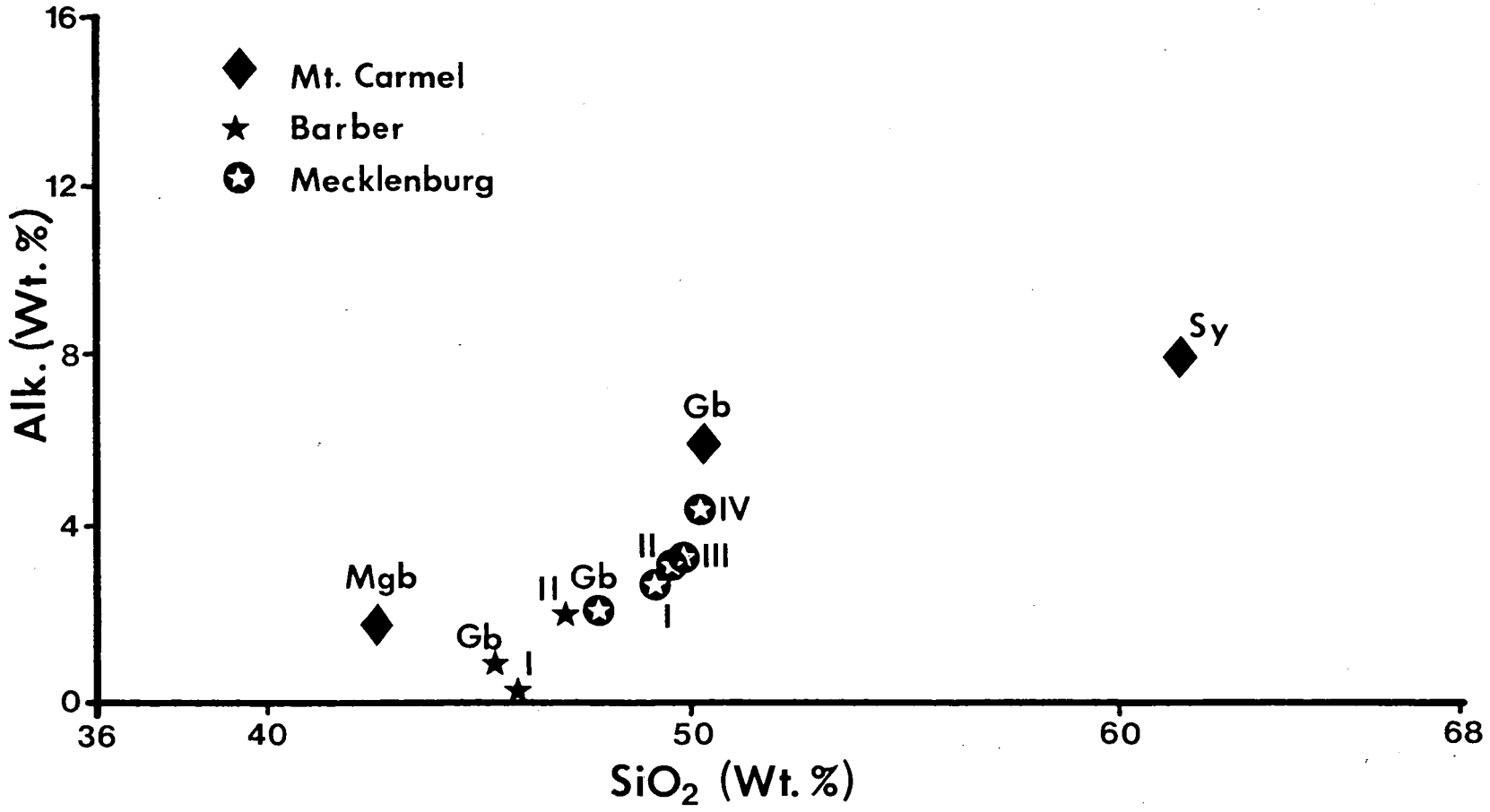

Figure 28. Total alkali vs. silica plot of average compositions of lithologies from the Mt. Carmel, Barber (Strange, 1983), and Mecklenburg (Hermes, 1968) complexes.

alkalis may be somewhat mobile, but silica on the other hand, should not vary extensively. Furthermore, these samples plot in approximately the same region as the Calhoun Falls and Greenwood complexes, although gabbros are more primitive than metagabbros in the Mecklenburg complex. Thus, Hermes (1968) is probably correct in considering the bulk chemistry to have survived metamorphism and to approximate the premetamorphic chemistry of the suites. In his data, Hermes (1968) listed two type 4 metagabbro analyses. These are compositionally banded, suggesting that they were metamorphosed in a stress field. The type 3 metagabbros are banded but do not contain compositional banding. All other metagabbros retain their original igneous textures.

Almost all intrusives in the southern Appalachian Piedmont contain cumulate textures in the unaltered gabbros (e.g., McSween and Nystrom, 1979; Fronabarger and McSween, 1983; and McSween et al., 1984). Mt. Carmel is unique in this respect because of its lack of such textural varieties.

In his study of the Mecklenburg complex, Hermes (1968) concluded that the following sequence of events occurred. Prior to the Taconic orogeny, a mafic magma was intruded into the Charlotte belt protolith and crystallized to form a mafic pluton. During the Taconic orogeny this pluton was regionally metamorphosed to form metagabbro, whose character was largely dependent on the local porosity and the distribution of water available for hydration of mafic phases. He hypothesized that an irregular distribution of water within the pluton

would account for the irregular distribution of the three types of metagabbro he described. After Taconic metamorphism, the Mecklenburg gabbro was intruded into the metagabbro. McSween (1981b) and McSween et al. (1984) have expanded this model to include all such gabbro-metagabbro associations found in the southern Appalachian Piedmont, suggesting that the early intrusive event would produce a zone of weakness along which later post-Taconic magmas could migrate.

This model is consistent with most of the data. It does not explain the preliminary Sm-Nd data from the Barber pluton (McSween et al., 1984), nor does it explain the continuous chemical trends seen in the Mt. Carmel bulk and trace element chemistry. It is consistent with the data obtained from the Mecklenburg complex by Hermes (1968) and the other plutons studied by McSween et al. (1984). The isotopic data from Barber and the chemical data from Mt. Carmel demand a single intrusive model, however.

Single Intrusive Model

Another model is to have one single intrusive event form all lithologies in a given complex. The timing of intrusion can be either pre-, or syn-Taconic (e.g., Barber complex) or post-Taconic (e.g., Mt. Carmel).

If the intrusive event is pre- or syn-Taconic, then the Barber Sm-Nd data of 567 my can be accepted as valid and the alteration of the metagabbro protolith was due to the Taconic regional metamorphic event as suggested by McSween et al. (1984). Unfortunately, too

many reliable isotopic ages have been obtained from other plutons (see Chapter I of this work) for this model to represent the "general case." Most of the gabbros are about 400 my, definitely post-Taconic.

If the intrusive event is post-Taconic, then the Sm-Nd data from Barber must be rejected, or the Barber pluton is different (as suggested by its chemistry, McSween et al., 1984). Furthermore, a mechanism must be found to form the metagabbro while preserving Hermes' (1968) textural classification of metagabbro. This difficulty can be resolved by taking recourse to the textural descriptions provided by McSween and Nystrom (1979), and McSween et al. (1984) in which they detail cumulate textures for the gabbros in the Charlotte belt. If early crystallization products in any given intrusive are formed with cumulate textures and subsequently autometasomatized, then the resulting textures should be essentially equivalent to those that would form through regional metamorphism. Under this mechanism, however, strong shearing stresses required to impart foliation (Hermes, 1968) are not needed. Indeed, most type 3 metagabbros do not exhibit cataclastic textures. The early crystallization products would be hydrated and altered by stewing in the residual liquids produced by advanced crystallization. Abundant brown hornblende and biotite in unaltered gabbros suggest that these intermediate rocks were formed under high fO_2 conditions. Many of the type 3 and type 4 metagabbros are banded, however, suggesting metamorphic segregation of mineral phases rather than autometasomatism was responsible for the alteration.

The Mecklenburg metagabbros are higher in silica (e.g., more evolved) than the gabbros (Hermes, 1968), apparently arguing against this model. Plagioclase is the mineral phase that imparts the layered fabric to most cumulates in the study area, while ferromagnesian minerals do not. If the early crystallization products in the Mecklenburg complex were composed primarily of cumulus plagioclase, an early fractionating phase (McSween et al., 1984), then they would appear to be more evolved than the later products. The limited variation in the chemical data as seen in Fig. 27, p. 111, also support this idea. The samples from the Greenwood and Calhoun Falls complexes both contain abundant cumulus textures and limited evolutionary trends, like Mecklenburg.

If this hypothesis is correct, then the later, more evolved magma must be saturated with respect to water, probably forming pegmatitic veins in the gabbro. Mafic pegmatities have been described in the Seroyer Branch mafic-ultramafic complex in the Inner Piedmont of Alabama (Clark, 1973), but none have been found in the Charlotte belt. Thus, it is not known if the mafic intrusives of the Charlotte belt became saturated with respect to water.

Recapitulation

Neither the multiple intrusive model, nor the single intrusive model explains all the data. It is possible that the plutons from each trend formed under different circumstances, some via two pulses, some via one single pulse, rendering identical results. If such is the case, then it appears logical that the plutons found in the northern magmatic

center were formed through two pulses and the plutons in the study area through a single pulse.

If all gabbro-metagabbro intrusives formed by the same mechanism, then more data are needed to resolve the problem. Isotopic ratios capable of remaining unchanged during the Taconic thermal event and that can be used on metagabbros (e.g., Sm-Nd systematics) would be invaluable. The best data, however, are direct views of a metagabbro-gabbro contact from which the existence of absence of cross-cutting relationships can be verified.

CHAPTER VI

HEAT FLOW IN GABBROIC ROCKS

Introduction

The previous chapters have shown that the gabbros of the southern Appalachians are often complex bodies composed of several different lithologies. These chapters not only offer a model for their formation, but they also provide considerable insight into the petrologic character of gabbros. It is the intent of this section to demonstrate that gabbroic bodies in general have some physical characteristics that other rock types do not have which may make them worth further consideration as nuclear waste repositories. Because the three complexes studied represent a wide range in chemical, lithologic, and petrologic characteristics, they are probably representative of mafic intrusives in general. Furthermore, the thermal characteristics of rocks are primarily a function of the mineral constituents of which the rocks are composed. Thus, the extremes of the thermal properties of mafic intrusives are probably represented by the plutons studied in the previous chapters (Table 9). Although the heat transfer phenomena are studied in this chapter, other petrologic criteria important to the study of gabbro plutons as potential repository sites are also summarized.

High-level radioactive waste from such sources as the commercial and defense nuclear industries contains significant quantities of short- and long-lived isotopes which generate heat during decay (E.I.

Table 9. Thermal properties for several rock types found in the study area, Daly et al. (1966).

Property	Symbol	Dunite	Gabbro	Syenite
Density	$\rho(kg/m^3)$	3350	2980	2950
Specific Heat	$c(m/s^2K)$	940	945	991
Thermal Conductivity	k(J/omK)	2.1	2.0	1.7

du Pont de Nemours and Company, 1980a, 1980b). The Department of Energy has considered burial of this radioactive waste in salt, basalt, shale and granite bodies (U.S. DOE, 1977, 1979; and Storch and Prince, 1979), and it has expended considerable effort in studying the thermal effect the waste will have on the rocks in which it is buried. Gabbroic bodies may have advantageous properties that the other proposed host rocks do not have, however (Ringwood, 1980). Although the thermal properties of most igneous rocks are similar (e.g., Mirkovich, 1968; Horai, 1971; Horai and Baldridge, 1972; and Hanley et al., 1978), the solidus temperatures are significantly different (about 650°C for granite and 1100°C for gabbro). For this reason, it is expected that either more waste of the same age, or younger (i.e., thermally hotter) waste can be buried in gabbro as compared to granite. Maximum temperatures at the canister-rock contact are currently restricted to less than 300°C, however, by DOE. Plutonic bodies such as granites and gabbros contain practically no intergranular permeability (Ringwood, 1980) as compared to the sedimentary and volcanic rocks. Ringwood (1980) suggested that quartz-free plutonic rocks such as slightly altered gabbros and diorites would be less apt to

contain significant secondary permeability (along joints and fractures) due to their higher degree of ductility as compared to granites. The objectives of this study are (1) to model the thermal effect of high-level radioactive waste in gabbro, and (2) to compare the age and amount of the waste that can be buried in gabbro and granite. In the following discussion all terms are used as defined in Appendix B.

Theoretical Development

Heat transfer within a system is governed by the energy balance equation:

$$\dot{E}in + \dot{E}g = \dot{E}out + \dot{E}s \qquad (6.1)$$

where $\dot{E}in$ = energy flowing into the system,

$\dot{E}g$ = energy generated inside the system,

$\dot{E}out$ = energy flowing out of the system, and

$\dot{E}s$ = energy stored in the system.

Because energy is conserved, the above equation must be satisfied. The amount of heat flow by conduction in any direction is given by

$$q = -kA\ \partial T/\partial x, \qquad (6.2)$$

where q = the heat flow,

k = thermal conductivity of the material,

A = the area perpendicular to the heat flow,

T = the temperature, and

x = the direction of heat flow.

The energy flux generated within a solid is given by

$$\dot{E}g = \dot{q}V \tag{6.3}$$

where $\dot{q}$ = the volume-specified heat flow rate, and

V = the volume within which it is defined.

The energy stored in a system is expressed as

$$\dot{E}s = \rho c V \, \partial T/\partial t, \tag{6.4}$$

where ρ = the density of the material,

c = the specific heat of the material,

V = the volume,

T = the temperature, and

t = time.

By substituting these rate equations (6.2-6.4) into the energy balance equation (6.1), the well known heat conduction equation (e.g., Carslaw and Jaeger, 1959) is derived as

$$\frac{\partial}{\partial x_i} \left(k_{x_i} \frac{\partial T}{\partial x_i}\right) + \dot{q} = \rho c \frac{\partial T}{\partial t} \tag{6.5}$$

where x_i = the cartesian directions. If kx = ky = kz = k = constant, then eq. (6.5) becomes

$$f(T) = \rho c \frac{\partial T}{\partial t} - k \frac{\partial^2 T}{\partial x_i^2} - \dot{q} \equiv 0 \tag{6.6}$$

Thus this equation expresses the temperature of a system as a function of time, position, and heat generation rate.

Since eq. (6.6) is second order and transient, two boundary conditions and one initial condition must be specified. The initial condition used in this work is

$$T_{(x_i)} = T_{0(x_i)} \qquad \text{at } t = 0 \tag{6.7}$$

and the boundary conditions are

$$k|_{x_i}^{t} \frac{\partial T}{\partial x_i} + \dot{q} = 0 \qquad \text{at } t > 0 \text{ on } S_1 \tag{6.8}$$

$$k|_{x_i}^{t} \frac{\partial T}{\partial x_i} + h(T - T_\infty) = 0 \qquad \text{at } t > 0 \text{ on } S_2 \tag{6.9}$$

where S_1 and S_2 are the boundary surfaces where the boundary conditions are applied. In the actual analysis, by setting S_1 and S_2 at infinity, equations (6.8) and (6.9) need not be evaluated to obtain a solution to eq. (6.6).

Finite Element Method

In the present case we want to find the temperature of a gabbro as a function of time and position after a decaying heat source (high-level radioactive waste) has been buried in it. Thus, the temperature of any given point in the gabbro will vary as a function of its distance from the source, with time, and as a function of the change in the heat generation rate of the source. An exact solution may or may not be determinable for this type of transient problem, depending on the nature of the heat generation decay curve, and the

complexity of the geometry and initial conditions that are imposed on the problem.

It is for this reason that the finite element method has been developed. The basic philosophy of the method is to replace the exact equation of the physical problem with an approximate one whose error can be controlled using precise mathematical tools. Since error is introduced, it is important to understand where the error occurs and how it is controlled so that the true solution to the problem can be deduced from the approximate solution.

Excellent descriptions of finite element computational analysis can be found in several textbooks on the subject (e.g., Rao, 1981; and Baker, 1983). The following summary is taken from these two sources. Although the mathematical tools used in finite element analysis vary, the basic method follows several rigorously defined steps:

1. discretization of the solution domain,
2. selection of an adequate interpolation equation,
3. derivation of characteristic element matrices and load vectors,
4. assembly of element equations into a global system of equations over the solution domain, and
5. calculation of the dependent variable at the nodal positions.

Each of these steps is described in the context of the present study.

Discretization

Once an equation is developed that governs the behavior of temperature in time and space, the domain over which the variation of

temperature is desired is divided into subdomains called finite elements. Each element is connected to other elements by boundaries along which points called nodes are defined. The temperature at each nodal point will be determined by calculating the equation of state of each element in contact with the node and solving these equations of state simultaneously. The selection of the position and shape of the finite elements affects the accuracy of the solution that will be obtained. In general, more elements provide a more accurate solution but the cost of computation also increases. Thus, accuracy is dictated in part by price, and a compromise between cost and accuracy must be made at this and other steps.

Interpolation Equations

After the solution domain is subdivided into finite elements, an equation approximating the variation of temperature with position in each element is selected. The Taylor's Series is most commonly used to describe the variation of temperature in space, and can be written as

$$T(x) = a_1 + a_2x + a_3x^2 + \ldots + a_{n+1}x^n \qquad (6.10)$$

This series is used because most functions can be so represented. If the variation of temperature in a small element can be considered linear, then eq. (6.10) becomes

$$T(x) = a + bx \qquad (6.11)$$

for any one dimension and

$$T(x) = a + bx + cx^2 \tag{6.12}$$

for quadratic variations. A discussion of the error associated with this approximation can be found in Baker (1983, pp. 169-175), who notes that it is second order accurate. In general, however, higher order approximation polynomials provide greater accuracy for more complex functions but require more computing time. On the other hand, error may be introduced by using a higher order function than is really represented by the real variation in the element.

Equations like (6.11) or (6.12) can be written in matrix form for an element e, as

$$T_{(e)_x} \equiv \{N_{k(x)}\}^T \{Q\}_e \tag{6.13}$$

where

$$\{N_{k(x)}\} = \begin{Bmatrix} N_i \\ N_j \\ N_k \\ \vdots \end{Bmatrix}^T = \begin{Bmatrix} a_i + b_i x + c_i x + \ldots \\ a_j + b_j x + c_j x + \ldots \\ a_k + b_k x + c_k x + \ldots \\ \vdots \end{Bmatrix}^T \tag{6.14}$$

and

$$\{Q\}_e = \begin{Bmatrix} q_1 \\ q_2 \\ q_3 \\ \vdots \end{Bmatrix} \equiv \begin{Bmatrix} T_1 \\ T_2 \\ T_3 \\ \vdots \end{Bmatrix} \tag{6.14}$$

The matrix $\{N_k(x)\}^T$ is standardized and the nodal coordinates of the element are i,j,...,p. Equation (6.13) describes the variation of temperature in each element in the solution domain and is substituted into the equations developed in the next step to obtain a solution to the problem.

Characteristic Element Matrices and Load Vectors

In this step, we wish to derive a functional (function of functions) that approximates the governing equation (6.6) using variational calculus. The objectives of this step is to find a set of equations for each element that adequately approximate equation (6.6) and that can be solved without recourse to calculus (i.e., that can be solved using a digital computer). The functional form that satisfies these criteria is

$$S_e \left[\int_{R_e^n} \{N_k\} \rho c \frac{\partial \bar{T}_e}{\partial t} d\tau - \int_{R_e^n} \{N_k\} \nabla \cdot k_e \nabla T_e d\tau - \int_{R_e^n} \{N_k\} \rho \dot{q}_e d\tau \right] \qquad (6.16)$$

where

R_e^n = domain of element e,

S_e = a matrix assembly operator, and

$\bar{T}_e$ = temperature distribution equation.

As shown by Baker (1983), this becomes

$$\sum_{e=1}^{M} \left[\Delta_e \rho_e c_e [M200] \{Q\}_e' - \Delta_e^{-1} k_e [M211] \{Q\}_e - \Delta_e \rho_e [M200] \{\dot{Q}\}_e \right] \qquad (6.17)$$

where [M200] and [M211] are characteristic matrices in n-dimensions. In qualitative terms, the three parts of eq. (6.17) express (1) the amount of heat the rock can store, (2) the rate the heat flows through the rock, and (3) the amount of heat generated per unit time (c.f., eq. 6.1).

Assembly of Element Equations

Once the equations expressing the variation of temperature for each element are derived, they are assembled into a global set of equations governing the entire solution domain. Thus equation (6.17) is solved for the temperature at each node for each time step. This assembly is performed by a matrix operator which is defined in Baker (1983, p. 77).

Calculation of Nodal Temperatures

The global system of matrix equations assembled in the previous step are solved for the temperature at each nodal point for one time step. The strength of the heat source is then calculated for the next time step, and the nodal temperatures are again calculated. Thus the solution is stepped through time over the solution domain.

Computer Implementation

A computer program, CFDL.TRAK, developed by A. J. Baker and M. O. Soliman (personal communication) was used to solve equation (6.6). It was modified to accept an unsteady heat source and to use variable time steps. The first modification was required in order to accurately model the nature of the decaying radioactive waste, and

the second, to increase efficiency in the solution. The program was used for two dimensional problems, and employs a tensor matrix Jocobian with time splitting for both linear and quadratic finite element cardinal basis.

The CFDL.TRAK program has several advantages. First, because both time steps and element sizes can be varied throughout the solution, the very-near-field, near-field, and far-field regions can be investigated simultaneously. Thus, it is not necessary to compute an average thermal loading for far-field investigations. For the purpose of this study, the very-near-field is defined as the interval within the canister to a distance of 3 meters from the center of the canister. The near-field is the interval from the very-near-field to a distance of 10 meters from the center of the canister. The far-field is the region greater than 10 meters from the center of the canister.

The second advantage of this program is that approximation error can be bounded by varying both the time step and the grid size throughout the solution domain. Thus, for an initially large, unsteady source term, approximation error is potentially more significant early in the solution and near the source. By using small time steps early in the solution, and small element spans near the source, this approximation error can be controlled.

Finally, it is possible to nondimensionalize the problem. In equation (6.17) a set of matrices are multiplied by scalar values (that represent physical properties), which can result in very large components in the resulting matrices after multiplication. Because the solution of these matrices requires the decomposition of them into

symmetrical upper and lower banded matrices (see Baker, 1983, for details), no solution can be found if there is a large difference in the individual components. Appendix C gives the details of the method of nondimensionalization that avoids this potential problem. An added benefit associated with nondimensionalization is that the physical rock properties (e.g., the scalar multipliers) can be changed after a solution is obtained. Thus, several solutions can be found for a given generic partial differential equation simply by changing the parameters of the rock properties.

Summary of the Finite Element Method

Once we can mathematically define what controls the variation of temperature in time and space, an equation is written that approximates this variation for a very small portion of space (a finite element) and for an instant in time. From this equation, and the known input data, we can solve for the temperature at any point (e.g., a node) in this small (relative to the whole area of interest) element with a low degree of error. Because this approximate function is the same for all other elements in space at any instant in time, we can assemble these equations into a large matrix containing p (number of nodes) equations with p unknowns. We then solve this matrix for one increment in time; then decide on a second interval of time, and substitute the results of the first time solution and resolve the matrix again. This is continued until the final time is reached. By using techniques noted in Baker (1983), approximation error can be bounded (hence controlled) during the solution through input parameter control including the time step and grid size.

Materials Properties

Mafic Rocks

The thermal properties of dunite, gabbro, and syenite in Table 9 were taken from Mirkovich (1968), Hanley et al. (1978), and Daly et al. (1966). These three igneous rock types were selected because they are representative of most mafic intrusives. All of these properties vary as a function of composition. Daly et al. (1966) found gabbro and olivine gabbro to range in density from 2,850 to 3,120 kg/m^3 for 27 samples that they measured, olivine gabbro being more dense. The median density is 2,985 kg/m^3 and the mean density is 2,976 kg/m^3. Thus a representative average of 2,980 kg/m^3 was selected. This value is identical to that determined for a diabasic gabbro by Mirkovich (1968).

The thermal conductivity of most materials varies as a function of temperature, and such is also the case with gabbro (Mirkovich, 1968; and Morgan and West, 1980) (Fig. 29). It is evident from this figure that the composition of the rock affects the conductivity more than does temperature. The large variation in thermal conductivity for the same rock types, as measured by different workers, may be due to experimental techniques rather than to inherent compositional differences (e.g., lines 2 vs. 6, or lines 3 vs. 5 in Fig. 29). Because the thermal conductivity for gabbro only varies between 1.5 and 2.5 J/smK over a temperature range of 800°C, a constant value of 2 J/smK was selected to be representative.

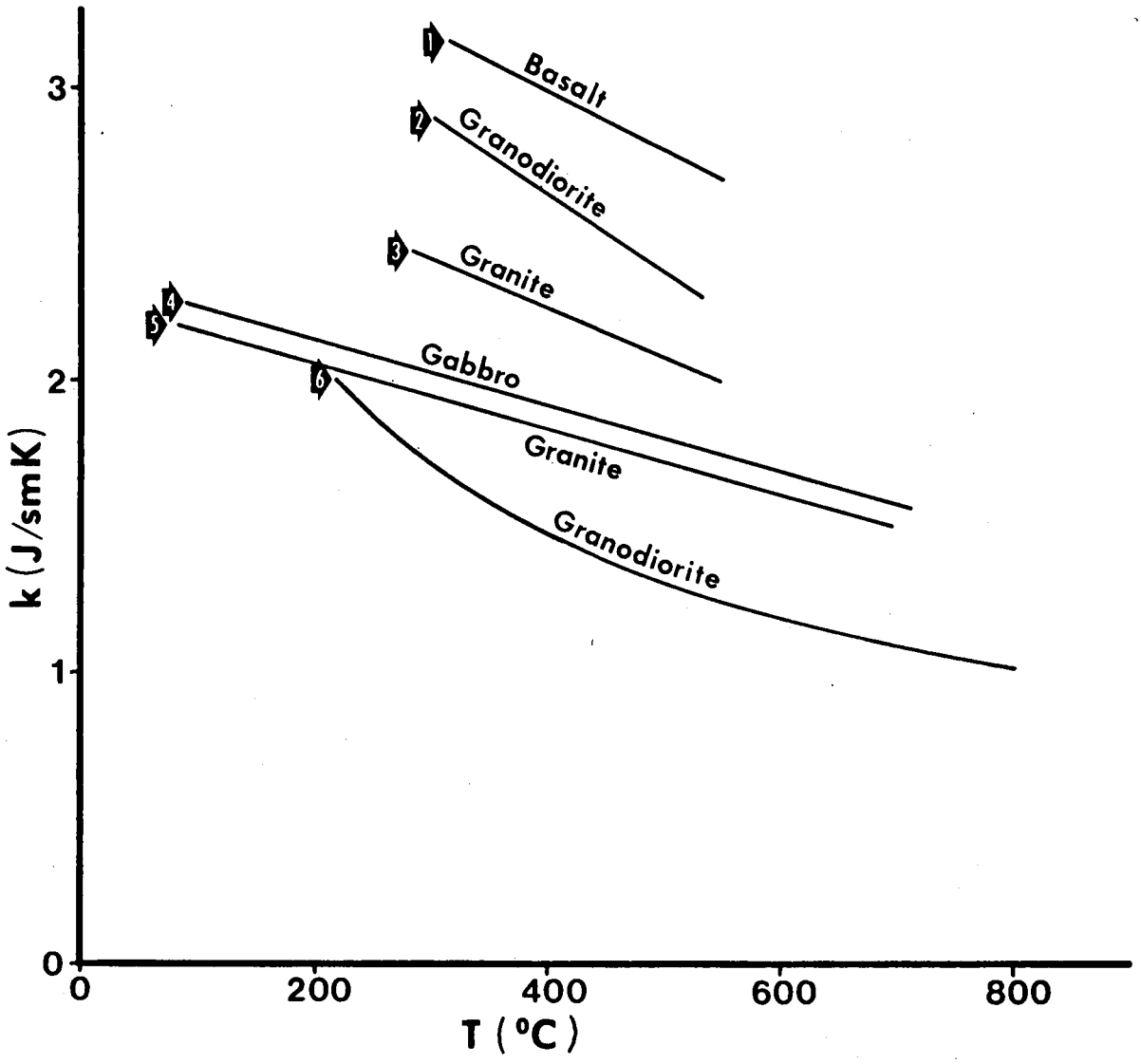

Figure 29. Variation of thermal conductivity with temperature for various igneous rock types. Samples 1-3 from Morgan and West (1980), and samples 4-6 from Mirkovich (1968).

The specific heat, c, of gabbro was reported in Mirkovich (1968) as being 945 m/s^2K. This is in good agreement with Hanley et al. (1978), who reported thermal diffusivities for several basalts. Thermal diffusivity is related to thermal conductivity by

$$a = k/\rho c \tag{6.18}$$

For the Dresser basalt, the thermal conductivity is 960 m/s^2K, using a specific heat of 3,140 J/smK (Morgan and West, 1980). The variation in the specific heat between gabbro and basalt is related to the higher porosity and interstitial water of the basalt.

Radioactive Waste

The properties of radioactive waste are functions of (1) the type of waste (identity and abundances of nuclides), and (2) the age of the waste. A comprehensive review of the many proposed packaging and emplacement procedures can be found in Office of Waste Isolation (1978). Waste types and expected ages of emplacement are covered in E. I. du Pont de Nemours and Company (1980a, 1980b). Two waste forms (Table 10 and Fig. 30) using the packaging and burial conditions reported in Claiborne et al. (1980), Rickertsen and Claiborne (1981), Rickertsen et al. (1982a), and Rickertsen et al. (1982b) (Table 11 and Fig. 31) have been selected. Only one canister is considered and very-near-field investigations are not within the scope of the present study.

Exponential regression equations were derived to characterize the thermal decay of the waste (Table 12). Several regression equations

Table 10. Thermal decay curves for waste derived from boiling water reactors (BWR), pressurized water reactors (PWR), and defense high-level waste (DHLW). (After Rickertsen et al., 1982a.) DHLW and PWR waste were selected for study.

Time (yrs)	q (w/canister) (DHLW)	(PWR)	(BWR)	Time (yrs)	q (w/canister) (DHLW)	(PWR)	(BWR)
0				700		34.5	12.4
1				800		31.2	11.2
2				900		27.9	10.1
3				1000	.7	25.2	9.2
4				2000	.4	13.2	4.9
5	540.6			3000		10.4	3.8
6				4000		9.3	3.5
7				5000	.3	8.8	3.3
8				6000		8.2	3.1
9				7000		7.7	2.7
10	358.5	548.0*	183.0*	8000		7.1	2.7
15	310.4*	458.7	154.1	9000		7.1	2.6
20	275.0	410.5	137.0	10000	.2	6.6	2.4
30	218.8	340.9	113.8	20000	.2	3.8	1.5
40	175.1	287.7	96.4	30000		2.7	.9
50	140.7	246.1	82.7	40000		1.6	.7
60		212.6	72.1	50000	.1	1.6	.5
70		185.8	63.1	60000			
80		164.4	56.0	70000			
90			50.5	80000			
100	50.2	133.2	45.8	90000			
200	10.3	75.1	26.4	100000	.1	.5	.2
300	4.1	59.2	21.0	200000		.5	.1
400	2.3	51.0	17.0	300000			
500	1.5	44.4	15.7	400000			
600		38.9	13.9	500000		.2	.1

*Expected age at time of burial.

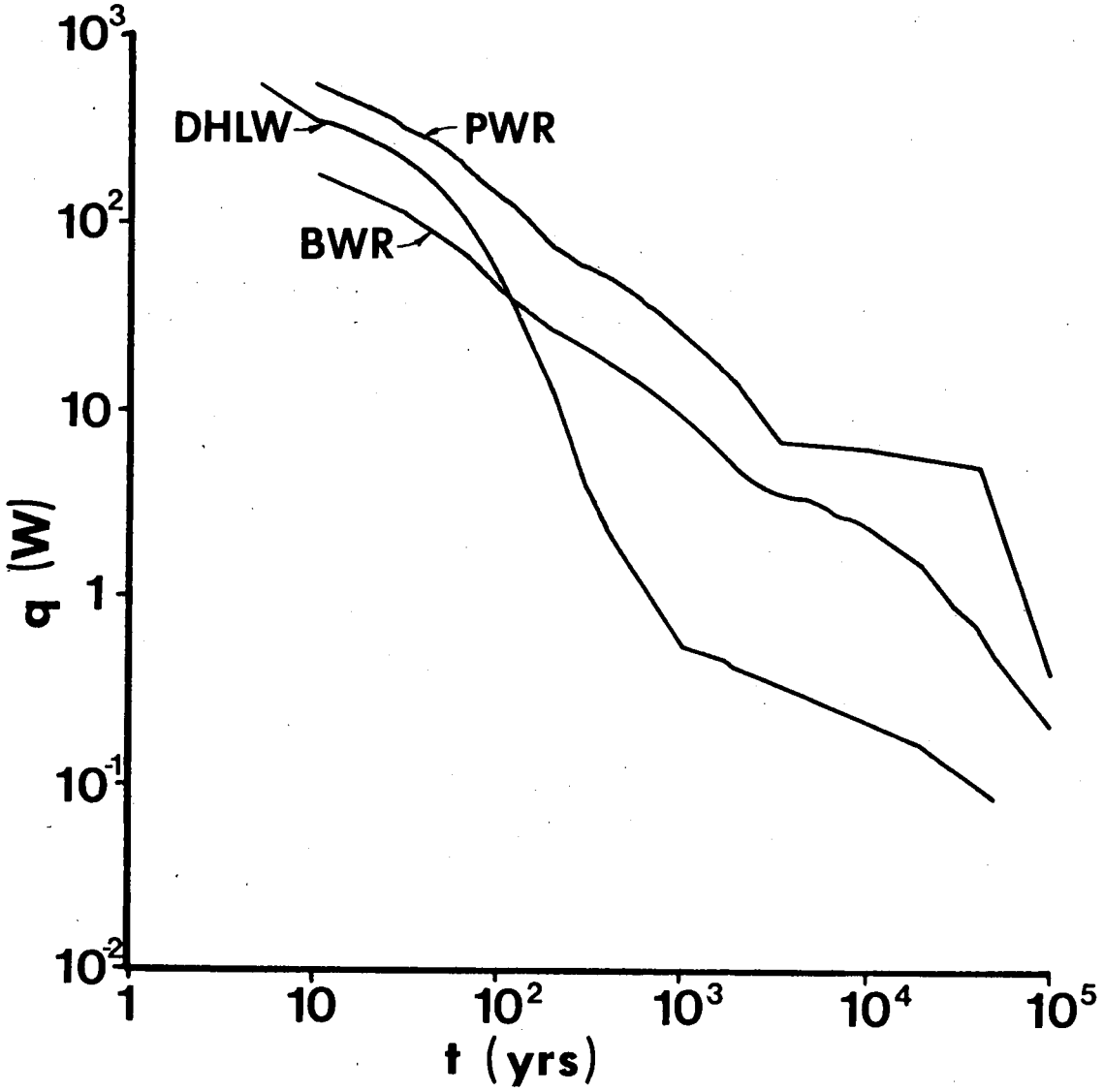

Figure 30. Thermal decay curves for waste derived from pressurized water reactors (PWR), boiling water reactors (BWR), and defense high-level waste (DHLW). DHLW and PWR were used in this study. (After Rickertsen et al., 1982a.)

Table 11. Packaging and burial conditions for defense high level waste (DHLW) and pressurized water reactor (PWR) waste. (After Rickertsen et al., 1982a.)

	DHLW	PWR
Heat generation rate at time of burial (w/can)	310.4	548.0
Heat generation rate at time of burial (w/m^3)	497.2	548.0*
Canister height (m)	3.01	4.52
Canister diameter (m)	0.61	0.324
Volume of waste in canister (m^3)	0.6245	--**
Waste forms	glass	fuel assembly (rods)
Backfull material	bentomite	bentomite
Borehole diameter (m)	1.56	1.18
Borehole depth (m)	4.25	6.29
Overpack material	titanium	--**
Overpack, length (m)	3.34	--**
Overpack diameter (OD) (m)	0.85	--**

*Assumed.

**Not applicable.

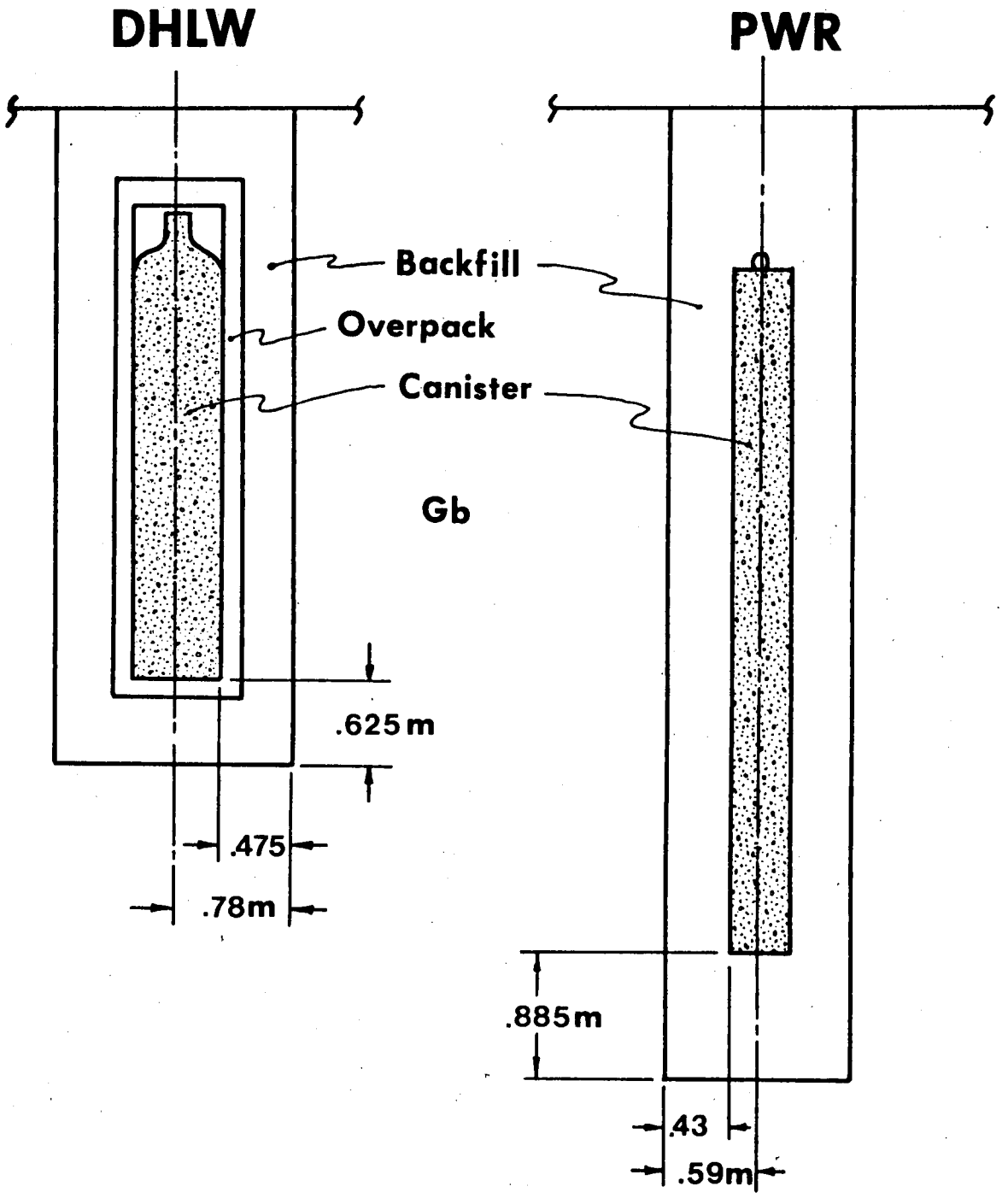

Figure 31. Schematic drawing of burial conditions for defense high level waste (DHLW) and pressurized water reactor (PWR) waste. (After Rickertsen et al., 1982a.)

Table 12. Regression equations used for the heat source.

Interval (yrs.)	DHLW	Interval (yrs.)	PWR
0-50	$e^{(-2.25614E-2)(time)}$	0-50	$e^{(-1.82336E-2)(time)}$
50-135	$e^{(-1.96815E-2)(time)}$	50-100	$e^{(-1.16027E-2)(time)}$
135-335	$e^{(-1.00869E-2)(time)}$	100-400	$e^{(-3.11798E-3)(time)}$
335-985	$e^{(-1.95688E-3)(time)}$	400-2000	$e^{(-1.14980E-3)(time)}$

were required for each type of waste as the decay does not follow a regular trend, due to the many long- and short-lived isotopes in the waste that contribute to the thermal energy. In each regression, the residual (R^2) was kept to greater than 0.995 for waste ages of less than 100 years and to 0.95 for ages greater than 100 years. The greater regression accuracy is required for the younger material that is contributing the most heat.

Physical Geometry Used in the Problem

Because the rock is assumed to be thermally isotropic (e.g., no variance with pressure or temperature and homogeneous composition) and because the waste canister is a right circular cylinder, the symmetry of the system degenerates to a two-dimensional problem (Fig. 32). A two-dimensional quarter section, the shaded area (Fig. 32), can be taken through the canister without losing any information in the solution. All results in the subsequent discussion refer to this quarter slice unless explicitly noted to the contrary.

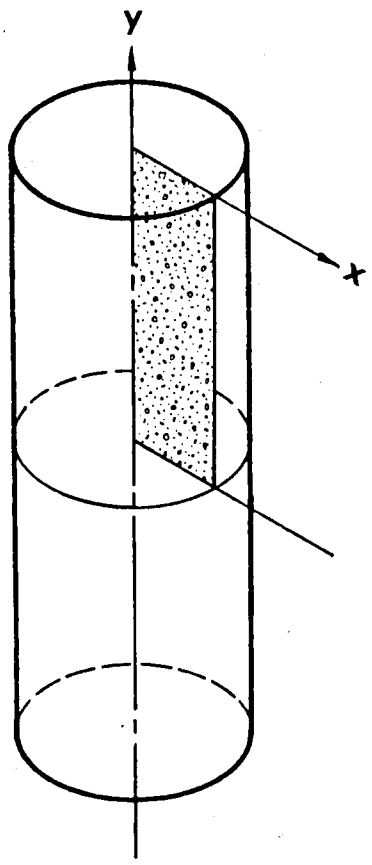

Figure 32. Idealized section through a waste canister showing the quarter section region (shaded) used in the problem.

Assumptions and Limitations

The following assumptions were made concerning the gabbro. Thermal conductivity, density, and specific heat do not vary with temperature or pressure, and there are no compositional variations in the gabbro. Furthermore, all secondary porosity such as fractures is assumed to be nil. The thermal conductivity and specific heat do not vary enough for gabbro (Fig. 29, p. 133) to warrant making them dependent on temperature. By assuming no compositional variation,

the problem is greatly simplified. The validity of this assumption is questionable, but, gabbro has one of the lower thermal conductivities of all igneous rocks (Mikrovich, 1968) and presents a worst case scenario. Rocks with higher conductivities transport heat faster, thereby reducing the maximum temperatures experienced in the repository. The assumption that there is no secondary porosity is not entirely valid. At depths of emplacement of about 600 meters (Claiborne et al., 1980) fracture closure may become significant. Furthermore, engineering design of the repository will attempt to avoid high fracture regions (U.S. DOE, 1980).

The following assumptions were made concerning the waste. All thermal properties of the waste, overpack, and backfill are considered to be the same as for the gabbro. The DLRW is composed of glass and has a thermal conductivity of about 1 J/msK (Rickertsen et al., 1982a). The titanium overpack and the bentonite backfill have thermal conductivities of 10.0 J/msK and 0.75 J/msK, respectively (Rickertsen et al., 1982a). These data indicate that the bentonite should experience higher thermal histories than predicted in the results, and the gabbro should attain lower maximum temperatures than predicted. The containment geometry has been simplified (Fig. 31 and Table 11). These simplifications should only effect a very-near-field analysis which is not considered in this study.

Error and Sensitivity Analysis

The properties of the gabbro and the radioactive waste were nondimensionalized to facilitate the computational aspects of the problem

(see Appendix C for details). The nondimensional values used in the problem are shown in Table 13. Several variations of the input parameters were run using the CFDL.TRAK code to insure that the results presented in this study do not contain significant error. As noted earlier, several potential sources of approximation error, that are independent of the variation of physical properties of the rocks and radioactive waste, exist in the finite element (as well as other numerical) methods. They include (1) the finite element grid size, (2) the truncation error in the Taylor's series polynomial approximation $\{N_k\}$ in equation (6.16), and (3) the time step. For a given finite element basis, the ratio of grid size and time step is the practical parameter for controlling error. To assess the magnitude of error associated with these parameters, three separate runs were made in which each parameter was varied independently.

Due to the very low thermal conductivity of gabbro and the high initial heat generation rates of the waste, the most significant spatial variation in temperature occurs early in the emplacement history and near the waste canister. It is with this large initial change in temperature in and near the canister that potentially large errors in predicted temperatures can result. For this reason, the assessment runs were conducted in the very-near-field; 3 meters in each direction, and for times not exceeding 50 years.

Reference Run

These runs are compared to a reference run that was used to compute the final solutions to the problems. The reference run

Table 13. True, reference, and nondimensional values used in the finite element procedure for Defense High-Level Waste (DHLW) and Pressurized Water Reactor (PWR) waste.

	DHLW			PWR		
	true	reference	nondim.	true	reference	nondim.
$\rho(kg/m^3)$	2980	2980	1	2980	2980	1
$c(m/s^2K)$	945	945	1	945	945	1
$k(J/smK)$	2	2	1	2	2	1
$q_i(J/m^3s)$	497.2	497.2	1	548.0	548.0	1
$l(m)$	1	1	1	1	1	1
$t(s)$	1	1.408×10^{6}	7.102×10^{-7}	1	1.408×10^{6}	7.102×10^{-7}
$T(°C)$	1	2	0.5	1	2	0.5

incorporates a linear finite element approximation, 20 elements of 0.15 meters length on a side in both directions (making a grid of 20 x 20 elements equivalent to 3.0 x 3.0 meters), and an initial time step size of 39.1 hours. The geometry of the set-up used in the error analysis is illustrated in Fig. 33, and the canister is represented by the quarter panel shown in the lower left. It is composed of two columns of eight elements each. In the subsequent figures, the x- and y-directions are keyed to Fig. 33.

Figure 34 shows two families of temperature-time-space (TTS) curves for the x- and y-directions, respectively. In this, and all subsequent TTS curves, the temperatures at the nodal points on the principal x- and y-axes are plotted.

Changing Grid Size

The grid size was increased from two elements to four elements in the x-direction, and the number of elements in the y-direction was left unchanged at 20 elements. Two important observations can be made by this refinement of the grid size (Fig. 35). The error increases in the very-near-field with a finer grid because the time step is proportionally larger in relation to the element length in the x-direction. This error manifests itself in the x-direction (Fig. 35a) in the slight roughness seen between 0.225 meters and 0.9 meters on the fine grid TTS curve. The curve is smooth; however, and at distances greater than 0.9 meters it indicates that this error is negligible in the far-field. This error is not apparent in the x-direction because the grid-time step ratio remains roughly constant in this direction (Fig. 35b).

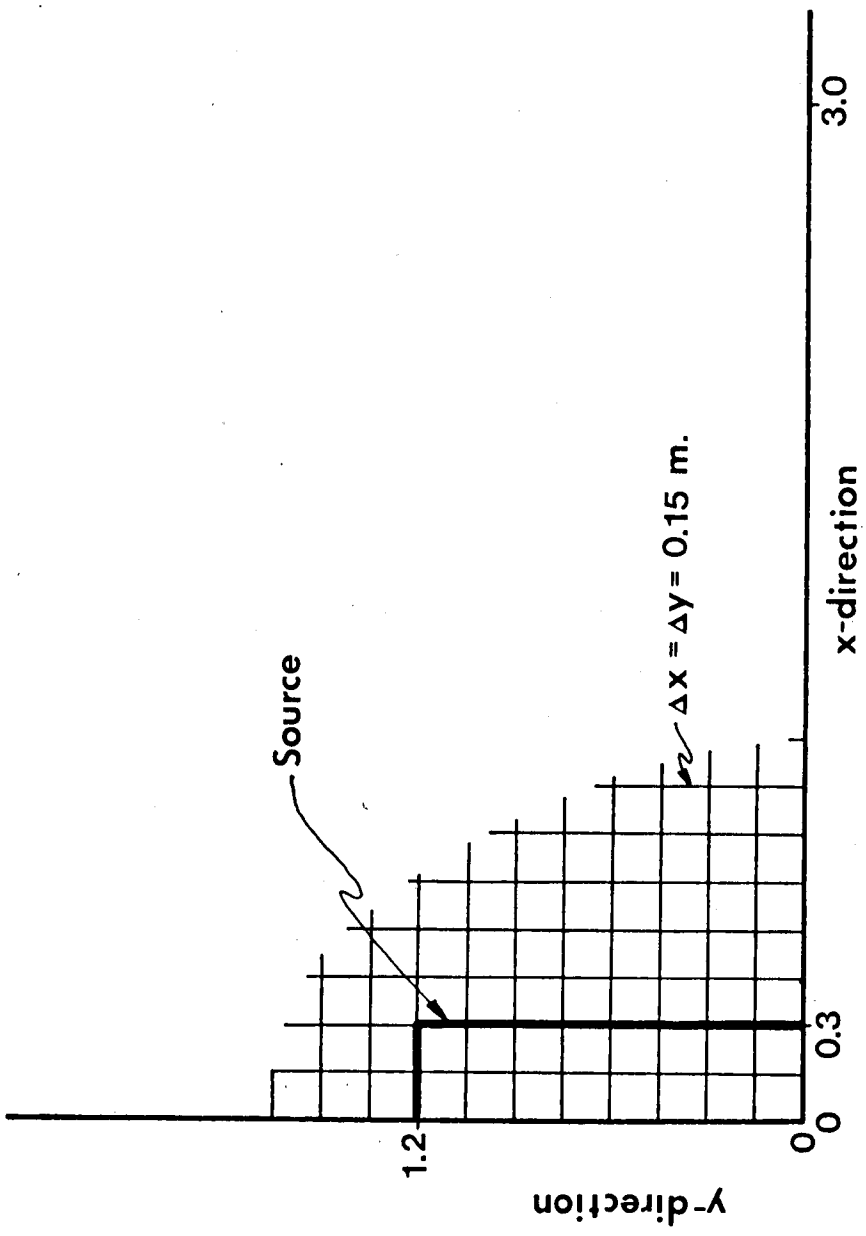

Figure 33. Finite element grid used in the near-field error and sensitivity analysis.

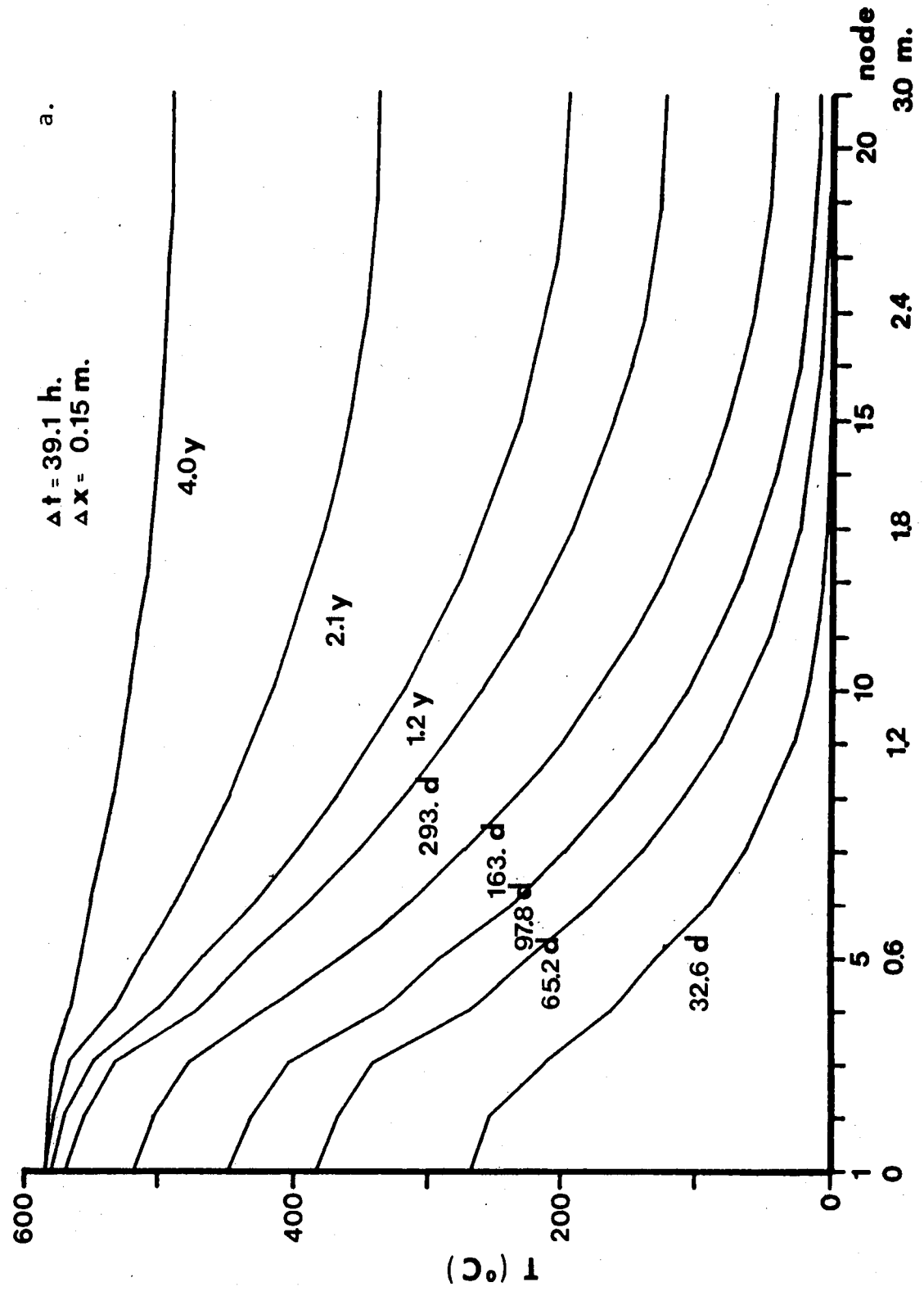

Figure 34. Time-temperature-space curves showing the results of the reference run for (a) the x-direction and (b) the y-direction.

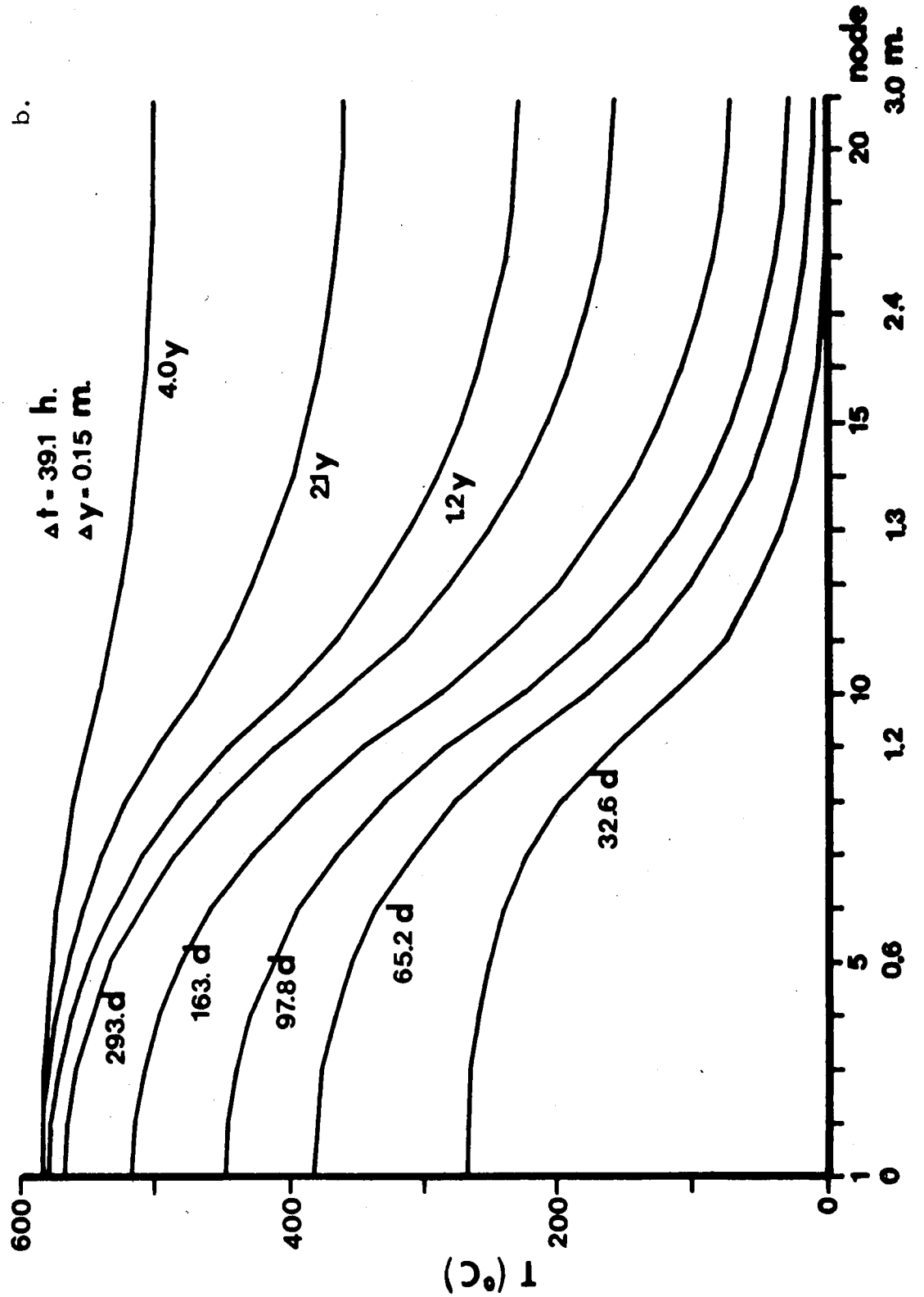

Figure 34 (continued)

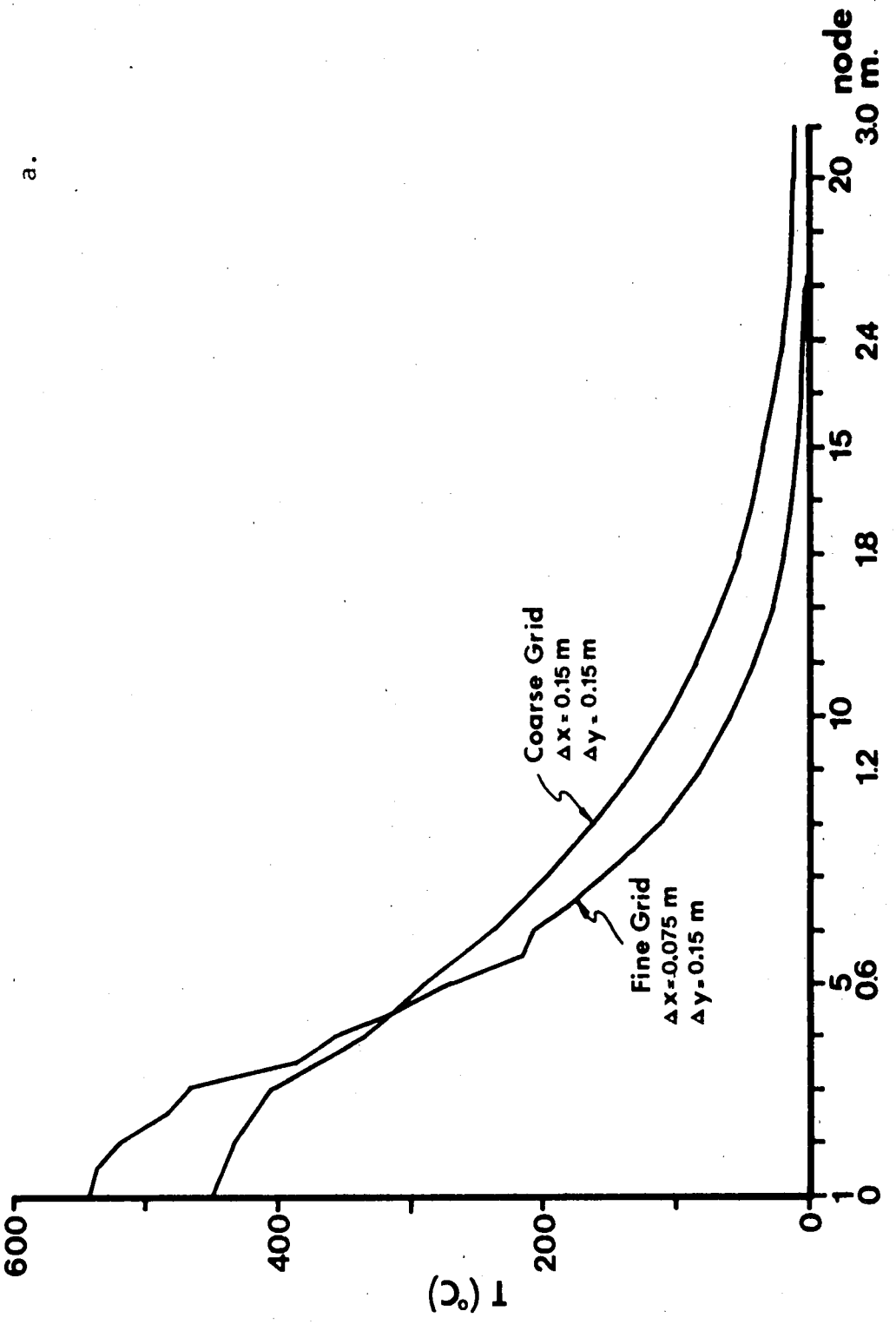

Figure 35. Time-temperature-space curves showing the effect of changing the grid size for (a) the x-direction and (b) the y-direction.

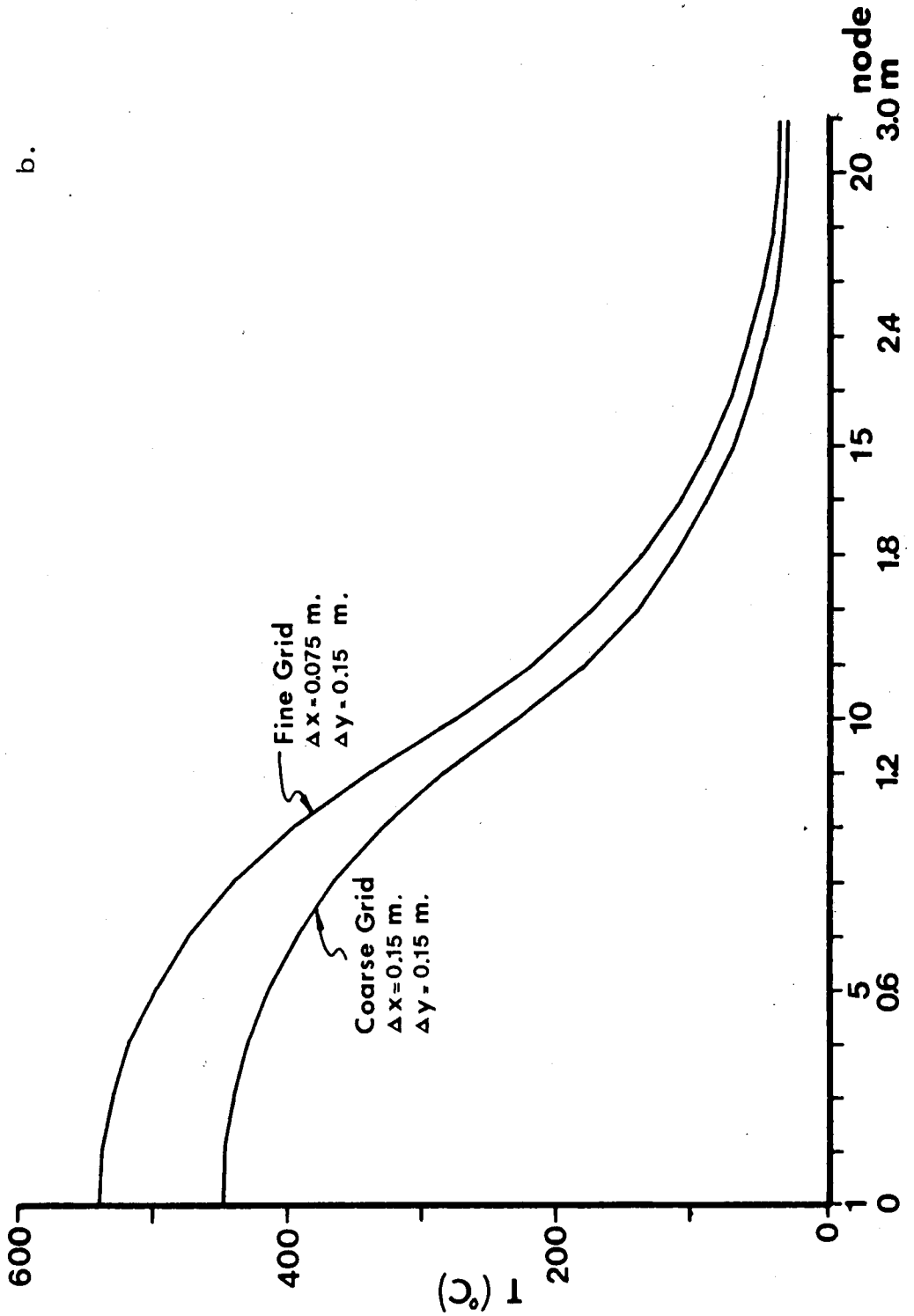

Figure 35 (continued)

The second important observation seen in Fig. 35 is that the finer grid yields different shaped temperature profiles in the x-direction. Higher temperature are calculated in the canister and lower temperatures are calculated far from the canister in the x-direction for the finer grid (Fig. 35a). The two curves become subparallel at distances greater than 2.0 meters. The two TTS profiles in the y-directions are subparallel, and do not cross (Fig. 35b). Thus, the coarse grid solution yields temperatures about 10°C too low in the x-direction and about 8°C too high in the y-direction, both at 3.0 meters. In both directions, however, the curves are convergent, indicating that this error is restricted only to the very-near-field.

No significant increase in accuracy is obtained by refining the grid size beyond 0.15 meters in the far-field. Due to the assumptions made, the very-near- and near-fields are of no interest in this problem.

Changing the Taylor's Series Approximation

Figure 36 results from the temperature approximation in an element assumed to vary in a quadratic manner. This assumption did not improve the solution in the near-field and was discarded as a possible method of increasing accuracy.

Changing the Time Step

By increasing the time step of a solution, additional time-like truncation error is introduced into the solution (Fig. 37). Keeping the ratio of time-grid size approximately constant at unity yields the

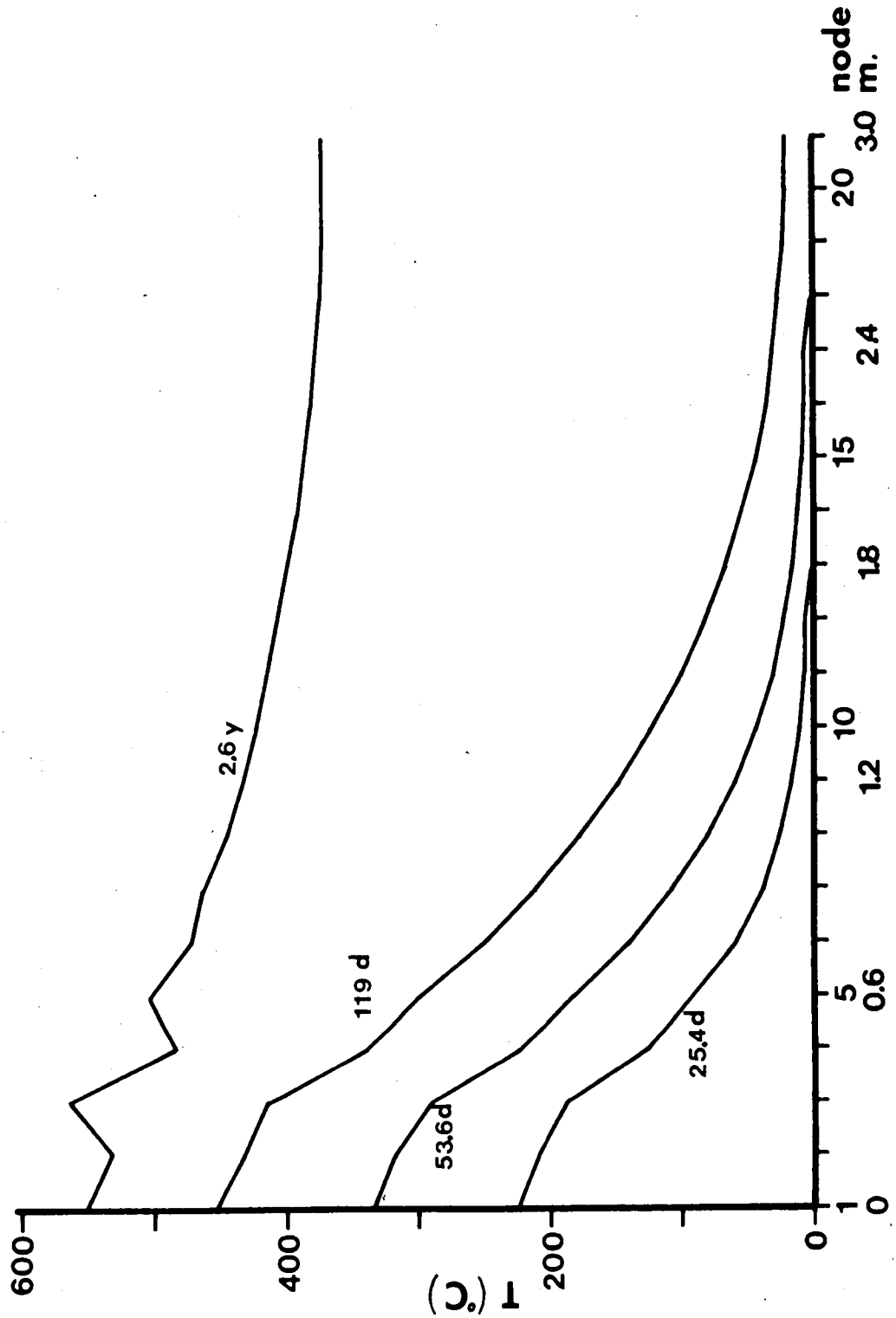

Figure 36. Time-temperature-space curves showing the effect of using a quadratic interpolation equation in the y-direction.

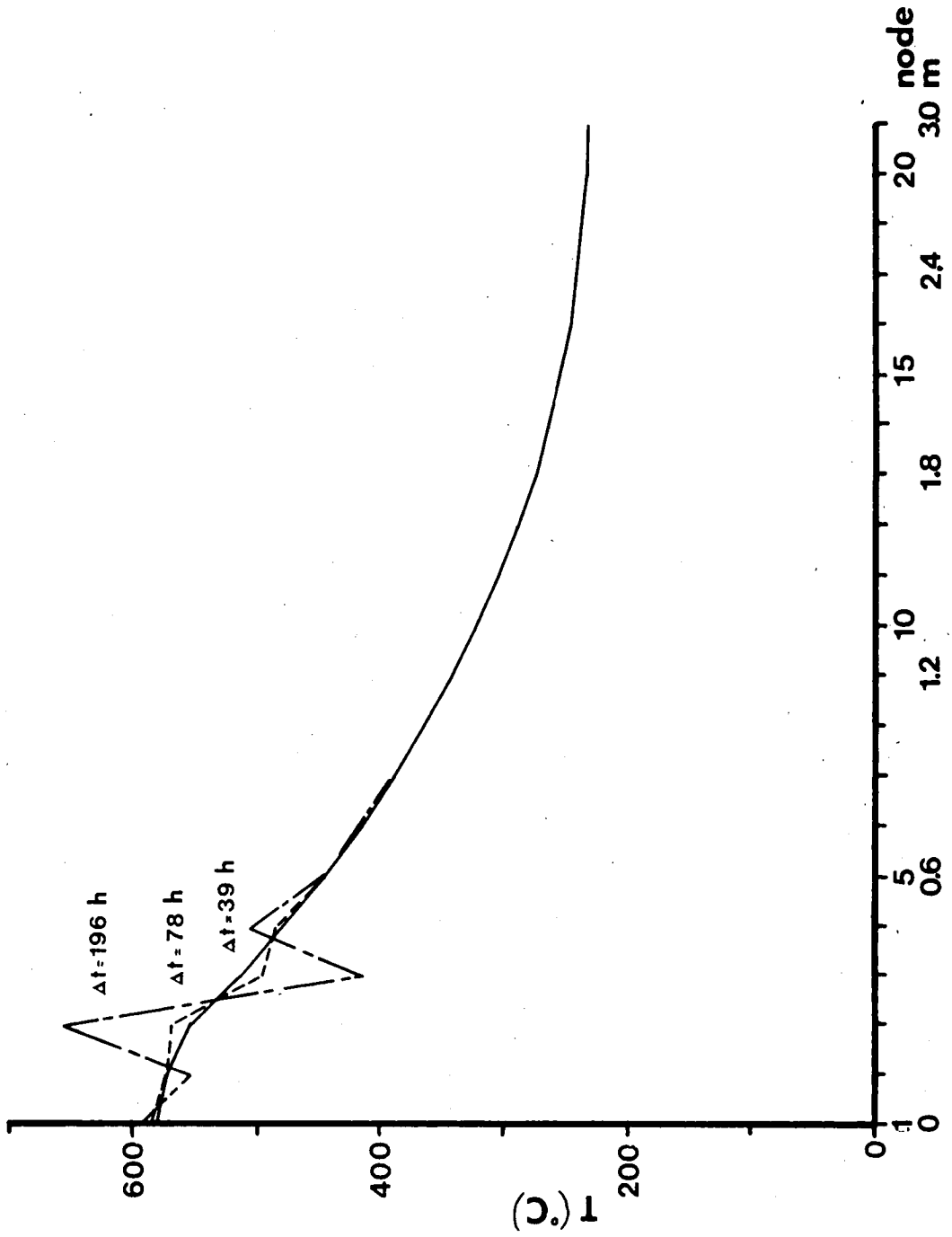

Figure 37. Time-temperature-space curves showing the effect of changing the time interval (Δt) between temperature calculations for the y-direction.

best (adequate) solution accuracy for the problem during the early time history when the heat source term is (relatively) large. Thereafter, for efficiency, this constant can be substantially increased as the problem state homogenizes.

Sensitivity Analysis

The two relationships

$$\frac{\rho_r c_r L^2}{k_r \tau} = C_1 \tag{6.19}$$

and

$$\frac{\dot{q}_r L^2}{k_r T_r} = C_2 \tag{6.20}$$

(Baker, personal communication) provide a means of evaluating the sensitivity of each physical parameter used in the problem. The rock density, specific heat, and thermal conductivity effectively control the time that any point will experience a given temperature (eqs. 6.19-6.20), in consert with the heat generation rate. Thus, for any point in the solution domain, a change of any physical parameter will result in a change in time or temperature and can be found from these equations. Table 14 shows the results for one such calculation for the maximum temperature (590°C) experienced at 4.2 years into the solution (Fig. 34). The reference values were used in the problem solution for DHLW and the changed values were taken from the expected variations discussed earlier. The change in heat source intensity is arbitrary for illustrative purposes.

Table 14. Sensitivity of time and temperature to changing rock and waste properties.

Property	Reference Value	Value change	Reference Temp.	Reference Time	New T (°C)	New t (yrs.)
Density	2980	3120	590	4.2	590	4.4
Sp. Ht.	945	960	590	4.2	590	4.3
Them Cad	2	3	590	4.2	393	2.8
q	497.2	300	590	4.2	356	4.2

As is evident in Table 14, the thermal conductivity can change the solution by a greater amount than the other parameters over the expected range of variability. For this reason, results must be considered order-of-magnitude correct in the final analysis.

Results

The predicted maximum temperature for DHLW in the rock (Fig. 38) is 368°C at the backfill-gabbro interface at 0.89 years (326 days). The maximum temperature for PWR waste in the rock (Fig. 39) is 400°C at 1.8 years. The U.S. DOE obtained maxima of about 200°C and 250°C for DHLW in granite and basalt host rocks, respectively. They obtained maxima of about 200°C for granite and 260°C for basalt for PWR waste. It is difficult to compare these results; however, because of the different baseline assumptions that were used in each case. In the U.S. DOE (1980) study, for example, they assumed 0.72 kw/canister with 6.5 year old waste. Furthermore, the method of calculating the waste decay curve is not specified, not is the geometry of emplacement. Their study assumed true thermal conductivities for

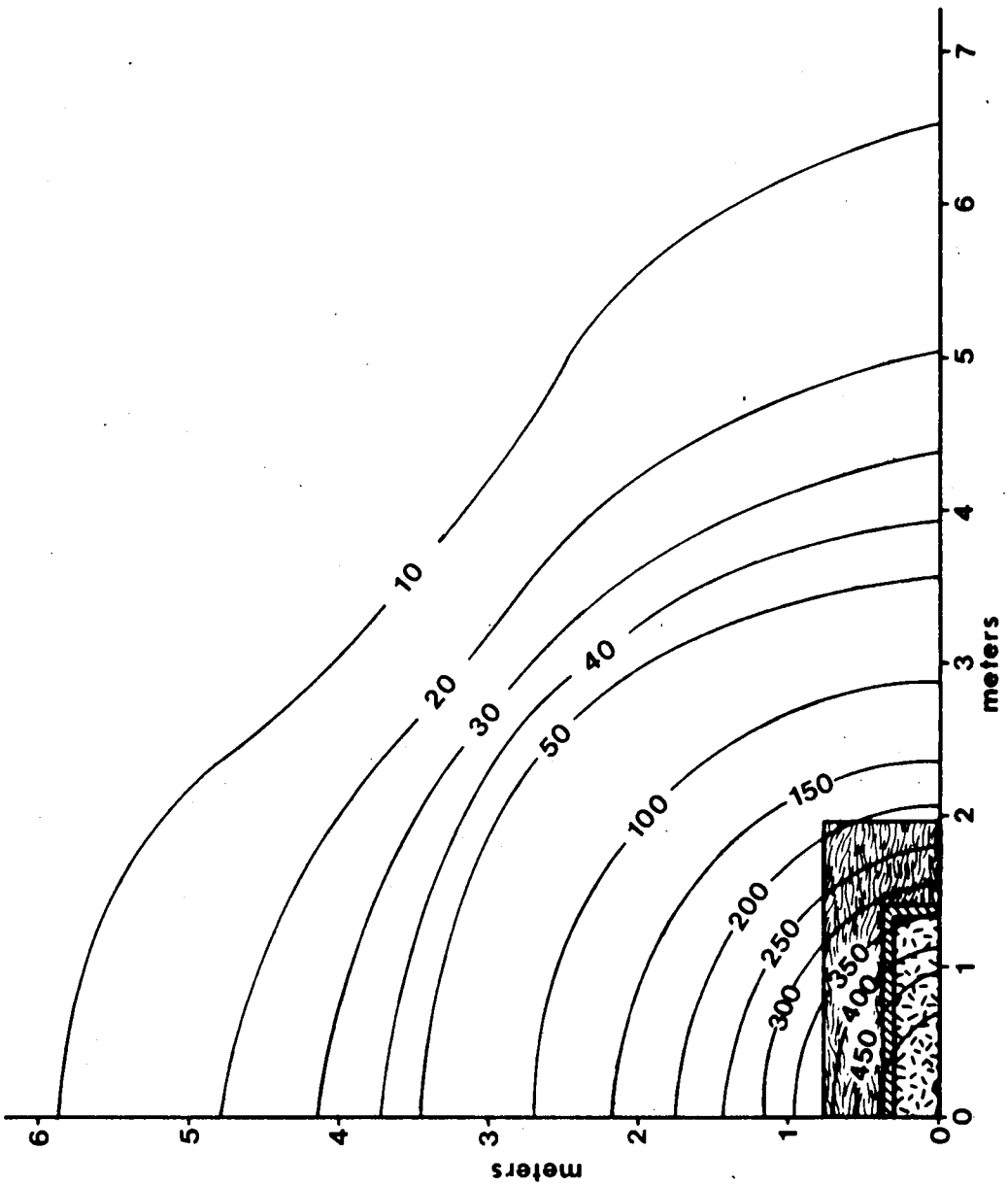

Figure 38. Isothermal curves at t = 0.89 years for Defense High Level Waste (DHLW) in gabbro. The four regions are (from coordinate origins outward) waste, overpack, bentonite backfill, and gabbro, respectively.

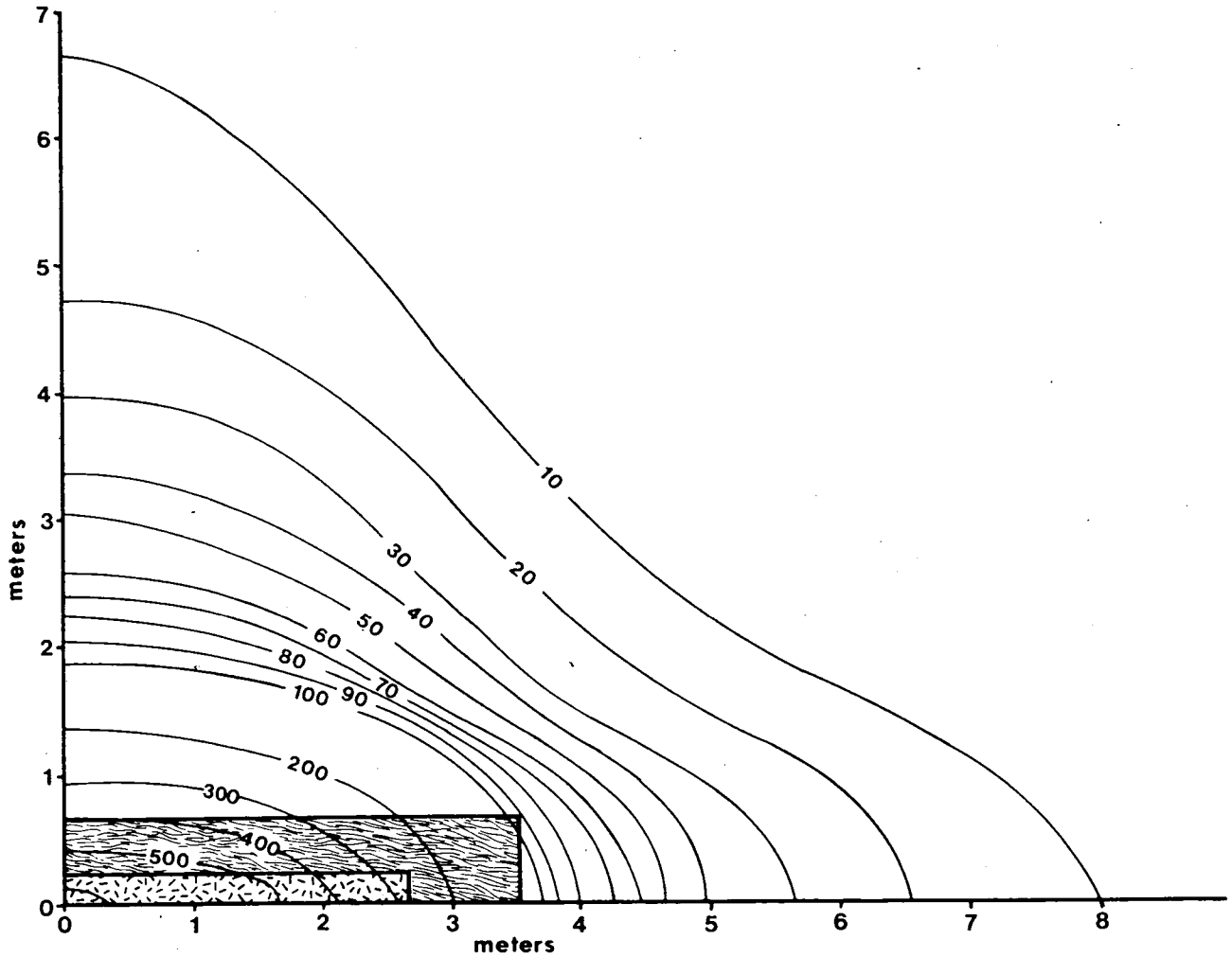

Figure 39. Isothermal curves at t = 1.8 years for Pressurized Water Reactor (PWR) waste in gabbro. The three regions are (from coordinate origins outward) waste, bentonite backfill, and gabbro,, respectively.

the waste, canister, and backfill, while this study did not. Despite these considerable differences in assumptions, and input parameters, the results are less than one magnitude different. This is well within the bounds prescribed in the sensitivity analysis performed for this study. The error associated with experimentally determined thermal properties of rocks (e.g., Fig. 29, p. 133) makes the comparison of these results to the U.S. DOE (1980) results more favorable.

In the near-field, the very-near-field assumptions have less effect on the predicted temperatures (c.f., error analysis, this chapter). At 5.0 meters, the maximum temperature is 160°C which is higher than the predicted maximum for granite and basalt which are about 140°C and 150°C, respectively (U.S. DOE, 1980), but which is within the range of expected values. This maximum temperature occurs at about 1.6 years after burial as compared to about 10 years for granites and basalts. The different times are due to the different initial thermal loadings in the respective studies [497.2 W for this study and 720 W for the DOE (1980)]. It is interesting to note that despite the different thermal loading, similar maximum temperatures are obtained for similar rock types.

Because the thermal maximum in the near-field is similar to those obtained for granite and basalt, then it is reasonable to assume similar thermal maxima in the very-near-field. If the maximum temperature predicted by this study are taken (425°C), and if it is assumed that acceptable packaging can be designed to withstand higher temperatures, then gabbros can accept a waste canister with higher heat

generation rates. The magnitude of the heat generation rate can be found by

$$q(sol) = T(sol) \times q(calc) \; / \; T(calc) \quad , \qquad (6.21)$$

where T(sol) is the solidus temperature of the gabbro, T(calc) is the temperature calculated, q(sol) is the maximum heat generation rate, and q(calc) is the calculated heat generation rate. The maximum heat generation rate for gabbro is calculated to be about 1200 W/m^3 to reach a temperature maximum of 1100°C, the solidus temperature for gabbro. The maximum heat generation rate for granite is about 700 W/can using the same equation. It is impossible to exactly compare the two values because this study does not use an average areal thermal loading, whereas the U.S. DOE (1980) study does. None the less, this is a 60% increase in waste per canister, or about 60% younger waste (assuming a linear decay in the very early history of the waste).

The highest temperature in gabbro that was obtained from this analysis is 400°C for PWR waste. As was shown in the previous chapters of this work, mafic intrusives rarely form large homogeneous plutons, rather, they form complexes composed of several lithologies (c.f., Chapters I and II). Table 9, p. 121, lists the expected range of thermal properties for the rock types found in the mafic intrusives of the study area. By taking advantage of the nondimensionalization characteristics of the CFDL.TRAK program, it is possible to translate the maximum temperature found for gabbro into maxima for dunite and

syenite (see Appendix C for methodology). The syenite will attain a maximum temperature of 340°C and dunite will attain a maximum of 440°C. This variation is reasonable when compared to the maximum variation in temperatures found for salt, shale, basalt, and granite (U.S. DOE, 1980). They found that for PWR waste, there is a maximum variation of about 172°C. Since there is a greater variation in the thermal properties of the rocks that they studied, the higher temperature variations are expected.

Recommendations

This study has shown that gabbros have approximately the same predicted thermal histories as does granite. Gabbros have higher solidus temperatures, however, and can accept more or thermally hotter waste, solely on the basis of thermal considerations. The very-near-field is where the maximum temperatures occur, and studies should be initiated to study this region.

Beyond the thermal properties of gabbro, other criteria make mafic intrusive rocks desirable candidates for further study. As Ringwood (1980) pointed out, slightly altered or metamorphosed gabbros have a higher degree of ductility than granites. This difference in ductility is due to the high degree of quartz contained in granite. The inherently higher ductility will have the effect of helping heal any fractures that may develop after high-level radioactive waste emplacement in gabbro. Furthermore, metamorphism of gabbroic rocks produces stable hydrous minerals such as amphiboles, micas, and clays. These hydrous minerals typically have higher

specific volumes than their unmetamorphosed precursors, thus further aiding in sealing any secondary permeability near the repository. Fried et al. (1977) found that plutonium and americium are strongly absorbed by the minerals in basalts. Thus, if a canister were breached, allowing radioactive waste to migrate along fractures, then absorption of these elements would most likely occur near the source. This is especially true if the breach occurred early in the emplacement history when the highest temperatures are experienced. These high temperatures would effectively metamorphose wall rocks of fractures along which water flow would occur. The hydrous phases thus formed would serve both to seal the fractures and to absorb radionuclides.

Although granites enjoy the same alteration characteristics (due to their high feldspar content), they contain very few ferromagnesian minerals. The ferromagnesians in gabbroic rocks tend to buffer hydrothermal solutions and form reducing environments (Hutchinson et al., 1980), thus preventing significant inorganic complexing of heavy metals. The study of oxidation-reduction reactions in association with uranium and thorium migration in sedimentary environments is well known (e.g., Trung and Poty, 1972; and Langmuir, 1978). They have shown that uranous (U^{+4}) and uranyl (U^{+6}) complexes can be easily formed in aqueous systems at almost any geologically reasonable pH, but only under higher Eh conditions. Thus, the reducing conditions expected to be found in mafic rocks is an advantage over granitic rocks in resisting radionuclide transport.

CHAPTER VII

CONCLUSIONS AND RECOMMENDATIONS

Summary

Calhoun Falls Complex

1. The Calhoun Falls complex is a layered intrusion composed of metagabbro, cumulus troctolite, cumulus gabbronorite, and serpentinized pyroxenite and periodotite.

2. The ultramafic units show no deformational features and are considered to have been intruded at the same time as the unaltered rocks. The timing of intrusion of the metagabbro is enigmatic.

3. Early fractionation of olivine plus clinopyroxene prior to plagioclase is responsible for the formation of the ultramafic units.

4. Limited iron enrichment of olivine and clinopyroxene as well as the limited range of many of the bulk rock components such as silica and the alkalis, are probably due to the processes that formed the cumulate textures.

5. Calculation of intercumulus liquid compositions indicates that about 20% of the plagioclase is cumulus, the rest being overgrowth. The intercumulus liquid composition is a primitive tholeiitic basalt.

Mt. Carmel Complex

1. The Mt. Carmel complex is composed of metagabbro, olivine-biotite gabbro, and syenite, all of which appear to be genetically related.

2. The suite has been shown to represent approximate liquid compositions from which it crystallized. The subsequent liquid line of descent is thoeliitic and includes all three lithologies.

3. Fractionation of olivine plus clinopyroxene formed the early metagabbros. Olivine plus clinopyroxene plus plagioclase fractionation produced the evolved metagabbro and the gabbro. Syenite was produced after all olivine crystallized.

4. For this pluton, it is hypothesized that one pulse of magma produced all three lithologies.

Greenwood Complex

1. The Greenwood complex is composed of cumulus gabbronorite, diorite, and metagabbro.

2. The fine grained diorite appears to grade into the medium grained cumulus gabbronorite, however, very limited sampling makes this conclusion tentative.

3. Geophysical and field evidence suggest that the Greenwood complex has barely been unroofed. Furthermore, the complex may be composed of three separate plutons: a larger elliptical body to the south, and two smaller bodies to the north.

4. Texturally, the cumulus gabbronorite is similar in both the Greenwood and Calhoun Falls complexes, but the Greenwood complex is more silica enriched. This observation may be due to the different depth of erosion of the two plutons, or to inherent parent magma differences.

The Plutons in the Study Area in Relation to Those to the North

1. The study area is composed of a cluster of mafic plutons separated from the others in the Charlotte belt by a gap of low plutonic activity.

2. Olivine plus clinopyroxene control the early crystallization history of the mafic plutons in the study area, while other workers have shown that olivine plus clinopyroxene plus plagioclase fractionation controlled the crystallization of plutons outside the study area.

3. On this basis, it is proposed that the study area is a magmatic center that was active contemporaneously with the northern plutons. Several possible hypotheses are proposed for the existence of these magmatic centers.

Thermal Heat Modeling in Mafic Intrusives

The thermal properties of gabbro have been shown to be favorable for the containment of high-level radioactive waste. The chemistry and hydrologic properties of gabbro also appear to be favorable. Thus, on this basis, it appears that mafic intrusives can also be considered as possible radioactive waste repository host rocks.

BIBLIOGRAPHY

BIBLIOGRAPHY

Albee, A. L. and Ray, L., 1970, Correction factors for electron probe microanalysis of silicates, oxides, carbonates, phosphates, and sulfates: Anal. Chem., v. 42, p. 1408-1444.

American Geological Institute, 1974, Glossary of Geology: Gary, M., McAfee, R., Jr., and Wolf, C. L. (eds.) Washington, D. C., 805 pp.

Baker, A. J., 1983, Finite Element Computational Fluid Mechanics: McGraw-Hill Book Co., Washington, D. C., 510 pp.

Barnes C. G., 1983, Petrology and upward zonation of the Wooley Creek batholith, Klamath Mountains, California: J. Petrol., v. 24, p. 495-537.

Barton, C. and Brown, L., 1983, Paleomagnetism of Carboniferous intrusions in North Carolina: J. Geophys. Resc., v. 85, p. 2327.

Bell, H., 1960, A synthesis of geologic work in the Concord area, North Carolina: U. S. Geol. Surv. Prof. Paper 400B, p. 189-191.

Bence, A. E. and Albee, A. L., 1968, Empirical correction factors for the electron microanalysis of silicates and oxides: Jour. Geol., v. 76, p. 382-403.

Bourland, W. C. and Farrar, S., 1980, Tectogenesis of the rocks surrounding the Winnsboro intrusive complex: S. C. Geol., v. 24, n. 1, p. 1-18.

Butler, J. R., 1966, Geology and mineral resources of York County, South Carolina: S. C. State Devel. Board, Bull. 33, 65 pp.

Butler, J. R. and Ragland, P. C., 1969, A petrochemical survey of plutonic intrusions in the Piedmont, southeastern Appalachians, USA: Contrib. Mineral. Petrol., v. 24, p. 164-190.

Butler, J. R. and Fullagar, P. D., 1982, Timing of orogenic events in the Carolinas: Geol. Soc. Amer., Abstr. with Pgms., v. 14, p. 8.

Butler, J. R. and McSween, H. Y., Jr., 1983, Mafic plutonic rocks of the southern Appalachians: Geol. Soc. Amer., Abstr. with Pgms., v. 15, p. 118.

Cabaup, J. J., 1969, Origin and differentiation of the gabbro in the Concord Ring Dike, North Carolina Piedmont: Unpubl. M.S. thesis, Univ. of N. C., Chapel Hill.

Camp, W. C. and Herren, E. C., 1980, Soil survey of Greenwood and McCormick Counties, South Carolina: U. S. Dept. of Agric., 68 pp. and maps.

Carpenter, R. H. and Hughes, T. C., 1970, Geochemical and geophysical survey of the Gladesville norite, Jasper County, Georgia: Geol. Surv. Ga., Infor. Circ. 37, 7 pp.

Carpenter, R. H., Odom, A. L., and Hartley, M. E., III, 1982, Geochronological investigations of the Lincolnton metadacite, Georgia and South Carolina: Geol. Soc. Amer., Special Paper 191, p. 145-152.

Carslaw, H. S. and Jaeger, J. C., 1959, Conduction of Heat in Solids: Oxford Press, London, 567 pp.

Chalcraft, R. G., 1970, Petrography and geophysics of the Rock Hill gabbro pluton, York County, South Carolina: Southeastern Geol., v. 11, n. 3, p. 153-171.

Chalcraft, R. G., 1977, A petrologic study of the Ogden pluton, York and Chester Counties, South Carolina: Geol. Soc. Amer., Abstr. with Pgms., v. 9, n. 2, p. 128.

Chalcraft, R. G., Lawrence, D. P., and Taylor, C. A., Jr., 1978, The petrology of the Greenwood pluton, Greenwood County, South Carolina: A preliminary report: Carol. Geol. Soc. Guidebook, p. 40-46.

Chalcraft, R. G., Lawrence, D. P., Taylor, C. A., Jr., and Duc, A. C., Jr., 1981, Geological interpretation of gravimetric surveying in a portion of Greenwood County, South Carolina: S. C. Geology, v. 25, n. 2, p. 79-89.

Claiborne, H. C., Wagner, R. A., and Just, R. A., 1979, A comparison of the results of several heat transfer computer codes when applied to a hypothetical nuclear waste repository: Oak Ridge Nat. Lab., ORNL/TM-7112, 66 pp.

Claiborne, H. C., Rickertsen, L. D., and Graham, R. F., 1980, Expected environments in high-level nuclear waste and spent fuel repositories in salt: Oak Ridge Nat. Lab., ORNL/TM-7201, 188 pp.

Clark, J. R., 1973, The petrology and geochemistry of the Seroyer Branch mafic-ultramafic complex, Chambers County, Alabama: Unpubl. M.S. thesis, Univ. of Ala., Tuscaloosa.

Clark, S. R., 1980, Petrology of the Bear Poplar and Barber mafic intrusives, North Carolina: Unpubl. M.S. thesis, Univ. of Tenn., Knoxville.

Constantino-Herrera, S. E., 1971, Geology of the Cleveland gabbro, Rowan County, North Carolina: Unpubl. M.S. thesis, Univ. of N. C., Chapel Hill.

Cook, F. A., Brown, L. D., Kaufmann, S., and Oliver, J. E., 1983, The COCORP seismic reflection traverse across the southern Appalachians: Amer. Assoc. Petrol. Geol., Studies in Geol., n. 14, 61 pp.

Cook, F. A., Brown, L. D., Kaufmann, S., Oliver, J., and Petersen, T., 1981, COCORP seismic profiling of the Appalachian orogen beneath the Coastal Plain of Georgia: Geol. Soc. Amer. Bull., v. 92, p. 738-748.

Cox, K. G., Bell, J. D., and Pakhurst, R. J., 1979, The Interpretation of Igneous Rocks: George Allen and Unwin, London, 450 pp.

Daly, R. A., Manger, G. E., and Clark, S. P., Jr., 1966, Density of rocks: in Clark, S. P., Jr. (ed.), Handbook of Physical Constants, Geol. Soc. Amer., Memoir 97, p. 19-26.

Dooley , D. E., 1983, Paleomagnetism of some mafic intrusions in the South Carolina Piedmont. I. Magnetic systems with single characteristic directions: Phys. Earth Planet. Int., v. 31, p. 241.

E. I. du Pont de Nemours and Company, 1980a, Preliminary technical data summary for the defense waste processing facility-stage 1: DPSTD-80-38, Savannah River Plant, Aiken, S. C.

E. I. du Pont de Nemours and Company, 1980b, Preliminary technical data summary no. 3 for the defense waste processing facility: DPSD-77-13-3, Savannah River Plant, Aiken, S. C.

Ellwood, B. B., 1982, Paleomagnetic evidence for the continuity and independent movement of a distinct major crustal block in the Southern Appalachians: J. Geophys. Resc., v. 87, p. 5339.

Elthon, D., 1983, Isomolar and isostructural pseudo-liquidus phase diagrams for oceanic basalts: Amer. Miner., v. 68, p. 506-511.

Elthon, D. and Scarfe, C. M., 1984, High-pressure phase equilibria of a high-magnesia basalt and the genesis of primary oceanic basalts: Amer. Miner., v. 69, p. 1-15.

Flanagan, F. J., 1973, 1972, Values for international geochemical reference samples: Geochim. et Cosmochim. Acta, v. 37, p. 1189-1200.

Fried, S., Friedman, A., Atcher, R., and Hines, J., 1977, Retention of plutonium and americium by rock: Science, v. 196, p. 1087-1089.

Fronabarger, A. K., 1984, Analysis of seven U. S. Geological Survey samples: AMH-1, BIR-1, GSM-1, DNC-1, DTS-2, TLM-1, and W-2: Geostandards Newsletter (In Press).

Fronabarger, A. K. and McSween, H. Y., Jr., 1983, Calhoun Falls complex, a mafic layered intrusion?: Geol. Soc. Amer., Abstr. with Pgms., v. 15, n. 2, p. 63.

Fullagar, P. D., 1971, Age and origin of plutonic intrusions in the Piedmont of the southeastern Appalachians: Geol. Soc. Amer. Bull., v. 82, p. 2845-2862.

Fullagar, P. D. and Butler, J. R., 1979, 325 to 265 m.y.--old granitic plutons in the Piedmont of the Southern Appalachians: Amer. Jour. Sci., v. 279, p. 161-185.

Gill, J. B., 1981, Orogenic Andesites and Plate Tectonics: Springer-Verlag, New York, 390 pp.

Glover, L., III and Sinha, A. K., 1973, The Virgilina deformation, a late preCambrian to early Cambrian(?) orogenic event in the central Piedmont of Virginia and North Carolina: Amer. Jour. Sci., Cooper Vol., 273-A, p. 234-251.

Glover, L., III, Speer, J. A., Russell, G. S., and Farrar, S. S., 1983, Ages of regional metamorphism and ductile deformation in the central and southern Appalachians: Lithos, v. 16, p. 223-245.

Griffin, V. S., Jr., 1970a, Position of the Kings Mountain belt in Abbeville County, South Carolina: Southeastern Geol., v. 12, n. 2, p. 105-113.

Griffin, V. S., Jr., 1970b, A probable pre-Triassic mafic intrusive in the Anderson 15-minute quadrangle, South Carolina: Geol. Notes, v. XIV, n. 4, p. 97-104.

Griffin, V. S., Jr., 1971, The Inner Piedmont belt of the southern crystalline Appalachians: Geol. Soc. Amer. Bull., v. 82, p. 1885-1898.

Griffin, V. S., Jr., 1972, Progress report of a geologic study in Abbeville and McCormick Counties, South Carolina: Geol. Notes, v. 16, n. 3 p. 59-78.

Griffin, V. S., Jr., 1978, Geology of the Calhoun Creek, Calhoun Falls and portions of the Chennault and Verdery quadrangles, South Carolina: S. C. Geol. Surv., MS-23, 1:24,000 maps and 47 p. text.

Griffin, V. S., Jr., 1979, Geology of the Abbeville East, Abbeville West, Latimer, and Lowndesville quadrangles, South Carolina: S. C. Geol. Surv., MS-24, 1:24,000 maps and 58 p. text.

Griffin, V. S., Jr., 1981, The Lowndesville belt north of the South Carolina-Georgia border: in Horton, J. W., Jr., Butler, J. R., and Milton D. M. (eds.), Geological investigations of the Kings Mountain belt and adjacent areas in the Carolinas, Carolina Geological Society Field Trip Guidebook, S. C. Geol. Surv., p. 166-173.

Hadley, J. B., 1973, Igneous rocks of the Oxford area, Granville County, North Carolina: Amer. Jour. Sci., Cooper Vol., 273-A, p. 217-233.

Hanley, E. J., Dewitt, D. P., and Roy, R. F., 1978, The thermal diffusivity of eight well-characterized rocks for the temperature range 300-1000 K: Engineering Geology, v. 12, p. 31-47.

Hatcher, R. D., Jr., Butler, J. R., Fullagar, P. D., Secor, D. T., and Snoke, A. W., 1980, Geologic synthesis of the Tennessee-Carolinas-Northeast Georgia southern Appalachians: in Wones, D. R. (ed.), Proc. The Calidonides in the USA, Vir. Poly. Inst. and State Univ., Mem. 2, p. 83-90.

Hatcher, R. D., Jr. and Zietz, I., 1980, Tectonic implications of regional aeromagnetic and gravity data from the southern Appalachians: Wones, D. R., (ed.), Proc. The Calidonides in the USA, Vir. Poly. Inst. and State Univ., Mem. 2, p. 235-244.

Hermes, O. D., 1968, Petrology of the Mecklenburg gabbro-metagabbro complex, North Carolina: Contrib. Mineral. Petrol., v. 18, p. 270-294.

Hermes, O. D., 1970, Petrochemistry of coexistent mafic silicates from the Mecklenburg gabbro-metagabbro complex, North Carolina: Geol. Soc. Amer. Bull. 81, p. 137-164.

Herren, E. C., 1980, Soil survey of Abbeville County, South Carolina, U. S. Dept. of Agricul., 82 pp. and maps.

Horai, K., 1971, Thermal conductivity of rock-forming minerals: J. Geophys. Resch., v. 76, p. 1278-1308.

Horai, K. and Baldridge, S., 1972, Thermal conductivity of nineteen igneous rocks, I Application of the needle probe method to the measurement of the thermal conductivity of rocks: Phys. Earth Planet. Int., v. 5, p. 151-156.

Horton, J. W., 1981, Shear zones between the Inner Piedmont and Kings Mountain belts in the Carolinas: Geol., v. 7, p. 28-33.

Hughes, C. J., 1982, Igneous Petrology: Elsevier Sci. Pub. Co., Amsterdam, 551 pp.

Hutchinson, R. W., Fyfe, W. S., and Kerrich, R., 1980, Deep fluid penetration and ore deposition: Min. Sci. Engng., v. 12, p. 107-120.

Iverson, W. and Smithson, S., 1982, Master decollement rootzones beneath the southern Appalachians and crustal balance: Geol., v. 10, p. 241-245.

Irvine, T. N., 1980, Magmatic infiltration metasomatism, double diffusive fractional crystallization, and adcumulus growth in the Muskox: in Hargraves, R. B., (ed.), Physics of Magmatic Processes, Princeton Univ. Press, p. 325-383.

Irvine, T. N., 1982, Terminology for layered intrusions: Jour. Petrol., v. 23, part 2, p. 127-162.

Irvine, T. N. and Baragar, W. R. A., 1971, A guide to the chemical classification of the common volcanic rocks: Can. Jour. Earth Sci., v. 8, p. 523-548.

Jackson, E. D., 1967, Ultramafic cumulates in the Stillwater, Great Dyke, and Bushveld intrusions: in Wyllie, P. J., (ed.), Ultramafic and Related Rocks, John Wiley and Sons, Inc., New York, p. 20-38.

Kane, M. F., 1983, Gravity evidence of crustal structure in the United States Appalachians: in Schenk, P. E. (ed.), Regional Trends in the Geology of the Appalachian-Caledonian-Hercynian-Mauritanide Orogen, D. Reidel Publ. Co., p. 45-54.

Kesler, T. L., 1972, Inner Piedmont belt of the southern crystalline Appalachians: Discussion: Geol. Soc. Amer. Bull., v. 83, p. 1895-1986.

King, P. B., 1955, A geologic section across the southern Appalachians: An outline of the geology in the segment in Tennessee, North Carolina, and South Carolina: in Russell, R. J., (ed.), Guides to Southeastern Geology, New York, Geol. Soc. Amer., p. 332-373.

Kuno, H., 1959, Origin of Cenozoic petrographic provinces of Japan and surrounding area: Bull. Volc., v. 20, p. 37-76.

Kuno, H., 1966, Lateral variation of basalt magma type across continental margins and island arcs: Bull. Volc., v. 29, p. 195-222.

Kuno, H., 1968, Origin of andesite and its bearing on the island arc structure: Bull. Volc., v. 32, p. 141-176.

Langmuir, D., 1978, Uranium solution--mineral equilibria at low temperatures with applications to sedimentary ore deposits: MAC Short Course, Toronto, pp. 17-55.

Larsen, E. S., Jr., 1938, Some new variation diagrams for groups of igneous rocks: J. Geol., v. 46, p. 505-520.

Leake, B. E., 1978, Nomenclature of amphiboles: Amer. Mineral., v. 63, p. 1023-1052.

LeMaitre, R. W., 1976, The chemical variability of some common igneous rocks: J. Petrol., v. 17, p. 589-637.

Long, L., 1979, The Carolina Slate belt--Evidence for a continental rift zone: Geol., v. 7, p. 180-184.

McCauley, J. R., 1961, Relationship between the Carolina Slate Belt and the Charlotte belt in Newberry County, South Carolina: Geol. Notes, v. 5, p. 59-71.

McConnell, K. I. and Griffin, V. S., Jr., 1973, Petrology of the Anderson Metagabbro: Geol. Notes, v. 17, n. 3, p. 68-82.

McSween, H. Y., Jr., 1970, Petrology of Charlotte and Kings Mountain belt rocks in northern Greenwood County, South Carolina: Geol. Notes, v. 14, p. 57-84.

McSween, H. Y., Jr., 1972, An investigation of the Dutchmans Creek gabbro, Fairfield County, South Carolina: Geol. Notes, v. 16, p. 19-42.

McSween, H. Y., Jr., 1981a, Petrology of the Ogden gabbroic intrusion, York County, South Carolina: S. C. Geol., v. 25, p. 91-100.

McSween, H. Y., Jr., 1981b, Gabbro-metagabbro complexes: a mechanism for magma ascent?: Geol. Soc. Amer., Abstr. with Pgms., v. 13, p. 508.

McSween, H. Y., Jr. and Nystrom, P. G., Jr., 1979, Mineralogy and petrology of the Dutchmans Creek gabbroic intrusion, South Carolina: Amer. Miner., v. 64, p. 530-545.

McSween, H. Y., Jr., Sando, T. W., Clark, S. R., Harden, J. T., and Strange, E. A., 1984, The gabbro-metagabbro association of the southern Appalachian piedmont: Amer. Jour. Sci., v. 284, p. 438-461.

Macdonald, G. A., 1968, Composition and origin of Hawaiian lavas: Geol. Soc. Amer. Mem. 116, p. 1541-1596.

Macdonald, G. A. and Katsura, T., 1964, Chemical composition of Hawaiian lavas: J. Petrol., v. 5, p. 82-133.

Matthews, V., III, 1967, Geology and petrology of the pegmatite district in southwestern Jasper County, Georgia: Unpubl. M.S. thesis, Univ. Ga.

Matthews, V., III, 1969, The Gladesville norite and its relationship to similar mafic plutons in the Georgia Piedmont: Geol. Soc. Amer. Abstr. with Pgms., v. 4, p. 50.

Medlin, J. H., 1968, Comparative petrology of two igneous complexes in the South Carolina Piedmont: Unpubl. Ph.D. thesis, Penn. State Univ.

Medlin, J. H., 1969, Petrology of two mafic igneous complexes in the South Carolina Piedmont: Geol. Soc. Amer., Abstr. with Pgms., v. 4, p. 52.

Medlin, J. H., Thornton, C. P., and Gold, D. P., 1972, Petrology of mafic igneous complexes in the southeastern U. S. Piedmont: II: The Buffalo mafic igneous complex, Union County, South Carolina: S. E. Geol., v. 14, p. 73-106.

Mirkovich, V. V., 1968, Experimental study relating thermal conductivity to thermal piercing of rocks: Int. J. Rock Mech. Min. Sci., v. 5, p. 205-218.

Misra, K. C. and McSween, H. Y., Jr., 1984, Mafic and ultramafic rocks of the Appalachian orogen--An Introduction: Amer. Jour. Sci., v. 284, p. 290-293.

Miyashiro, A., 1974, Volcanic rock series in island arcs and active continental margins: Amer. J. Sci., v. 274, p. 321-355.

Morgan, B. A., 1963, A gravity survey of a ring-dike near Concord, North Carolina: Unpubl. M.S. thesis, Univ. of N. C. at Chapel Hill.

Morgan, M. T. and West, G. A., 1980, Thermal conductivity of the rocks in the Bureau of Mines standard rock suite: Oak Ridge Nat. Lab., ORNL/TM-7052, 54 p.

Myers, C. W., 1968, Geology of the Presley Mill gabbro, Putnam County, Georgia: Unpubl. M.S. thesis, Univ. Ga.

Nelson, A. E., 1981, Polydeformed rocks of the Lowndsville shear zone in the Greenville 2 degree quadrangle, South Carolina: in Horton, J. W., Jr., Butler, J. R., and Milton, D. M., (eds.), Geological Investigations of the Kings Mountain Belt and Adjacent Areas in the Carolinas, Carolina Geol. Soc. Field Trip Guidebook, S. C. Geol. Surv., p. 181-193.

Office of Nuclear Waste Isolation, 1979, Conceptual Reference Repository Description (CRRD), Office of Nuclear Waste Isolation: ONWI/SUB/79/E512-01600.16, v. 3.

Office of Waste Isolation, 1978, Contribution to draft generic environmental impact statement on commercial waste management: Radioactive waste isolation in geologic formation: Y/OWI/TM-44.

O'Hara, M. J., 1968, The boundary of phase equilibria studies on the origin and evolution of basic and ultrabasic rocks: Earth Sci. Rev., v. 4, p. 69-133.

O'Hara, M. J., 1976, Data reduction and projection schemes for complex compositions: Progress in Experimental Petrology, Nat. Environ. Res. Council Publ. series D, n. 6, p. 103-126.

O'Hara, M. J., 1977, Geochemical evolution during fractionation crystallization of a periodically refilled magma chamber: Nature, v. 266, p. 503-507.

Olsen, B. A., 1982, Petrogenesis of the Concord gabbro-syenite complex, Cabarrus County, North Carolina: Unpubl. M.S. thesis, Univ. Tenn., Knoxville.

Olsen, B. A., McSween, H. Y., Jr., and Sando, T. W., 1983, Petrogenesis of the Concord gabbro-syenite complex, North Carolina: Amer. Miner., v. 68, p. 315-333.

Otten, M. T., 1983, The Magmatic and Subsolidus Evolution of the Artfjallet Gabbro Central Swedish Caledonides: Offsetdrukkerij Kanters B. V., Alblasserdam, 185 pp.

Overstreet, W. C. and Bell, H., III, 1965a, The crystalline rocks of South Carolina: U. S. Geol. Surv. Bull. 1183, 126 pp.

Overstreet, W. C. and Bell, H., III, 1965b, Geologic map of the crystalline rocks of South Carolina: U. S. Geol. Surv. Misc. Geol. Inv. Map I-413, 1:250,000 map.

Pirkle, W. A., 1977, Geology of the Red Hill quadrangle, Edgefield County, South Carolina: Geol. Notes, v. 21, p. 75-83.

Pirkle, W. A., 1978, Preliminary report on the geology of the Parksville quadrangles, McCormick and Edgefield Counties, South Carolina: Geol. Notes, v. 22, p. 95-104.

Pirkle, W. A., 1982, Geologic framework of the Winterseat quadrangle in the southwestern portion of the Carolina Slate belt, South Carolina: S. C. Geol., v. 26, p. 69-79.

Price, V. P., Jr., 1966, Distribution of trace elements in plutonic rocks of the southeastern Piedmont: Unpubl. Ph.D. thesis, Univ. North Carolina, Chapel Hill.

Price, V. P., Jr., 1969, Note on a fault in Abbeville County, South Carolina: Geol. Notes, v. 13, p. 81-82.

Rao, S. S., 1982, The Finite Element Method in Engineering: Pergammon Press, New York, 625 pp.

Ragland, P. C. and Butler, J. R., 1972, Crystallization of the West Farrington Pluton, North carolina, U.S.A.: Jour. Petrol., v. 13, p. 381-404.

Rickertsen, L. D. and Claiborne, H. C., 1981, Expected environments for a defense high-level waste repository in salt: Oak Ridge nat. Lab., ORNL/TM-7597, 43 pp.

Rickertsen, L. D., Arbital, J. G., and Claiborne, H. C., 1982a, Expected near-field thermal environments in a sequentially loaded spent-fuel or high-level waste repository in salt: Oak Ridge Nat. Lab., ORNL/TM-8083, 58 pp.

Rickertsen, L. D., Misplon, M. A., Claiborne, H. C., 1982b, Expected very-near-field thermal environments for advanced spent-fuel and defense high-level waste packages: Oak Ridge Nat. Lab., ORNL/TM-8109, 62 pp.

Ringwood, A. E., 1980, Safe disposal of high-level radioactive wastes: Fortsch. Mineral., v. 58, p. 149-168.

Rogers, J. J. W., 1982, Criteria for recognizing environments of formation of volcanic suites in the Carolina Slate belt: Geol. Soc. Amer. Special Paper 191, p. 99-107.

Rozen, R. W., 1981, The Middleton-Lowndesville cataclastic zone in the Elberton East quadrangle, Georgia: in Horton, J. W., Jr., Butler, J. R., and Milton, D. M. (eds.), Geological Investigations of the Kings Mountain Belt and Adjacent Areas in the Carolinas, Carolina Geol. Soc. Field Trip Guidebook, S. C. Geol. Surv., p. 174-180.

Salpas, P. A., Haskin, L. A., and McCallum, I. S., 1983, Stillwater anorthosites: A lunar analogy?: Proc. 14th Lunar and Planet. Sci. Conf., Pt. 1., J. Geophys. Resc., v. 88, p. B27-B39.

Secor, D. T., Jr., Peck, L. S., Pitcher, D. M., Prowell, D. C., Simpson, D. H., Smith, W. A., and Snoke, A. W., 1982, Geology of the area of induced seismic activity at Monticello Reservoir, South Carolina: Jour. Geophys. Resch. v. 87. n. B8, p. 6945-6957.

Secor, D. T., Jr., Samson, S. L., Snoke, A. W., and Palmer, A. R., 1983, Confirmation of the Carolina Slate belt as an exotic terrain: Science, v. 221, p. 649-650.

Secor, D. T. and Snoke, A. W., 1978, Stratigraphy, structure and plutonism in the central South Carolina Piedmont: in Snoke, A. E. (ed.), Geological Investigations of the Eastern Piedmont of the Southern Appalachians, Carolina Geol. Soc. Field Trip Guidebook for 1978, S. C. Geol. Surv. Columbia, S. C., p. 61-99.

Spry, A., 1969, Metamorphic Textures: Pergamon Press, New York, N. Y., 350 pp.

Stolper, E., 1980, A phase diagram for mid-ocean ridge basalts: Preliminary results and implications for petrogenesis: Contrib. Mineral. Petrol., v. 74, p. 13-27.

Stroch, S. N. and Prince, B. E., 1979, Assumptions and ground rules used in nuclear waste projections and source term data: Office of Nuc. Waste Isol., ONWI-24, 137 pp.

Strange, E. A., 1983, The geochemistry of the Barber mafic complex, Rowan County, North Carolina: Unpubl. M.S. thesis, Univ. Tenn., Knoxville.

Streckeisen, A. L., 1973, Plutonic rock classification and nomenclature recommended by the IUGS subcommission on the systematics of igneous rocks: Geotimes, v. 18, n. 10, p. 26-30.

Talwani, P., Long, L. T., and Bridges, S. R., 1975, Simple Bouger anomaly map of South Carolina: S. C. Geol. Surv., MS-21, 1:500,000 map and 27 pp. text.

Taylor, C. A., Jr. and Butler, J. R., 1982, Geology and gravity of the northern end of the Charlotte belt, and Davie County Mesozoic basin, central North Carolina Piedmont: Geol. Soc. Amer., Abstr. with Pgms., v. 14, p. 88-89.

Thurmond, C. J. and Whitney, J. A., 1979, Structural and stratigraphic development of the Charlotte and Northern Slate belts within the Chennault quadrangle, Georgia and South Carolina: Geol. Soc. Amer. Abstr. with Pgms., v. 11, n. 4, p. 215.

Trung, C. N. and Poty, B., 1976, Solubilité de UO_2 en milieu aqueux à 400 et 500°, et 1 kilobar: Rapport Annuel 1976, CNRS, France, p. 37-39.

Upton, B. G., J., 1974, The alkaline province of southeast Greenland: in Sorensen, H. (ed.), The Alkaline Rocks, John Wiley, London, 622 pp.

U. S. Department of Energy, 1977, conceptual Design Report--National Waste Terminal Storage Repository Waste in a Dome Salt Formation--Conceptual Design Study No. 6--Thermal Analysis: DOE Contract No. EY-77-C-05-5367.

U. S. Department of Energy, 1979, Management of Commercially Generated Radioactive Waste: DOE/EIS-0046-D, v. 2.

U. S. Department of Energy, 1980, Final Environmental impact statement: management of commercially generated radioactive waste: DOE/EIS-0046F.

U. S. Geological Survey, 1978, Aeromagnetic survey of northwest South Carolina: Open File Map 78-847, scale: 1-250,000, Reston, Va.

Van der Plas, L. and Tobi, A. C., 1965, A chart for judging the reliability of point counting results: Amer. Jour. Sci., v. 263, p. 87-90.

Wagener, H. D., 1974, The York-Chester gabbro-metagabbro-amphibolite complex: Geol. Notes, v. 18, p. 1-3.

Wagener, H. D., 1977, The granitic stone resources of South Carolina: S. C. Geol. Surv., Miner. Resources Series 5, 65 pp. plus maps.

Walker, D., Shibata, T., and DeLong, S. E., 1979, Abyssal tholeiites from the Oceanographer fracture zone: Contrib. Mineral. Petrol., v. 70, p. 111-125.

Weisenfluh, G. A. and Snoke, A. W., 1978, an epizonal trondhjemite-quartz keratophyre complex near Calhoun Falls, South Carolina: Geol. Notes, v. 22, p. 47-73.

Wheeler, B. D., 1982, Chemical analysis of coal by energy dispersive X-ray fluorescence utilizing artificial standards: Adv. in X-ray Anal., v. 26, p. 457-466.

Whitney, J. A., Paris, T. A., Carpenter, R. H., and Hartley, M. E., III, 1978, Volcanic evolution of the southern Slate belt of Georgia and South Carolina: A primitive oceanic island arc: Jour. Geol., v. 86, p. 173-193.

Wicks, F. J. and Whittaker, E. J. W., 1977, Serpentine textures and serpentinization: Can. Mineral., v. 15., p. 459-488.

Wicks, F. J., Whittaker, E. J. W., and Zussman, J., 1977, An idealized model for serpentine textures after olivine: Can. Mineral., v. 15, p. 446-458.

Wilson, F. A., 1981, Geologic interpretation of geophysical data from the "Mecklenburg-Weddington" gabbro complex, southern Mecklenburg County, North Carolina: Horton, J. W., Jr., Butler, J. r., and Milton, D. M. (eds.), Geological Investigation of the Kings Mountain belt and adjacent areas in the Carolinas, Carolina Geological Society Field Trip Guidebook, S. C. Geol. Surv., p. 28-38.

Wright, T. L. and Doherty, P. C., 1970, A linear programming and least squares computer method for solving petrologic mixing problems: Geol. Soc. Amer. Bull., v. 81, p. 1995-2008.

APPENDICES

APPENDIX A

Table A1. Representative modal analyses (volume percent) from Calhoun Falls complex.

	PcPO (Gabbronorite)				PO (Troctolite)				Metagabbro				Pyroxonite	Serpentinite		
	CF1	CF21	CF26	CF50	CF31	CF32	CF33	CF34	CF6	CF12	CF22	CF29	CF14*	CF15	CF19	CF27
Pg	45.8	59.6	72.6	63.1	58.1	64.4	62.4	64.0	28.9	44.4	49.5	41.1	∿1.5			
Ol	Tr	5.2	Tr	6.6	12.8	3.0	9.1	10.0					Tr			
Cpx	26.0	16.6	13.4	13.6	Tr	0.2	Tr	Tr		4.9		Tr	∿2.0	.5		Tr
Opx	20.2	1.6	Tr	1.8	7.3	2.0	7.3	6.8					∿95.0			
Hbl	3.2	14.8	1.8	9.6	18.3	25.2	15.2	17.6		1.0	Tr	25.0	∿1.0	.5	Tr	7.3
Bt		.6	1.0	1.1	1.8	3.0	2.5	1.0		Tr	Tr	Tr				
Opq	4.8	1.6	8.6	2.9	1.4	1.8	1.7	.6	9.6	Tr	6.1	12.1	.5	5.1	.7	15.1
Act					Tr		Tr		38.9	41.0	44.3	20.8			63.5	
Epid		Tr	2.2	1.2	.2	.4			4.7	4.6	Tr					
Chl									9.0		Tr					
Tc									8.3	4.1	Tr	1.0		49.8	26.4	42.7
Ap				Tr												
Serp														44.2	9.4	34.9
Total	100.0	100.0	100.0	100.0	100.0	100.0	100.0	100.0	100.0	100.0	100.0	100.0	∿100.0	100.0	100.0	100.0
Counts	1000	1000	1000	1025	1000	1000	1000	1000	508	705	512	924	500	575	948	782

*Very fine-grained; low confidence on modal results.

Table A2. Representative modal analyses (volume percent) from Mt. Carmel complex.

	Olivine-Biotite Gabbro						Metagabbro							
	MC13	MC19	MC21	MC36	MC42	MC43	MC2	MC7	MC12	MC14	MC20	MC23	MC26	MC28
Pg	68.4	37.1	59.3	50.2	69.3	65.4	60.0	7.9	23.4	--	60.1	45.5	21.7	33.4
Ol	4.2	--	6.5	--	5.6	1.8	--	--	--	--	--	--	--	--
Cpx	7.8	--	3.3	7.0	9.1	10.0	20.9	4.1	1.0	16.5	14.6	17.6	--	10.4
Opx	--	--	--	3.2	.6	--	--	--	--	--	--	--	--	--
Hbl	--	39.2	22.9	27.4	5.1	--	--	22.9	--	--	1.1	--	--	--
Bt	15.3	20.2	--	1.0	1.4	14.8	--	--	--	--	--	--	--	--
Opq	4.3	Tr	3.5	4.4	5.9	5.4	5.2	5.7	11.8	15.0	5.4	7.8	11.3	16.9
Act	Tr	--	--	--	--	--	9.5	53.1	58.1	63.7	9.3	25.6	65.4	35.7
Epid	--	1.8	--	1.8	--	--	5.4	6.3	5.7	4.5	4.0	6.5	1.6	3.5
Chl	--	--	--	--	--	--	Tr	--	--	--	5.5	--	--	--
Ap	1.0	--	1.8	--	3.0	1.6	--	Tr	Tr	--	--	--	Tr	--
Chl	--	2.0	--	4.0	--	--	--	--	--	--	--	--	--	--
Total	100.0	100.0	100.0	100.0	100.0	100.0	100.0	100.0	100.0	100.0	100.0	100.0	100.0	100.0
Counts	1000	1000	1000	1000	1000	1000	1000	1000	1000	1000	1000	1000	1000	1000

Table A3. Representative modal analyses (volume percent) from Greenwood complex.

	Fine-Grained Gabbro				POP (Gabbronorite)		Metagabbro	
	GW7	GW13	GW15	GW14	GW8	GW9	GW11	GW10
Pg	50.0	53.5	56.6	57.3	63.7	60.8	60.3	34.8
Ol	37.6	29.9	31.0	28.1	14.4	15.3	8.5	1.8
Cpx	.8	3.2	3.9	4.5	5.1	4.5	8.5	29.7
Opx	1.3	6.7	2.8	3.9	--	--	--	--
Hbl	1.1	.7	.2	Tr	13.1	18.4	4.9	.7
Bt	4.3	3.2	1.7	2.1	Tr	Tr	1.2	
Opq	4.6	2.8	3.9	3.8	2.4	1.1	6.5	1.5
Act.	.3			.3	1.3	Tr	10.2	31.5
Total	100.0	100.0	100.0	100.0	100.0	100.0	100.0	100.0
Counts	1000	1000	1000	1000	1000	1000	1000	1000

Table A4. Representat

		Greenwood Complex								
Wt. % Oxide	CF50 Core	GW9 Rim	GW14 Core	GW14 Rim	GW8 Core	GW8 Rim	GW10 Core	GW10 Rim	GW13 Core	GW13 Rim
SiO_2	51.0	49.99	52.72	57.21	49.61	53.64	47.88	51.94	55.68	65.70
Al_2O_3	31.8	32.77	29.42	26.98	33.63	31.13	34.04	30.75	29.14	22.86
FeO*	.41	.17	.45	.59	.14	.15	.41	.25	.63	.33
CaO	14.1	14.55	12.00	8.95	14.84	12.52	16.27	11.64	10.42	3.50
Na_2O	3.39	3.11	4.11	6.45	2.49	3.86	1.80	3.36	4.39	7.03
K_2O	.11	.04	.44	.71	.03	.08	.07	.09	.48	2.32
Total	100.7	100.64	99.14	100.89	100.73	101.38	100.48	98.02	100.75	101.75
		Cations/8 Oxygens								
Si	4.995	2.265	2.410	2.557	2.240	2.388	2.180	2.383	2.486	2.856
Al	2.304	1.748	1.585	1.421	1.790	1.633	1.827	1.063	1.533	1.109
Fe	.014	.005	.016	.021	.005	.005	.015	.009	0.23	.011
Ca	.682	.705	.587	.428	.717	.597	.792	.572	.498	.162
Na	.297	.272	.363	.559	.217	.333	.159	.297	.380	.591
K	.005	.001	.025	.041	.001	.004	.004	.004	.026	.128
Total	4.995	4.995	4.987	5.025	4.970	4.959	4.979	4.929	4.946	4.915

[a]Values in wt. % (

*All iron reporte

Table A5. Representative electron microprobe analyses: olivine.

	Calhoun Falls Complex					Mt. Carmel Complex			Greenwood Complex				
	CF50 [5]	CF33 [5]	CF21 [5]	CF34 [5]	CF32 [5]	MC42 [5]	MC13 [4]	MC13 [5]	GW14 [5]	GW9 [6]	GW9 [5]	GW13 [5]	GW8 [6]
SiO_2	39.0 (2)	38.3 (8)	38.1 (4)	28.9 (2)	38.8 (3)	32.24(6)	30.56(2)	31.08(14)	36.98(6)	38.78(12)	29.13(13)	36.75(12)	38.88(18)
Cr_2O_3	.00(0)	.00(0)	.02(2)	.27(2)	.25(3)	NA	NA	NA	NA	NA	NA	.00(2)	.00
TiO_2	NA	NA	NA	NA	NA	.03(1)	.03(0)	.03(3)	.09(0)	.05(1)	.03(1)	.03(1)	.00(1)
FeO*	20.0 (2)	19.0 (13)	21.0 (5)	15.4 (2)	16.3 (7)	53.38(8)	58.30(8)	57.47(60)	30.16(7)	17.48(8)	16.54(7)	30.83(50)	19.52(34)
MnO	NA	NA	NA	NA	NA	1.99(2)	3.26(6)	3.36(4)	.50(5)	.44(3)	.27(2)	.55(3)	.35(2)
CaO	.00(0)	.02(2)	.02(1)	ND	ND	.02(0)	.07(4)	.07(2)	.18(1)	.04(1)	.02(1)	.13(1)	.00(0)
MgO	41.7 (5)	41.9(34)	39.7 (7)	44.7 (4)	43.8 (5)	13.62(4)	6.68(1)	6.39(10)	33.59(3)	44.15(2)	44.40(12)	31.23(12)	41.22(5)
NiO	.07(2)	.21(5)	.04(3)	ND	ND								
Total	100.8	99.5	98.9	99.3	99.2	101.27	98.90	98.41	101.51	100.95	100.39	99.51	99.98
	Cations/4 Oxygens					Cations/4 Oxygens			Cations/4 Oxygens				
Si	.993	.986	.996	.978	.990	0.981	0.993	1.010	0.985	0.978	0.986	1.003	0.998
Cr_2O_3												.000	.000
Tf						.000	.000	.000	.001	.000	.000	.000	.000
Fe	.425	.410	.458	.327	.348	1.359	1.585	1.563	.671	.368	.348	.704	.418
Cr	.000	.000	.000	.005	.005								
Ca	.000	.000	.001			.000	.001	.001	.004	.000	.000	.003	.000
Mg	1.584	1.609	1.547	1.691	1.665	.619	.323	.309	1.333	1.660	1.668	1.271	1.577
Ni	.001	.003	.000										
Total	3.004	3.009	3.002	3.010	3.008	3.011	2.993	2.976	3.006	3.016	3.007	2.993	3.000

[a]Unit in [ ] is the number of replicate analyses averaged.

[b]Values in wt. % oxides.

[c]Units in ( ) represent one standard deviation in terms of least units cited.

*All iron reported as FeO.

NA = Oxide not analyzed.

ND = Oxide not detected.

Table A6. Representative

				Calhoun Falls Complex			
	CF3.35 [6] 7]	MC35 [7]	MC13 [6]	GW8 [5]	GW10 [5]	GW11 [5]	GW14 [4]
SiO_2	54.42 .82(60)	49.26(77)	50.92(45)	51.54(28)	55.02(42)	50.51(19)	48.75(28)
TiO_2	.10 .32(13)	.46(0)	.25(3)	.63(12)	.08(4)	.83(4)	1.52(3)
Al_2O_3	1.68 .85(8)	.95(8)	1.18(11)	2.40(39)	.85(20)	3.49(4)	3.79(25)
Cr_2O_3	NA --	--	--	.12(3)	.02(3)	--	--
FeO*	13.62 .20(49)	22.50(53)	17.18(30)	3.85(28)	14.98(35)	6.95(41)	9.52(4)
MnO	.51 .30(9)	.93(8)	1.04(5)	.19(4)	.41(3)	.27(8)	.24(2)
MgO	29.08 .11(7)	4.83(20)	9.76(8)	15.79(13)	27.34(39)	15.84(28)	14.78(17)
CaO	.55 .92(20)	20.74(11)	20.02(10)	24.21(42)	.66(17)	20.87(47)	19.64(18)
Na_2O	.01 --	--	--	--	--	--	--
Total	99.97 .52	99.68	100.35	98.70	99.36	98.77	98.23
					Cations/6 Oxygens		
Si	1.94 .980	1.970	1.962	1.917	1.988	1.888	1.854
Ti	.00 .009	.013	.006	.017	.002	.023	.042
Al	.07 .040	.043	.053	.104	.036	.153	.109
Cr	--	--	--	.003	.000	--	--
Fe	.40 .855	.752	.553	.119	.453	.217	.302
Mn	.01 .044	.030	.034	.005	.011	.007	.006
Mg	1.55 .188	.287	.560	.874	1.471	.882	.837
Ca	.02 .866	.888	.827	.965	.024	.835	.800
Na	.00 --	--	--				
Total	4.01 .982	3.983	3.994	4.004	3.984	4.005	4.011

[a]Unit in [ ] is the

[b]Values in wt. % oxi

[c]All Fe reported as

NA = Oxide not analy

ND = Oxide not detec

Table A7. Representative electron microprobe analysis: amphibole.

	MC7 [4]	MC14 [5]	CF32 [5]	CF50 [6]
SiO_2	51.64(10)	40.09(10)	38.56(12)	40.45(16)
TiO_2	.36(13)	1.89(12)	2.58(10)	3.46(18)
Al_2O_3	4.90(30)	13.04(27)	12.63(32)	11.93(14)
FeO*	7.22(23)	9.96(20)	10.56(22)	10.59(22)
MnO	.14(5)	.27(10)	.40(3)	.22(7)
MgO	16.42(20)	15.15(12)	14.34(23)	14.42(28)
CaO	12.71(14)	11.96(60)	11.55(12)	11.63(23)
Na_2O	.74(10)	2.52(31)	2.39(27)	2.54(14)
K_2O	.04(23)	1.22(19)	1.18(19)	1.14(21)
Total	94.16	96.11	94.20	96.37
		Cations/24 oxygens		
Si	7.542	6.018	5.938	6.065
Ti	.038	.211	.298	.387
Al	.840	2.304	2.291	2.108
Fe	.878	1.247	1.355	1.325
Mn	.013	.031	.049	.026
Mg	3.574	3.387	3.290	3.222
Ca	1.988	1.92	01.902	1.866
Na	.206	.731	.709	.735
K	.004	.229	.230	.215
Total	15.083	16.078	16.064	15.951

[a]Unit in [ ] is the number of replicate analyses averaged.

[b]Values in wt. % oxide.

[c]Units in ( ) represent one standard deviation in terms of least unit cited.

*All Fe is reported as FeO.

Table A8. Major element constituents (wt. %) and CIPW normative mineralogy for Calhoun Falls complex.

	PcPO (Gabbronorite)				PO (Troctolite)				Pyroxenite	Metagabbro					Serpentinites				
Wt. % Oxide	CF1	CF21	CR26	CF50	CF31	CF32	CF33	CF34	CF14	CF12	CF18	CR29	CF40	CF51	CF4	CF11	CF19	CF29	CF45
Major Element Constituents																			
SiO_2	47.10	48.75	46.44	46.24	47.42	47.90	45.61	45.37	51.33	50.03	51.99	41.83	49.82	41.57	53.03	53.16	50.08	42.79	43.49
TiO_2	0.54	0.35	3.10	0.58	0.66	0.57	0.40	0.64	0.31	.50	.56	2.19	1.10	3.33	0.36	0.34	1.10	0.49	1.18
Al_2O_3	16.09	16.63	16.41	16.10	20.18	22.70	20.73	18.75	3.68	17.19	18.09	13.77	15.10	12.20	2.89	3.08	12.35	5.54	8.89
Fe_2O_3*	2.20	1.63	3.15	2.22	1.62	1.40	1.38	1.53	3.70	1.15	1.78	3.87	1.92	3.71	5.07	4.31	4.31	4.75	4.44
FeO	6.26	4.64	8.96	6.33	4.60	3.71	3.92	4.36	8.64	3.28	5.07	11.01	5.46	10.55	8.63	7.34	7.34	8.09	7.55
MnO	0.23	0.11	0.24	0.15	0.10	0.08	0.09	0.10	0.35	.09	.15	.16	.16	.21	0.36	0.29	0.30	0.33	0.23
MgO	12.24	12.96	7.74	15.62	14.99	11.69	15.83	16.58	25.96	14.27	10.41	10.10	10.97	8.91	24.80	25.42	16.71	35.89	24.63
CaO	14.36	11.02	10.14	10.28	11.22	11.36	10.23	10.91	6.33	12.74	7.00	11.98	9.50	11.07	2.76	4.87	5.50	3.10	6.42
Na_2O	1.04	2.55	3.42	2.02	2.35	2.84	2.13	1.95	0.31	2.22	2.75	1.90	2.45	1.97	0.14	ND	ND	ND	0.39
K_2O	0.07	0.24	0.35	0.26	0.48	0.48	0.36	0.41	ND	0.33	1.36	0.71	0.82	0.41	ND	ND	0.28	ND	0.03
P_2O_5	0.29	0.28	1.62	0.27	0.36	0.49	0.28	0.53	0.10	0.23	0.31	2.51	0.43	2.70	0.05	0.07	0.61	0.28	0.48
Total	100.42	99.16	101.57	100.07	103.98	103.24	100.96	101.13	100.71	102.03	99.47	100.03	97.73	96.63	98.09	98.88	98.58	101.26	97.73
CIPW Norm																			
Q	--	--	--	--	--	--	--	--	--	--	--	--	--	--	5.56	3.88	10.2	--	--
Or	0.41	1.43	2.03	1.53	2.73	2.75	2.11	2.39	--	1.91	8.08	4.19	4.96	2.50	--	--	1.68	--	--
Ab	8.76	21.75	28.46	17.08	13.66	17.64	13.45	11.76	2.60	18.41	23.39	16.04	21.20	17.22	1.21	--	--	--	3.38
An	38.85	33.49	27.92	34.06	41.44	46.26	45.50	40.72	8.59	35.24	32.89	26.89	28.42	24.00	7.40	8.50	23.67	13.40	22.93
Ne	--	--	--	--	2.96	3.05	2.39	2.46	--	--	--	--	--	--	--	--	--	--	--
Cor	--	--	--	--	--	--	--	--	--	--	0.10	--	--	--	--	--	3.54	0.56	--
Di Wo	12.61	8.27	4.69	6.32	4.11	2.19	1.24	3.92	9.16	10.54	--	6.77	7.07	6.13	2.60	6.46	--	--	2.70
Di En	8.86	6.16	2.98	1.10	3.15	1.68	0.97	3.06	6.87	8.32	--	4.14	5.13	3.83	1.96	4.99	--	--	2.11
Di Fs	2.71	1.31	1.43	--	0.53	0.28	0.14	0.44	1.39	1.05	--	2.28	1.31	1.95	0.38	0.79	--	--	0.30
Hy En	7.78	3.13	3.33	0.40	--	--	--	--	47.03	1.01	20.13	1.20	15.22	11.74	60.99	59.02	42.19	23.40	27.91
Hy Fs	2.35	0.66	1.59	0.09	--	--	--	--	9.42	.12	5.59	.65	3.86	5.93	11.59	9.23	8.87	2.81	3.95
Ol Fo	9.60	16.29	8.86	23.70	22.94	18.58	26.68	26.46	7.20	17.87	4.15	13.86	5.32	5.15	--	--	--	45.44	22.93
Ol Fa	3.20	3.78	4.65	6.12	4.20	3.41	4.15	4.15	1.59	2.45	1.27	8.31	1.49	2.86	--	--	--	6.02	3.57
Mt	3.17	2.38	4.49	3.22	2.26	1.99	1.98	2.19	5.33	1.63	2.59	5.60	2.85	5.56	7.49	6.32	6.34	6.80	6.58
Il	1.02	0.67	5.79	1.10	1.21	1.05	0.75	1.20	0.58	.93	1.07	4.15	2.14	6.53	0.70	0.65	2.12	0.92	2.29
Ap	0.68	0.67	3.77	0.64	0.82	1.12	0.66	1.24	0.24	.53	.74	5.93	1.04	6.60	0.12	0.17	1.47	0.65	1.16

* $\frac{Fe^{3+}}{Fe^{2+} + Fe^{3+}} = 0.26$ (Le Maitre, 1976), assumed.

Table A9. Major element cor

Wt. % Oxide	MC2†	MC7	26-34	Olivine-Biotite Gabbro 180-12	180-19	180-22	180-268	124-3a	124-3	Syenite 124-2	124-2a	124-12	180-20	180-25
Major Element Constituents†														
SiO_2	44.4	41.83	45.10	53.30	51.50	47.50	53.50	54.00	55.80	60.20	58.00	65.30	60.00	62.70
TiO_2	2.96	3.14	0.92	2.04	2.42	2.52	1.72	1.63	1.26	0.72	0.85	0.10	0.46	0.52
Al_2O_3	19.98	14.10	22.80	19.50	17.70	22.50	16.30	16.80	19.70	16.70	16.70	18.00	18.00	17.60
Fe_2O_3*	2.70	4.33	6.69	1.72	2.05	2.01	1.64	10.75	1.35	1.62	1.59	0.55	0.98	0.82
FeO	6.61	10.60	5.47	7.71	9.64	5.79	9.21	9.64	6.19	7.28	7.16	2.45	4.42	3.68
MnO	0.09	0.24	0.095	0.12	0.15	0.105	0.14	0.80	0.23	0.29	0.35	0.05	0.18	0.12
MgO	5.06	9.35	5.30	5.00	6.90	5.30	6.10	5.50	4.50	0.50	0.70	0.10	0.45	0.35
CaO	11.81	10.22	14.10	6.50	6.50	7.50	5.20	5.50	5.40	2.80	3.70	0.50	2.20	0.18
Na_2O	2.59	1.56	2.70	4.65	3.95	4.75	5.45	4.98	5.42	4.93	6.16	7.25	6.75	5.65
K_2O	0.63	0.47	0.05	1.51	0.79	0.96	2.40	1.70	2.52	4.04	3.04	5.44	5.34	6.43
P_2O_5	0.13	0.97	NA	NA	NA	NA	NA	NA	NA	NA	NA	NA	NA	NA
SrO	NA	NA	0.07	0.07	0.08	0.08	0.065	0.055	0.065	0.035	0.04	0.21	0.025	0.014
BaO	NA	NA	0.01	0.04	0.025	0.04	0.05	0.06	0.06	0.15	0.08	0.005	0.13	0.055
Cr_2O_3	NA	NA	0.02	0.02	0.025	0.005	0.005	0.025	0.005	0.005	0.005	0.005	0.01	0.015
NiO	NA	NA	0.01	0.005	0.045	0.015	0.005	0.005	0.005	0.005	0.005	0.005	0.005	0.005
Total	97.81	97.99	00.29	99.64	99.72	97.56	98.35	101.11	98.62	99.26	98.37	99.95	98.95	99.75
CIPW Norm														
Qz	--	--	--	--	0.02	--	0.33	--	--	4.61	--	--	--	1.82
Or	3.84	2.78	0.27	8.96	4.68	5.82	14.43	9.96	15.10	24.07	18.27	32.18	31.91	38.74
Ab	19.54	13.20	17.48	39.50	33.54	31.30	46.91	41.78	46.51	42.06	57.99	61.40	45.40	48.74
An	40.97	30.08	41.37	23.05	27.24	25.59	15.92	21.83	18.14	11.60	9.09	0.51	3.08	1.05
Ne	1.29	--	2.87	--	--	5.37	--	--	--	--	--	--	6.69	--
C	--	--	--	--	--	--	--	--	--	--	--	--	--	0.99
Di Wo	6.87	5.97	11.94	4.00	2.25	5.37	4.43	2.29	3.89	1.16	4.10	1.14	3.49	--
Di En	4.52	3.78	7.81	1.52	0.92	2.15	3.83	0.51	1.00	0.13	0.61	0.07	0.53	--
Di Fs	1.86	1.81	3.33	2.57	1.36	3.31	0.0	1.95	3.15	1.17	3.91	1.21	3.30	--
Hy En	--	9.37	--	3.77	9.07	--	1.75	1.99	0.65	1.13	0.29	0.06	--	0.89
Hy Fs	--	4.49	--	6.30	13.27	--	0.0	7.49	2.03	10.31	1.83	0.93	--	5.53
Ol Fo	5.66	7.10	2.36	1.38	--	4.93	--	1.19	1.15	--	0.61	0.08	0.42	--
Ol Fa	2.57	3.75	1.10	2.53	--	8.26	--	4.95	3.98	--	4.30	1.42	2.82	--
Mt	3.91	6.28	9.67	2.50	2.98	2.99	1.12	2.95	1.99	2.37	2.34	0.80	1.44	1.21
Hm	--	--	--	--	--	--	7.95	--	--	--	--	--	--	--
Il	5.62	5.96	1.74	3.89	4.61	4.91	3.32	3.07	2.43	1.38	1.64	0.19	0.88	1.01
Ap	0.42	2.25	--	--	--	--	--	--	--	--	--	--	--	--
Cc	--	--	0.03	0.03	0.04	0.02	0.02	0.04	0.02	0.01	0.02	0.01	0.02	0.03

*$Fe^{3+}/Fe^{3} + Fe^{2+} = 0.2($

†Sample numbers with MC

Table A10. Major element constituents (wt. %) and CIPW normative mineralogy for Greenwood complex.

	Fine-Grained Gabbro (Diabase)										POcP Cumulate (Gabbronorite)									Metagabbro					
	GW1	GW3	GW9	GW12	GW13	GW15	GW17	GW19	GW20	GW21	GW8	GW9	GW10	GW11	GW16	GW18	GW22	GW23	GW25	GW2	GW4	GW6	GW30	GW31	GW32
Major Element Constituents																									
SiO_2	56.38	48.14	49.57	41.94	49.12	46.59	47.87	48.19	50.17	54.36	47.09	46.72	51.04	46.77	48.82	44.77	47.53	51.77	45.97	45.57	53.70	53.03	51.21	49.30	45.07
TiO_2	1.26	1.17	1.62	1.13	1.46	2.32	1.62	2.61	1.68	0.92	0.73	0.40	0.25	0.97	0.53	2.34	1.45	1.49	2.89	2.13	1.89	0.71	0.73	0.40	1.65
Al_2O_3	13.98	16.18	14.88	20.08	14.81	15.81	20.22	17.22	22.09	23.90	23.06	23.41	12.58	20.90	16.61	20.11	20.90	22.55	17.97	17.47	16.22	14.87	15.64	17.58	13.95
Fe_2O_3*	2.34	3.35	3.60	3.35	3.62	3.45	2.56	3.41	3.50	2.36	1.52	1.34	3.85	2.16	2.68	3.45	2.75	0.90	3.27	3.29	2.62	2.32	2.60	1.94	3.46
FeO	5.74	8.19	8.80	8.21	8.86	8.46	6.28	8.34	8.63	5.78	3.72	3.28	9.42	5.28	6.47	8.44	6.74	2.21	7.99	8.06	6.40	5.68	6.36	4.74	8.47
MnO	0.11	0.17	0.17	0.20	0.17	0.17	0.15	0.17	0.24	0.16	0.07	0.08	0.20	0.11	0.13	0.19	0.11	0.18	0.15	0.17	0.14	0.13	0.14	0.10	0.18
MgO	6.26	9.04	9.15	6.79	9.83	8.80	4.97	7.56	4.07	1.70	8.21	9.00	16.48	9.77	10.74	7.10	5.68	2.28	5.64	6.75	4.58	10.01	9.42	12.43	14.42
CaO	5.69	9.58	8.63	14.48	8.73	9.59	9.36	9.12	3.09	1.16	11.78	12.07	9.34	11.15	12.36	7.37	11.28	12.47	10.00	9.79	6.48	9.39	9.67	12.52	9.44
Na_2O	3.00	1.48	2.48	1.15	1.99	1.78	3.11	1.81	2.92	4.28	1.46	1.05	ND	1.30	0.34	1.01	2.38	4.14	3.54	2.83	3.43	0.79	1.53	0.79	0.71
K_2O	2.81	0.38	1.31	0.29	1.19	0.27	0.68	0.18	0.67	3.80	0.11	0.15	0.11	0.14	0.22	0.25	0.31	0.36	0.57	1.13	2.26	1.30	0.63	0.12	0.38
P_2O_5	0.73	0.22	0.37	0.42	0.37	0.57	0.47	0.73	0.02	0.04	0.13	0.08	0.05	0.12	0.16	1.16	0.23	0.26	0.96	1.18	1.02	0.20	0.09	0.12	0.54
Total	98.94	98.81	101.56	98.95	101.14	98.75	97.99	100.26	98.07	99.10	98.30	97.94	104.37	99.26	99.90	97.13	100.11	98.86	99.84	99.27	99.45	99.04	98.63	100.57	99.21
CIPW Norm																									
Qz	7.17	1.94	--	--	--	4.02	--	4.81	13.16	6.62	--	--	2.22	--	3.46	10.67	--	0.33	--	--	4.91	8.14	4.38	--	--
C	--	--	--	--	--	--	--	--	10.99	10.73	--	--	--	--	--	7.55	--	--	--	--	--	--	--	--	--
Or	16.61	2.25	7.74	1.71	7.03	1.60	4.02	1.06	3.96	22.46	0.65	0.89	0.65	0.83	1.30	1.48	1.83	2.13	3.37	6.68	13.36	7.68	3.72	0.71	2.25
Ab	26.39	12.52	20.99	7.48	16.84	15.06	26.32	15.32	24.71	36.22	12.35	8.89	--	11.00	2.88	8.55	20.14	35.03	29.63	23.95	29.02	6.69	12.95	6.69	6.01
An	16.38	36.38	25.60	48.77	27.96	34.35	39.21	38.33	15.20	5.49	55.91	58.72	34.00	50.78	43.15	28.99	43.22	41.89	31.46	31.63	22.19	33.19	33.95	44.07	33.76
Pg	41.77	48.91	46.59	56.25	44.80	49.42	65.52	53.65	39.91	41.71	68.26	67.61	34.00	61.78	46.03	37.54	63.36	76.92	61.09	55.58	51.21	39.88	46.90	50.76	39.76
Ne	--	--	--	1.22	--	--	--	--	--	--	--	--	--	--	--	--	--	--	0.18	--	--	--	--	--	--
Lc	--	--	--	--	--	--	--	--	--	--	--	--	--	--	--	--	--	--	--	--	--	--	--	--	--
Di En	1.92	2.58	3.92	4.93	3.46	2.60	1.05	0.58	--	--	0.52	0.20	3.44	1.12	4.90	--	2.84	5.68	3.05	1.10	0.82	3.54	3.79	5.36	2.83
Di Fs	0.83	1.22	1.86	3.16	1.58	1.09	0.60	0.26	--	--	0.11	0.04	1.17	0.30	1.69	--	1.59	1.19	1.63	0.58	0.49	1.08	1.39	1.15	0.81
Di Wo	2.96	4.05	6.18	8.49	5.40	3.97	1.74	0.90	--	--	0.70	0.27	5.01	1.57	7.15	--	4.69	7.62	4.96	1.79	1.38	5.05	5.61	7.21	3.99
Wo	--	--	--	--	--	--	--	--	--	--	--	--	--	--	--	--	--	0.02	--	--	--	--	--	--	--
Hy En	13.67	19.94	12.26	--	16.98	19.31	8.38	18.25	10.14	4.23	18.14	19.64	37.85	18.76	21.85	17.68	9.73	--	--	6.39	10.58	21.39	19.67	25.42	23.91
Hy Fs	5.90	9.44	5.82	--	7.70	8.08	4.75	8.24	10.60	7.44	3.99	3.86	12.90	5.02	7.53	9.14	5.45	--	--	3.38	6.24	6.51	7.20	5.44	6.86
Ol Fo	--	--	4.63	8.39	2.83	--	2.07	--	--	--	1.25	1.80	--	3.11	--	--	1.10	--	7.70	6.53	--	--	--	0.12	6.43
Ol Fa	--	--	2.42	5.92	1.42	--	1.29	--	--	--	0.30	0.39	--	0.92	--	--	0.68	--	4.52	3.80	--	--	--	0.03	2.03
Mt	3.39	4.86	5.22	4.86	5.25	5.00	3.71	4.94	5.12	3.42	2.20	1.94	5.58	3.13	3.89	5.00	3.99	1.30	4.74	4.77	3.80	3.36	3.77	2.81	5.02
Hm	--	--	--	--	--	--	--	--	--	--	--	--	--	--	--	--	--	--	--	--	--	--	--	--	--
Il	2.39	2.22	3.08	2.15	2.77	4.41	3.08	4.96	3.19	1.75	1.39	0.76	0.47	1.84	1.01	4.44	2.75	2.83	5.49	4.05	3.59	1.35	1.39	0.76	3.13
Ap	1.69	0.51	0.86	0.97	0.86	1.32	1.09	1.69	0.05	0.09	0.30	0.19	0.12	0.28	0.37	2.69	0.53	0.60	2.22	2.73	2.36	0.46	0.21	0.28	1.25

* $\frac{Fe^{3+}}{Fe^{3+} + Fe^{2+}}$ = 0.26 (Le Maitre, 1976) assumed.

Table A11. Trace element constituents (in ppm) for Calhoun Falls complex.

	PcPO (Gabbronorite)				PO (Troctolite)				Pyrorenite	Metagabbro					Serpentinitas				
	CF1	CF21	CF26	CF50	CF31	CF32	CF33	CF34	CF14	CF12	CF18	CF29	CF40	CF51	CF4	CF11	CF19	CF27	CF45
Ba	314	379	621	381	469	506	463	453	249	476	660	613	758	644	260	232	424	686	283
Cr	502	281	129	449	324	210	169	318	1923	298	284	295	488	224	1650	1905	1024	2098	1577
La	<5	<5	31	<5	53	<5	<5	<5	<5	<5	<5	8	<5	<5	<5	18	<5	22	<5
Nb	5	5	12	6	7	6	5	7	5	5	7	6	9	9	5	6	25	6	8
Nd	<5	<5	<5	<5	<5	<5	<5	<5	<5	<5	7	<5	<5	<5	<5	<5	<5	<5	<5
Ni	146	301	12	210	315	388	436	501	297	427	237	12	95	12	168	275	252	401	330
Pb	<5	7	<5	7	11	13	6	10	6	20	21	<5	10	7	13	12	13	16	10
Rb	6	5	<2	4	<2	<2	<2	<2	8	<2	34	11	8	5	6	8	14	9	7
Sr	174	913	1081	657	1387	1609	1448	1482	82	1656	985	780	853	856	17	25	228	150	197
Th	<3	<3	<3	<3	<3	<3	<3	<3	6	<3	<3	<3	<3	<3	<3	5	9	4	<3
V	35	<5	543	33	33	6	<5	34	<5	5	5	412	111	612	6	5	110	30	144
Y	9	8	35	14	10	7	7	11	10	13	13	21	25	35	8	14	31	13	19
Zr	40	100	139	92	141	153	133	143	40	144	139	83	151	113	39	40	174	52	58

Table A12. Trace element constituents (in ppm) for Mt. Carmel complex.

	Metagabbro												Olivine-Biotite Gabbro				Syenite				
	MC2	MC7	MC13	MC14	MC18	MC27	MC28	MC29	MC31	MC32	MC34	MC38	MC21	MC36	MC42	MC43	MC3	MC35	MC11	MC12A	MC40
Ba	262	246	352	315	223	210	265	217	253	225	287	254	320	324	338	725	1275	906	895	1127	914
Cr	19	22	16	20	20	22	24	29	19	18	32	17	19	21	19	17	9	9	9	9	19
La	--	--	--	--	--	--	--	--	--	--	--	--	--	--	--	--	--	--	--	--	--
Nb	<1	<1	<1	<1	<1	<1	<1	<1	<1	<1	<1	<1	127	47	120	144	27	110	56	150	2
Nd	--	--	--	--	--	--	--	--	--	--	--	--	--	--	--	--	--	--	--	--	--
Ni	--	--	--	--	--	--	--	--	--	--	--	--	--	--	--	--	--	--	--	--	--
Pb	5	<5	<5	10	<5	5	<5	6	<5	<5	5	<5	<5	7	7	5	8	10	10	5	13
Rb	9	13	6	10	12	11	8	13	8	8	13	12	11	17	12	31	38	44	45	46	20
Sr	1106	485	969	790	450	536	743	300	673	719	278	619	553	382	553	392	328	254	267	167	899
Th	<3	<3	<3	<3	<3	<3	<3	<3	<3	<3	<3	<3	<3	<3	<3	<3	<3	<3	<3	<3	<3
V	524	570	655	879	1061	1157	871	1157	737	770	951	806	488	733	471	339	19	5	5	33	248
Y	8	14	5	7	5	3	8	6	16	18	8	5	52	24	53	37	35	25	10	56	21
Zr	66	105	58	95	113	112	102	140	93	89	136	97	151	204	146	598	149	1149	413	420	149

Table A13. Trace element constituents (in ppm) for Greenwood complex.

	Fine-Grained Gabbro (Diabase)										POcP Cumulate (Gabbronorite)									Metagabbro					
	GW1	GW3	GW7	GW12	GW13	GW15	GW17	GW19	GW20	GW21	GW8	GW9	GW10	GW11	GW16	GW18	GW22	GW23	GW25	MC2	MC4	MC6	MC30	MC31	MC32
Ba	2640	292	659	324	664	580	718	510	442	909	235	277	383	257	484	383	387	380	465	721	1237	467	366	270	398
Cr	19	27	27	21	28	35	18	23	23	12	17	22	27	19	25	26	19	15	19	19	16	29	24	40	39
Nb	25	<1	<1	<1	<1	78	31	94	18	57	<1	<1	<1	<1	<1	59	<1	88	47	24	44	<1	<1	<1	<1
Pb	20	10	13	6	12	10	11	7	5	6	<5	10	6	<5	13	6	10	12	5	16	13	17	15	8	9
Rb	43	18	24	13	22	13	12	10	22	83	9	9	11	14	10	11	9	7	10	33	45	45	23	8	9
Sr	1368	354	629	309	635	638	767	609	229	109	570	641	485	450	562	489	727	793	689	708	1191	774	627	483	836
Th	<3	<3	<3	4	<3	<3	<3	<3	4	11	<3	<3	<3	<3	<3	<3	<3	<3	<3	<3	<3	<3	<3	<3	<3
V	225	182	261	212	228	388	279	441	307	138	49	<5	<5	103	55	405	244	110	506	390	336	91	109	<5	278
Y	17	17	19	15	18	31	49	21	11	55	8	7	6	11	14	29	13	76	44	46	40	18	10	10	25
Zr	109	135	145	119	141	165	187	178	277	250	106	91	96	119	94	186	87	302	108	109	174	95	90	103	87

APPENDIX B

Table B1. Units used in heat flow modeling and sample problem set up.

Quantity	Symbol	Dimensions	Units
Length	L,x,l	L	m
Time	t	t	s
Mass	M	M	kg
Force	F	$ML\ t^{-2}$	$kgms^{-2}$
Temperature	T	T	K, °C
Heat	q	ML^2t^{-2}	$kg\ m^2s^{-2}$
Vol. Heat Flow Rate	$\dot{q}$	$Mt^{-3}L^{-1}$	$W\ m^{-3}$
Density	ρ	$M\ L^{-3}$	$kg\ m^{-3}$
Sp. Heat	c	$L^2t^{-2}T^{-1}$	$m^2s^{-2}K^{-1}$
Therm. Cond.	k	$MLt^{-3}T^{-1}$	$kgms^{-3}K^{-1}$
Therm. Diff.	a	L^2t^{-1}	m^2s^{-1}
Unit Surf. Conv.	h	$Mt^{-3}T^{-1}$	$kgs^{-3}K^{-1}$

APPENDIX C

Nondimensionalization

As noted in Chapter VI, nondimensionalization of the finite element equation (6.16) reduces computational error and provides an option to obtain several solutions for a single computer run. Nondimensionalization of a problem is obtained in the following manner. Let

$$F(T) = \rho c\frac{\partial T}{\partial t} - k\frac{\partial^2 T}{\partial x_i^2} - \dot{q} \equiv 0 \qquad (C.1)$$

For each variable in equation C.1, a non-dimensional variable can be found by dividing the variable by any arbitrary constant (a reference value) that has the same units as the variable. For example,

$$c^* = \frac{c\ (m^2/s^2K)}{c_r(m^2/s^2K)} \qquad (C.2)$$

where c^* is the unitless, nondimensional specific heat, and c_r is any arbitrary reference specific heat, and c is the true specific heat for a given problem. Thus, for equation C.1:

$$\begin{aligned} \rho &= \rho_r\rho^* \\ c &= c_r c^* \\ k &= k_r k^* \\ x &= L\, x^* \\ t &= \tau\, t^* \\ \dot{q} &= \dot{q}_r\dot{q}^* \\ T &= T_r T^* \end{aligned} \qquad (C.3)$$

Substituting the equations for C.3 into C.1 yields

$$f(T^*) = \frac{\rho_r \rho^* c_r c^* T_r}{\tau} \frac{\partial T^*}{\partial t^*} - \frac{k_r k^* T_r}{L^2} \frac{\partial^2 T^*}{\partial x_i^{*2}} \quad \dot{q}_r \dot{q}^* \equiv 0 \quad . \tag{C.4}$$

By letting

$$\rho = \rho_r \rho^* = \rho_r(1) = \rho_r$$
$$c = c_r c^* = c_r(1) = c_r$$
$$k = k_r k^* = k_r(1) = k_r$$

then equation C.4 becomes

$$f(T^*) = \frac{\rho_r c_r T_r}{\tau} \frac{\partial T^*}{\partial t^*} - \frac{k_r T_r}{L^2} \frac{\partial^2 T}{\partial x_i^{*2}} - \dot{q}_r q^* \equiv 0 \quad , \tag{C.5}$$

and dividing by $L^2/K_r T_r$ yields

$$f(T^*) = \frac{\rho_r c_r L^2}{\tau \; k_r} \frac{\partial T^*}{\partial t^*} - \frac{\partial^2 T^*}{\partial x_i^{*2}} - \frac{\dot{q}_r L^2}{k_r T_r} \; \dot{q} \equiv 0 \tag{C.6}$$

Because all of the reference variables are scalar quantities, the multipliers of each differential in equation C.6 are also scalar constants. That is,

$$\frac{\rho_r c_r L^2}{\tau \; k_r} \equiv C_1 \quad , \text{ and} \tag{C.7}$$

$$\frac{q \; L^2}{k_r T_r} \equiv C_2 \quad . \tag{C.8}$$

From equations C.7 and C.8 it follows that

$$\tau = \frac{\rho_r c_r L^2}{C_1 k_r} \quad , \text{ and} \tag{C.9}$$

$$T = \frac{\dot{q}_r L^2}{C_2 k_r} \quad . \tag{C.10}$$

It is apparent from equation C.6 that the solution is unitless and that real time and temperature can be found by substituting equations C.6 and C.10 into equations C.3, or

$$t = \frac{\rho_r c_r L^2}{C_1 k_r} t^* \tag{C.11}$$

$$T = \frac{\dot{q}_r L^2}{C_2 k_r} T^* \tag{C.12}$$

From a theoretical point of view C_1/C_2 can be any value, but from a practical (computational) point of view, this ratio should vary between 10^{-3} and 10^{3}. Solving the functional equivalent of equation C.6 (e.g., using eq. 6.18) requires the decomposition of global matrices into symmetrical upper and lower banded matrices with ones on the diagonal. If the components are much greater or smaller than unity (e.g., $10^{\pm 8}$) a solution cannot be found.

Because a solution is obtained in unitless space, it is possible to change the reference parameters of equations C.7 and C.8 to obtain a set of real solutions for any single partial differential equation after

one computer run. Thus, if the density chagnes by a factor of 2 then C1 in equation C.7 changes by a factor of 2 and C2 in equation C.8 remains constant.

VITA

Kem Fronabarger was born in Las Vegas, New Mexico, in 1948. He received his B.S. degree in geology from the Missouri School of Mines and Metallurgy at Rolla in June 1972, after which he served in the U.S. Peace Corps as an exploration geologist in Upper Volta for two years. In this capacity, he was responsible for gold and diamond exploration under the auspices of the Direction de la Géologie et Mines de Haute Volta.

Upon completion of his tour of duty, he returned to Meulan, France, and married Chantal Rousselin in July 1974. After returning to the United States, he worked for the Federal Power Commission as a staff geologist, auditing natural gas reserves from federally owned off-shore leases in the Gulf Coast. In 1976, Mr. Fronabarger moved to Oak Ridge to work as an exploration geologist with the National Uranium Resource Evaluation Program directed by the Oak Ridge National Laboratory.

He completed his M.S. degree in 1980 in Economic Geology at the Department of Geological Sciences, The University of Tennessee, Knoxville, under the direction of Dr. Kula C. Misra and immediately started on his dissertation.

After completing requirements for the Ph.D. degree in 1984, Mr. Fronabarger accepted an appointment as Assistant Professor of Geology at the College of Charleston, Charleston, South Carolina.